Single-ion and exchange anisotropy effects and multiferroic behavior in high-symmetry tetramer single molecule magnets

Richard A. Klemm[1,*] and Dmitri V. Efremov[2,†]

[1]*Department of Physics, University of Central Florida, Orlando, FL 32816 USA*
[2]*Institut für Theoretische Physik, Technische Universität Dresden, 01062 Dresden, Germany*

(Dated: February 2, 2008)

We study single-ion and exchange anisotropy effects in equal-spin s_1 tetramer single molecule magnets exhibiting T_d, D_{4h}, D_{2d}, C_{4h}, C_{4v}, or S_4 ionic point group symmetry. We first write the group-invariant quadratic single-ion and symmetric anisotropic exchange Hamiltonians in the appropriate local coordinates. We then rewrite these local Hamiltonians in the molecular or laboratory representation, along with the group-invariant Dzyaloshinskii-Moriya (DM), and isotropic Heisenberg, biquadratic, and three-center quartic Hamiltonians. Using our exact, compact forms for the single-ion spin matrix elements, we evaluate the eigenstate energies analytically to first order in the microscopic anisotropy interactions, corresponding to the strong exchange limit, and provide tables of simple formulas for the energies of the lowest four eigenstate manifolds of ferromagnetic (FM) and anitiferromagnetic (AFM) tetramers with arbitrary s_1. For AFM tetramers, we illustrate the first-order level-crossing inductions for $s_1 = 1/2, 1, 3/2$, and obtain a preliminary estimate of the microscopic parameters in a Ni_4 from a fit to magnetization data. Accurate analytic expressions for the thermodynamics, electron paramagnetic resonance absorption and inelastic neutron scattering cross-section are given, allowing for a determination of three of the microscopic anisotropy interactions from the second excited state manifold of FM tetramers. We also predict that tetramers with symmetries S_4 and D_{2d} should exhibit both DM interactions and multiferroic states, and illustrate our predictions for $s_1 = 1/2, 1$.

PACS numbers: 75.75.+a, 75.50.Xx, 73.22.Lp, 75.30.Gw, 75.10.Jm

I. INTRODUCTION

Single molecule magnets (SMM's) have been a topic of great interest for more than a decade,[1] because of their potential uses in quantum computing and/or magnetic storage,[2] which are possible due to magnetic quantum tunneling (MQT) and entangled states. In fits to a wealth of data, the Hamiltonian within an SMM cluster was assumed to be the Heisenberg exchange interaction plus weaker total (global, or giant) spin anisotropy interactions, with a fixed overall total spin quantum number s.[1] MQT and entanglement were only studied in this simple model.

The simplest SMM clusters are dimers.[3, 4, 5] Surprisingly, two antiferromagnetic dimers, an Fe_2, $[Fe(salen)Cl]_2$, where salen is N,N'-ethylenebis(salicylideneiminato), and a Ni_2, $Na_2Ni_2(C_2O_4)_3(H_2O)_2$, appear to have substantial single-ion anisotropy without any appreciable total spin anisotropy.[5, 6, 7] The presence of single-ion or exchange anisotropy actually precludes the total spin s from being a good quantum number.[4, 5] Although the most common SMM clusters have ferromagnetic (FM) intramolecular interactions and contain $n \geq 8$ magnetic ions,[8, 9] a number of intermediate-sized FM SMM clusters with $n = 4$ and rather simple molecular structures were recently studied. Fits to electron paramagnetic resonance (EPR) Ni_4 data assuming a fixed s were also problematic, suggesting single-ion or exchange anisotropy in that tetramer, as well.[10, 11] The Cu_4 tetramer $Cu_4OCl_6(TPPO)_4$, where TPPO is triphenylphosphine oxide, has four spin 1/2 ions on the corners of a regular tetrahedron, with an $s = 2$ ground state and approximate T_d symmetry.[12, 13, 14] In this case, there are no single-ion anisotropy effects, but anisotropic symmetric exchange interactions were thought to be responsible for the zero-field energy splittings.[12, 15] The Co_4, $Co_4(hmp)_4(MeOH)_4Cl_4$, where hmp is hydroxymethylpyridyl, and Cr_4, $[Cr_4S(O_2CCH_3)_8(H_2O)_4](NO_3)_2{\cdot}H_2O$, compounds have $s = 6$ ground states with spin 3/2 ions on the corners of tetrahedrons.[16, 17] Those compounds have S_4 and approximate D_{2d} symmetry, respectively.[16, 17] A number of high symmetry $s = 4$ ground state Ni_4 structures with spin 1 ions were reported.[18, 19, 20, 21, 22] Two of these, $[Ni(hmp)(ROH)Cl]_4$, where R is an alkyl group, such as methyl, ethyl, or 3,3-dimethyl-1-butyl and hmp is 2-hydroxymethylpyridyl, form tetramers with precise S_4 group symmetry.[21, 22] Two others, $Ni_4(ROH)L_4$, where R is methyl or ethyl and H_2L is salicylidene-2-ethanolamine, had approximate S_4 symmetry, although the precise symmetry was only C_1.[18] Several planar Mn_4 compounds with the Mn^{+3} spin 2 ions on the corners of squares were made, with overall $s = 8$ tetramer ground states.[23] Although two of these complexes had only approximate S_4 symmetry, one of these complexes, $Mn_4Cl_4(L')_4$, where H_2L' is 4-*t*-butyl-salicylidene-2-ethanolamine, had perfect S_4 symmetry.[23] Inelastic neutron scattering (INS) experiments provided strong evidence for single-ion

anisotropy in a Co_4 and a Ni_4 with approximate S_4 symmetry.[17, 18]

We note that *ab initio* calculations of the intramolecular spin-spin interactions in SMM clusters have not yet been always successful in calculating even the strongest, intramolecular isotropic Heisenberg interactions accurately, and have been incapable of calculating any of the local anisotropic spin-spin interactions within an SMM cluster.[24, 25, 26] Even to obtain the Heisenberg interactions accurately, it seems one needs to extend the local spin-density approximation (LSDA) to include on-site repulsions with strength U (the LSDA+U model), which would have to be introduced phenomenologically to fit the lowest two energy level manifolds in zero applied magnetic field.[26, 27, 28, 29, 30] We therefore define a microscopic model to be a model constructed in terms of the individual spins and from the local interactions between them, with parameters describing the strengths of the various types of local spin-spin interactions and interactions between the local spins and the magnetic field. This is distinct from a model constructed solely from the anisotropies of the total spin of an SMM cluster, which we denote as a phenomenological model. Our definition of a microscopic model is analogous to the standard model of the interactions of quarks and gluons within a hadron.

Recently there have been microscopic treatments of dimers,[4, 5] trimers, and tetramers, including Zeeman g-tensor anisotropy, single-ion anisotropy, and anisotropic exchange interactions.[31] Most of those treatments and their recent extensions to more general systems expressed the single-spin matrix elements only in terms of Wigner $3j$, $6j$, and $9j$ symbols.[31, 32] While such treatments are very helpful in fitting experimental data, more compact analytic forms are desirable to study microscopic models of FM SMM clusters in which the MQT and entanglement issues crucial for quantum computing can be understood. We constructed the quadratic single-ion and anisotropic near-neighbor (NN) and next-nearest-neighbor (NNN) exchange SMM cluster Hamiltonians from the respective local axial and azimuthal vector groups for equal-spin tetramer SMM clusters with point group symmetries $g = T_d$, D_{4h}, D_{2d}, C_{4h}, C_{4v}, and S_4, and found compact analytic expressions for the single-spin matrix elements of four general spins. Each local vector group generates site-dependent molecular single-ion and exchange anisotropy. We then show that for D_{2d} and S_4 symmetries, the antisymmetric exchange interactions lead to non-vanishing spin currents that may be accompanied by electric polarizations, leading to multiferroic effects. We evaluate the magnetization, specific heat, EPR and INS transitions in the Hartree approximation, and provide a procedure for extracting three of the effective site-independent microscopic parameters using EPR. We also show analytically how to include the effects of weak biquadratic exchange.

An outline of the paper is as follows. In Sec. II, we discuss the six structures and the general quadratic spin Hamiltonian. In Sec. III, we write the single-ion and symmetric anisotropic exchange Hamiltonians in terms of the local coordinates, and the antisymmetric exchange Hamiltonian in the molecular coordinates. In Sec. IV, we impose the operations of the six group symmetries, and discuss the effects of antisymmetric anisotropic exchange interactions and the related electric polarizations in lower symmetry systems. In Sec. V, the resulting group-symmetric Hamiltonians are written in the molecular representation, and the isotropic biquadratic exchange interactions are introduced. Section VI contains the eigenstates of the full Hamiltonian to first order in the anisotropy and NN biquadratic exchange interactions. These eiqenstates are used to obtain the level-crossing inductions for AFM tetramers, and particular examples with $s_1 = 1/2, 1, 3/2$ are presented. In Sec. VI, we also evaluate quantitatively some effects of antisymmetric anisotropic exchange and provide our related predictions for multiferroic behavior. In Sec. VII, the self-consistent Hartree approximation (or strong-exchange limit) is used to provide simple but accurate results for the thermodynamics, EPR resonant inductions, and INS

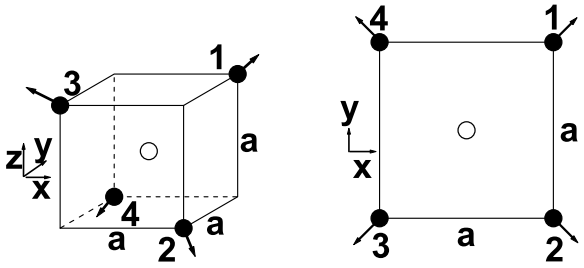

FIG. 1: T_d (left) and D_{4h} (right) ion sites (filled). Circle: origin. Arrows: local axial $\hat{\boldsymbol{z}}_n^{T_d}$ (left), azimuthal $\hat{\boldsymbol{x}}_n^{D_{4h}}$ (right) single-ion vectors. The axial vectors $\hat{\boldsymbol{z}}_n^{D_{4h}} = \hat{\boldsymbol{z}}$, normal to the ionic plane.

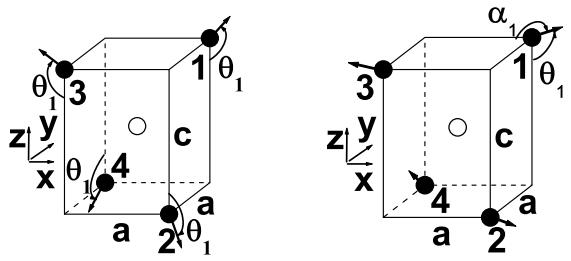

FIG. 2: D_{2d} (left) and S_4 (right) ion sites (filled). Circle: origin. Arrows: local axial single-ion vectors. The $g = D_{2d}, S_4$ axial vectors $\hat{\boldsymbol{z}}_1^g$ make the angles θ_1^g with the z axis, and the S_4 axial vector $\hat{\boldsymbol{z}}_1^{S_4}$ also makes the angle α_1 with the x axis, where $\cos\alpha_1 = \sin\theta_1^{S_4}\cos\phi_1^{S_4}$.

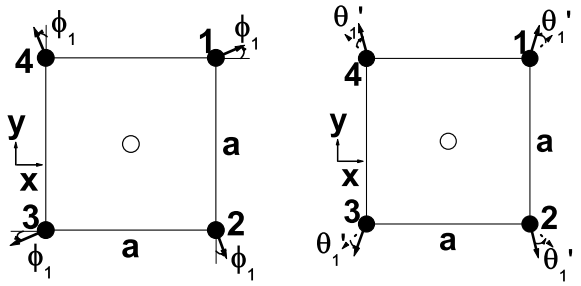

FIG. 3: C_{4h} (left) and C_{4v} (right) ion sites (filled). Circle: origin. Arrows: local azimuthal $\hat{\boldsymbol{x}}_n^{C_{4h}}$ (left) axial $\hat{\boldsymbol{z}}_n^{C_{4v}}$ (right) single-ion vectors. The axial vectors $\hat{\boldsymbol{z}}_n^{C_{4h}} = \hat{\boldsymbol{z}}$. The C_{4v} axial vectors each make the angle $\theta_1 = \pi/2 - \theta_1'$ with the z axis. The dotted arrows (equivalent to the D_{4h} azimuthal single-ion vectors $\hat{\boldsymbol{x}}_n^{D_{4h}}$) are their projections in the xy plane.

cross-sections, and describe how EPR experiments in the excited states of FM tetramers can provide a measure of some of the microscopic anisotropy interations strengths. Finally, in Sec. VIII, we discuss the significance of our results, and provide a preliminary fit to magnetization data on an AFM Ni_4 tetramer, and in Sec. IX, we present our conclusions.

II. STRUCTURES AND BARE HAMILTONIAN

For SMM clusters with ionic site point groups $g = T_d, D_{4h}$, we assume the four equal-spin s_1 ions sit on opposite corners of a cube or square of side a centered at the origin, as pictured in Fig. 1. For clusters with $g = D_{2d}, S_4$, we take the ions to sit on opposite corners of a tetragonal prism with sides (a, a, c) centered at the origin, as in Fig. 2. The ions for $g = C_{4h}, C_{4v}$ also sit on the corners of a square of side a centered at the origin, as pictured in Fig. 3, but the ligand groups have different symmetries than for the simpler D_{4h} case pictured in Fig. 1.[33] In each case, we take the origin to be at the geometric center, so that $\sum_{n=1}^{4} \boldsymbol{r}_n = 0$, where the relative ion site vectors are

$$\boldsymbol{r}_n = \frac{a}{\sqrt{2}}\Big[\sin\Big(\frac{(2n-1)\pi}{4}\Big)\hat{\boldsymbol{x}} + \cos\Big(\frac{(2n-1)\pi}{4}\Big)\hat{\boldsymbol{y}}\Big] - \frac{c}{2}(-1)^n\hat{\boldsymbol{z}}. \quad (1)$$

Tetrahedrons with $g = T_d$, $c/a = 1$, approximately as in Cu_4,[12] are a four-spin example of the equivalent-neighbor model.[34] In squares with $g = D_{4h}$, C_{4h}, or C_{4v}, $c = 0$. The high D_{4h} symmetry is approximately exhibited by the square Nd_4 compound, $Nd_4(OR)_{12}$, where R is 2,2-dimethyl-1-propyl, in which the Nd^{+3} ions have equal total angular momentum $j = 9/2$.[35, 36] We note that the Mn_4 clusters with approximate or exact S_4 symmetry also have $c = 0$.[23] In tetragonal prisms with $g = D_{2d}$ or S_4, $c/a > 1$, approximately as in a Co_4,[17] or $c/a < 1$, as in some Mn_4 and a Ni_4.[19, 23] For comparison with the planar symmetries $g = C_{4h}, D_{4h}$, and D_{4v}, we assume for $g = D_{2d}, S_4$ that $c/a < 1$, so that there are four NN sites and two NNN sites. For each g, $\hat{\boldsymbol{x}}, \hat{\boldsymbol{y}}, \hat{\boldsymbol{z}}$ are the molecular (or laboratory) unit coordinate axis vectors.

The most general Hamiltonian quadratic in the four spin operators $\boldsymbol{S}_n$ may be written for group g as

$$\mathcal{H}^g = -\mu_B \sum_{n=1}^{4} \boldsymbol{B} \cdot \overleftrightarrow{\boldsymbol{g}}_n^g \cdot \boldsymbol{S}_n + \sum_{n,n'=1}^{4} \boldsymbol{S}_n \cdot \overleftrightarrow{\boldsymbol{D}}_{n,n'}^g \cdot \boldsymbol{S}_{n'}, \quad (2)$$

where μ_B is the Bohr magneton and $\boldsymbol{B} = B(\sin\theta\cos\phi, \sin\theta\sin\phi, \cos\theta)$ is the magnetic induction at an arbitrary direction (θ, ϕ) relative to the molecular (or cluster) coordinates $(\hat{\boldsymbol{x}}, \hat{\boldsymbol{y}}, \hat{\boldsymbol{z}})$.[31, 37]

For simplicity, we take $\overleftrightarrow{\boldsymbol{g}}_n^g$ to be diagonal, isotropic, and site-independent, so that the Zeeman interaction may be written in terms of a single gyromagnetic ratio $\gamma \approx 2\mu_B$. Thus in the following, g only refers to the molecular group. We separate $\overleftrightarrow{\boldsymbol{D}}_{n,n'}^g$ into its symmetric and antisymmetric parts, $\overleftrightarrow{\boldsymbol{D}}_{n,n'}^g = \overleftrightarrow{\boldsymbol{D}}_{n,n'}^{g,s} + \overleftrightarrow{\boldsymbol{D}}_{n,n'}^{g,a}$, respectively. For $n' = n$, the single-ion $\overleftrightarrow{\boldsymbol{D}}_{n,n}^g$ is necessarily symmetric, so $\overleftrightarrow{\boldsymbol{D}}_{n,n}^{g,a} = 0$. For each g, the four $\overleftrightarrow{\boldsymbol{D}}_{n,n}^{g,s}$ contain the local single-ion structural information, and the six distinct symmetric $\overleftrightarrow{\boldsymbol{D}}_{n,n'}^{g,s}$ contain the local symmetric exchange structural information, which lead to the isotropic, or Heisenberg, exchange interactions, and the remaining symmetric anisotropic exchange interactions. The six distinct antisymmetric $\overleftrightarrow{\boldsymbol{D}}_{n,n'}^{g,a}$ contain additional local structural information which lead to the Dzyaloshinskii-Moriya (DM) interactions.[38, 39] Physically, the symmetric anisotropic exchange interactions also contain the intramolecular dipole-dipole interactions, which can be even larger in magnitude than the terms originating from actual anisotropic exchange.[37, 40]

As is well known, each of the symmetric rank-three tensors (or matrices) $\overleftrightarrow{\boldsymbol{D}}_{n,n'}^g$ can be diagonalized by three rotations: a rotation by the angle $\phi_{n,n'}^g$ about the molecular z axis, then a rotation by the angle $\theta_{n,n'}^g$ about the rotated $\tilde{x}$ axis, followed by a rotation by the angle $\psi_{n,n'}^g$ about the rotated $\tilde{z}$ axis.[41] This necessarily leads to the three principal axes $\hat{\tilde{\boldsymbol{x}}}_{n,n'}^g$, $\hat{\tilde{\boldsymbol{y}}}_{n,n'}^g$, and $\hat{\tilde{\boldsymbol{z}}}_{n,n'}^g$. For the single-ion axes with $n' = n$, we denote these principal axes to be $\hat{\tilde{\boldsymbol{x}}}_n^g$, $\hat{\tilde{\boldsymbol{y}}}_n^g$, and $\hat{\tilde{\boldsymbol{z}}}_n^g$, respectively, which are written explicitly in Sec. III. The non-vanishing matrix elements in these locally-diagonalized symmetric matrix coordinates are $\tilde{D}_{n,n',xx}^{g,s}$, $\tilde{D}_{n,n',yy}^{g,s}$ and $\tilde{D}_{n,n',zz}^{g,s}$. Since the structural information in each of the $\overleftrightarrow{\tilde{\boldsymbol{D}}}_{n,n'}^{g,s}$ depends upon the local environment, in the absence of molecular group g symmetry, each of these angles would in principle be

different from one another.

Although an antisymmetric exchange matrix $\overleftrightarrow{\boldsymbol{D}}^{g,a}_{n,n'}$ can generally be diagonalized by a unitary transformation, it contains at most three independent, real parameters, which can be incorporated into the components of a three-vector, $\boldsymbol{d}^g_{n,n'}$, with an effective spin-spin interaction of the form $\boldsymbol{d}^g_{n,n'}\cdot(\boldsymbol{S}_n\times\boldsymbol{S}_{n'})$,[38, 39] which is easiest to write in the molecular representation.

For the six high-symmetry groups under study, we analyze the effects of molecular group symmetry upon the single-ion and anisotropic exchange parts of $\mathcal{H}^g$. The group symmetries further restrict the number of independent parameters.

In the absence of any anisotropy interactions, the bare Hamiltonian $\mathcal{H}^g_0$ is given by the Zeeman and Heisenberg interactions,

$$\begin{aligned}\mathcal{H}^g_0 &= -\gamma\boldsymbol{B}\cdot\boldsymbol{S}-J'_g(\boldsymbol{S}_1\cdot\boldsymbol{S}_3+\boldsymbol{S}_2\cdot\boldsymbol{S}_4)\\ &\quad -J_g(\boldsymbol{S}_1\cdot\boldsymbol{S}_2+\boldsymbol{S}_2\cdot\boldsymbol{S}_3+\boldsymbol{S}_3\cdot\boldsymbol{S}_4+\boldsymbol{S}_4\cdot\boldsymbol{S}_1),\end{aligned}\tag{3}$$

which can be rewritten as

$$\mathcal{H}^g_0 = -\frac{J_g}{2}\boldsymbol{S}^2-\gamma\boldsymbol{B}\cdot\boldsymbol{S}-\frac{(J'_g-J_g)}{2}(\boldsymbol{S}^2_{13}+\boldsymbol{S}^2_{24}),\tag{4}$$

where $\boldsymbol{S}_{13}=\boldsymbol{S}_1+\boldsymbol{S}_3$, $\boldsymbol{S}_{24}=\boldsymbol{S}_2+\boldsymbol{S}_4$, and $\boldsymbol{S}=\boldsymbol{S}_{13}+\boldsymbol{S}_{24}$ is the total spin operator,[36] and we dropped an irrelevant, overall constant. In Eq. (4),

$$J'_{T_d} = J_{T_d},\tag{5}$$

$$J'_g \neq J_g\tag{6}$$

for $g=D_{2d},S_4,D_{4h},C_{4h}$, and C_{4v}. In terms of the diagonalized matrix elements, $-2J_g=\tilde{D}^{g,s}_{1,2,xx}+\tilde{D}^{g,s}_{1,2,yy}$ and $-2J'_g=\tilde{D}^{g,s}_{1,3,xx}+\tilde{D}^{g,s}_{1,3,yy}$, for instance. For our $c/a<1$ convention, $-J_g$ and $-J'_g$ are the NN and NNN Heisenberg interactions for $g=D_{2d},S_4,C_{4v},C_{4h}$ and D_{4h}.

III. THE SINGLE-ION AND ANISOTROPIC EXCHANGE HAMILTONIANS

To take account of the molecular group g symmetries, it is useful to write the single-ion and symmetric anisotropic exchange interactions in terms of the local coordinates. In this section, we write the local Hamiltonian for these interactions, and the molecular Hamiltonian for the antisymmetric exchange interactions. In Sec. IV, we then impose the group symmetries on these interactions for $C_{4h},D_{4h},C_{4v},S_4,D_{2d}$, and T_d molecular group symmetries, respectively.

A. Local single-ion Hamiltonian

For the single-ion anisotropy, we define the local vector basis for the nth site to be $\{\hat{\tilde{\boldsymbol{x}}}^g_n,\hat{\tilde{\boldsymbol{y}}}^g_n,\hat{\tilde{\boldsymbol{z}}}^g_n\}$ for each g. These basis elements are the vectors that diagonalize the single ion matrix from $\overleftrightarrow{\boldsymbol{D}}^g_{n,n}$ to $\overleftrightarrow{\tilde{\boldsymbol{D}}}^g_{n,n}$.[41] Since we employ these vectors repeatedly, we write them here for simplicity of presentation. The diagonalized vector set elements may be written in the molecular $(\hat{\boldsymbol{x}},\hat{\boldsymbol{y}},\hat{\boldsymbol{z}})$ representation as

$$\hat{\tilde{\boldsymbol{x}}}^g_n = \begin{pmatrix}\cos\phi^g_n\cos\psi^g_n-\cos\theta^g_n\sin\phi^g_n\sin\psi^g_n\\ \sin\phi^g_n\cos\psi^g_n+\cos\theta^g_n\cos\phi^g_n\sin\psi^g_n\\ \sin\theta^g_n\sin\psi^g_n\end{pmatrix},\tag{7}$$

$$\hat{\tilde{\boldsymbol{y}}}^g_n = \begin{pmatrix}-\cos\phi^g_n\sin\psi^g_n-\cos\theta^g_n\sin\phi^g_n\cos\psi^g_n\\ -\sin\phi^g_n\sin\psi^g_n+\cos\theta^g_n\cos\phi^g_n\cos\psi^g_n\\ \sin\theta^g_n\cos\psi^g_n\end{pmatrix},\tag{8}$$

$$\hat{\tilde{\boldsymbol{z}}}^g_n = \begin{pmatrix}\sin\theta^g_n\sin\phi^g_n\\ -\sin\theta^g_n\cos\phi^g_n\\ \cos\theta^g_n\end{pmatrix},\tag{9}$$

which satisfy $\hat{\tilde{\boldsymbol{x}}}^g_n\times\hat{\tilde{\boldsymbol{y}}}^g_n=\hat{\tilde{\boldsymbol{z}}}^g_n$. We then write the most general quadratic single-ion anisotropy interaction as

$$\begin{aligned}\mathcal{H}^{g,\ell}_{si} &= -\sum_{n=1}^{4}\Big(J^g_{a,n}(\boldsymbol{S}_n\cdot\hat{\tilde{\boldsymbol{z}}}^g_n)^2\\ &\quad +J^g_{e,n}[(\boldsymbol{S}_n\cdot\hat{\tilde{\boldsymbol{x}}}^g_n)^2-(\boldsymbol{S}_n\cdot\hat{\tilde{\boldsymbol{y}}}^g_n)^2]\Big),\end{aligned}\tag{10}$$

in terms of the site-dependent axial and azimuthal interactions $J^g_{a,n},J^g_{e,n}$, analogous in notation to that for homoionic dimers.[4, 5] In terms of the diagonalized matrix elements, $-J^g_{a,n}=\tilde{D}^{g,s}_{n,n,zz}-(\tilde{D}^{g,s}_{n,n,xx}+\tilde{D}^{g,s}_{n,n,yy})/2$ and $-J^g_{e,n}=(\tilde{D}^{g,s}_{n,n,xx}-\tilde{D}^{g,s}_{n,n,yy})/2$.

B. Local symmetric anisotropic exchange Hamiltonian

In addition to the single-ion interactions, the other microscopic anisotropic interactions are the anisotropic exchange interactions, which include the intracluster dipole-dipole interactions.[40] The intercluster dipole-dipole interactions can lead to low-T hysteresis in the phenomenological total spin model,[42] but in the microscopic individual spin model, are generally much weaker than the intracluster ones due to the larger distances involved. Hence, we neglect those and all other intercluster interactions, such as those mediated by phonons. As for the single-ion interactions, we first construct the symmetric anisotropic exchange Hamiltonian $\mathcal{H}^g_{ae}$ in the local group coordinates. In this case, there are distinct local vector sets for the NN and NNN exchange interactions. Diagonalization of the symmetric anisotropic exchange matrix $\overleftrightarrow{\boldsymbol{D}}^{g,s}_{n,n'}$ leads to $\overleftrightarrow{\tilde{\boldsymbol{D}}}^{g,s}_{n,n'}$ and the vector basis $\{\hat{\tilde{\boldsymbol{x}}}^g_{n,n'},\hat{\tilde{\boldsymbol{y}}}^g_{n,n'},\hat{\tilde{\boldsymbol{z}}}^g_{n,n'}\}$, given by Eqs. (7)-(9) with the subscript n replaced by n,n'.

The local symmetric anisotropic exchange Hamiltonian

$\mathcal{H}^{g,\ell}_{ae}$ is then generally given by

$$\mathcal{H}^{g,\ell}_{ae} = -\sum_{q=1}^{2}\sum_{n=1}^{6-2q}\Big[J^{f,g}_{n,n+q}(\boldsymbol{S}_n\cdot\hat{\tilde{\boldsymbol{z}}}^{g}_{n,n+q})(\boldsymbol{S}_{n+q}\cdot\hat{\tilde{\boldsymbol{z}}}^{g}_{n,n+q}) + J^{c,g}_{n,n+q}\Big((\boldsymbol{S}_n\cdot\hat{\tilde{\boldsymbol{x}}}^{g}_{n,n+q})(\boldsymbol{S}_{n+q}\cdot\hat{\tilde{\boldsymbol{x}}}^{g}_{n,n+q}) - (\boldsymbol{S}_n\cdot\hat{\tilde{\boldsymbol{y}}}^{g}_{n,n+q})(\boldsymbol{S}_{n+q}\cdot\hat{\tilde{\boldsymbol{y}}}^{g}_{n,n+q})\Big)\Big], \quad (11)$$

where we define $\boldsymbol{S}_5 \equiv \boldsymbol{S}_1$, as if the four NN spins were on a ring. In Eq. (11), the axial and azimuthal interaction strengths $-J^{f,g}_{n,n'} = \tilde{D}^{g,s}_{n,n',zz} - (\tilde{D}^{g,s}_{n,n',xx} + \tilde{D}^{g,s}_{n,n',yy})/2$ and $-J^{c,g}_{n,n'} = (\tilde{D}^{g,s}_{n,n',xx} - \tilde{D}^{g,s}_{n,n',yy})/2$, as for the single-ion interaction strengths. The subscripts a, e and superscripts f, c correspond to our dimer notation.[5]

C. Antisymmetric anisotropic exchange Hamiltonian

As noted above, we write the antisymmetric anisotropic exchange, or Dzyaloshinskii-Moriya (DM),[38, 39] Hamiltonian $\mathcal{H}^{g}_{DM}$ in the molecular representation,[37]

$$\mathcal{H}^{g}_{DM} = \sum_{q=1}^{2}\sum_{n=1}^{6-2q}\boldsymbol{d}^{g}_{n,n+q}\cdot\Big(\boldsymbol{S}_n\times\boldsymbol{S}_{n+q}\Big). \quad (12)$$

We note that in these molecular coordinates, the DM interaction three-vectors $\boldsymbol{d}^{g}_{n,n+q}$ depend explicitly upon the exchange bond indices $n, n+q$ for each group g. We then employ the local group symmetries to relate them to one another.

The rules for the directions of the $\boldsymbol{d}^{g}_{n,n+q}$ were given by Moriya,[38] and were employed for a dimer example by Bencini and Gatteschi.[37] The Moriya rules are: (1) $\boldsymbol{d}^{g}_{n,n'}$ vanishes if a center of inversion connects $\boldsymbol{r}_n$ and $\boldsymbol{r}_{n'}$. (2) When a mirror plane contains $\boldsymbol{r}_n$ and $\boldsymbol{r}_{n'}$, $\boldsymbol{d}^{g}_{n,n'}$ is normal to the mirror plane. (3) When a mirror plane is the perpendicular bisector of $\boldsymbol{r}_n - \boldsymbol{r}_{n'}$, $\boldsymbol{d}^{g}_{n,n'}$ lies in the mirror plane. (4) When a two-fold rotation axis is the perpendicular bisector of $\boldsymbol{r}_n - \boldsymbol{r}_{n'}$, then $\boldsymbol{d}^{g}_{n,n'}$ is orthogonal to the rotation axis. (5) When $\boldsymbol{r}_n - \boldsymbol{r}_{n'}$ is an r-fold rotation axis with $r > 2$, then $\boldsymbol{d}^{g}_{n,n'}$ is parallel to $\boldsymbol{r}_n - \boldsymbol{r}_{n'}$. As noted above, we shall incorporate these rules in the molecular representation. For example, in NaV_2O_5, the lack of inversion symmetry between interacting spins has been shown to lead to a DM interaction.[43]

IV. GROUP SYMMETRY INVARIANCE

A. General considerations

In this section, we impose the set of allowed group g symmetry operations upon the full Hamiltonian $\mathcal{H}^{g}$.

g	θ^{g}_1	ϕ^{g}_1	ψ^{g}_1
C_{4h}	0	ϕ^{g}_1	0
D_{4h}	0	$\frac{\pi}{4}$	0
C_{4v}, D_{2d}	θ^{g}_1	$\frac{3\pi}{4}$	$-\frac{\pi}{2}$
S_4	$\theta^{S_4}_1$	$\phi^{S_4}_1$	$\psi^{S_4}_1$
T_d	$\tan^{-1}\sqrt{2}$	$\frac{3\pi}{2}$	0

TABLE I: Lists of the single-ion parameter sets μ^{g}_1.

These symmetry operations are represented by the matrices $\mathcal{O}_\lambda$ for $\lambda = 1, \ldots, 26$ listed in Subsection A of the Appendix. For each g, we require $\mathcal{H}^{g}$ to be invariant under each symmetry operation $\mathcal{O}^{g}_\lambda$ for each allowed λ.

For the six g cases under study, the set $\{\mathcal{O}^{g}_\lambda\}$ of group operations greatly reduces the number of single-ion and symmetric anisotropic exchange parameters. As we shall see, in each group g, these reduce the single-ion and symmetric anisotropic exchange interaction strength set to

$$\{J^{g}_j\} \equiv \{J^{g}_a, J^{g}_e, J^{g}_{f,q}, J^{g}_{c,q}\}, \quad (13)$$

for $q = 1, 2$, which are independent of the site index n. That is, for each g, there are at most two single-ion, two NN and two NNN symmetric anisotropic exchange interaction strengths. In addition, for these six g cases, the group operations further limit the number of vector set parameters to

$$\mu^{g}_1 = \{\theta^{g}_1, \phi^{g}_1, \psi^{g}_1\}, \quad (14)$$

$$\mu^{g}_{1q} = \{\theta^{g}_{1p}, \phi^{g}_{1p}, \psi^{g}_{1p}\}, \quad (15)$$

where $p = q + 1 = 2, 3$, and we used the notation $\theta^{g}_1 = \theta^{g}_{1,1}$, $\theta^{g}_{1p} = \theta^{g}_{1,p}$, etc. Some of these parameters may be further restricted. In addition, however, the molecular single-ion and anisotropic exchange Hamiltonians contain both site-independent and site-dependent terms.

For $\mathcal{H}^{g}_{DM}$, we first impose the Moriya rules on each anisotropic exchange pair,[37, 38] and then impose the required group symmetries on the six pairs. For the six groups under study, the group symmetries place restrictions upon the $\boldsymbol{d}^{g}_{n,n+q}$, leading to the anisotropic exchange parameter set

$$d^{g} = \{d^{g}_z, d^{g}_{x1}, d^{g}_{y1}, d^{g}_{x2}, d^{g}_{y2}\}. \quad (16)$$

For each of the six g cases, the NNN DM parameter set has at least one more restriction than does the NN DM parameter set. Some g symmetries lead to site-dependent signs of the components of d^{g}.

C. Imposing the group symmetries

In Subsection A of the Appendix, we describe the matrices $\mathcal{O}_\lambda$ for $\lambda = 1, \ldots, 26$ representing the group symmetry operations for $g = C_{4h}, D_{4h}, C_{4v}, S_4, D_{2d}$, and T_d.

g	θ^g_{1p}	ϕ^g_{1p}	ψ^g_{1p}
C_{4h}	0	$\phi^{C_{4h}}_{1p}$	0
D_{4h}	0	$\frac{\pi}{4}$	0
C_{4v}	0	$\frac{(p-2)\pi}{4}$	0
S_4	$\theta^{S_4}_{1p}$	$\phi^{S_4}_{1p}$	$\psi^{S_4}_{1p}$
D_{2d}	$\theta^{D_{2d}}_{12}\delta_{p,2}+\frac{\pi}{2}\delta_{p,3}$	$\frac{(-1)^p\pi}{2(p-1)}$	$\frac{(p-2)\pi}{2}$

TABLE II: Lists of the relevant NN ($p=2$) and NNN ($p=3$) parameter sets μ^g_{1p}.

g	d^g_z	d^g_{x1}	d^g_{y1}	d^g_{x2}	d^g_{y2}
C_{4h}, D_{4h}	d^g_z	0	0	0	0
S_4	$d^{S_4}_z$	$d^{S_4}_{x1}$	$d^{S_4}_{y1}$	$d^{S_4}_{x2}$	$d^{S_4}_{y2}$
D_{2d}	$d^{D_{2d}}_z$	0	$d^{D_{2d}}_{y1}$	$d^{D_{2d}}_{x2}$	0
T_d, C_{4v}	0	0	0	0	0

TABLE III: Lists of the DM parameter sets d^g.

For each molecular group g, the allowed symmetry operations $\mathcal{O}_\lambda$ commute with the Hamiltonian. For a particular λ, $\mathcal{O}_\lambda \boldsymbol{r}_n = \boldsymbol{r}_{n'(\lambda)}$. We therefore take $\boldsymbol{S}_n = \boldsymbol{S}(\boldsymbol{r}_n)$, so that $\mathcal{O}_\lambda \boldsymbol{S}_n = \boldsymbol{S}(\mathcal{O}_\lambda \boldsymbol{r}_n) = \boldsymbol{S}(\boldsymbol{r}_{n'(\lambda)}) = \boldsymbol{S}_{n'(\lambda)}$.

For C_{4h} symmetry, besides the trivial identity operation, the allowed group operations are clockwise and counterclockwise rotations by $\pi/2$ about the z axis, and reflections in the xy plane.[33] These operations are represented respectively by the matrices $\mathcal{O}_{1,2,6}$. We use this simple case to illustrate how the symmetries are imposed. We first consider the axial part of $\mathcal{H}^{C_{4h},\ell}_{si}$, and set

$$\sum_{n=1}^{4} J^{C_{4h}}_{a,n} (\boldsymbol{S}_n \cdot \hat{\tilde{\boldsymbol{z}}}^{C_{4h}}_n)^2 \;=\; \sum_{n=1}^{4} J^{C_{4h}}_{a,n} \mathcal{O}_1 (\boldsymbol{S}_n \cdot \hat{\tilde{z}}^{C_{4h}}_n)^2 \mathcal{O}_1^T. \tag{17}$$

We interpret $\hat{\tilde{\boldsymbol{z}}}^{C_{4h}}_n$ as its vector transpose, $(\hat{\tilde{\boldsymbol{z}}}^{C_{4h}}_n)^T$ in Eq. (17), and obtain

$$\mathcal{O}_1 \boldsymbol{S}_n \;=\; \boldsymbol{S}_{n+1}, \tag{18}$$

$$(\hat{\tilde{\boldsymbol{z}}}^{C_{4h}}_n)^T \mathcal{O}_1^T \;=\; \Big(-\sin\theta^{C_{4h}}_n \cos\phi^{C_{4h}}_n, \; -\sin\theta^{C_{4h}}_n \sin\phi^{C_{4h}}_n, \cos\theta^{C_{4h}}_n \Big). \tag{19}$$

Substituting these into the right-hand side of Eq. (17), setting $n \to n+1$ in the left-hand side, and equating coefficients of $S_{n+1,\alpha} S_{n+1,\beta}$ for $\alpha, \beta = x, y, z$ leads to

$$J^{C_{4h}}_{a,n} \;=\; J^{C_{4h}}_{a,n+1} = J^{C_{4h}}_a, \tag{20}$$

$$\theta^{C_{4h}}_n \;=\; \theta^{C_{4h}}_{n+1} = \theta^{C_{4h}}_1, \tag{21}$$

$$\phi^{C_{4h}}_n \;=\; \phi^{C_{4h}}_{n+1} + \frac{\pi}{2}. \tag{22}$$

Then, imposing $\mathcal{O}_6$ symmetry, we have $\mathcal{O}_6 \boldsymbol{S}_n = \boldsymbol{S}_n$, and either $\theta^{C_{4h}}_1 = \pi/2$ or $\theta^{C_{4h}}_1 = 0$, both of which lead to invariance of this part of the Hamiltonian under $\mathcal{O}_6$ We therefore take the easy-axis case, $\theta^{C_{4h}}_1 = 0$. Carrying out similar transformations on the azimuthal single-ion Hamiltonian leads to

$$J^{C_{4h}}_{e,n} \;=\; J^{C_{4h}}_e, \tag{23}$$

$$\chi^{C_{4h}}_n \;=\; \phi^{C_{4h}}_n + \psi^{C_{4h}}_n = \chi^{C_{4h}}_{n+1} + \frac{\pi}{2}. \tag{24}$$

We could then choose $\psi^{C_{4h}}_1 = 0$, leaving one free angle parameter $\phi^{C_{4h}}_1$, as listed in Table I, plus the two interaction strengths $J^{C_{4h}}_a, J^{C_{4h}}_e$.

The symmetric anisotropic exchange Hamiltonian, $\mathcal{H}^{C_{4h},\ell}_{ae}$ can be made invariant under $\mathcal{O}_1, \mathcal{O}_2, \mathcal{O}_6$ in a very similar fashion. The operations for the other five g symmetries are listed in Subsection A of the Appendix, along with the associated matrices. Our results for the single-ion, symmetric anisotropic exchange, and DM interaction parameters are compiled in Tables I-III.

D. Induced electric polarizations

As shown by Katsura *et al.*,[44] the spin-orbit interactions between spins at sites n and n' can induce an electric polarization

$$\boldsymbol{P}_{n,n'} \sim \hat{\boldsymbol{r}}_{n,n'} \times (\boldsymbol{S}_n \times \boldsymbol{S}_{n'}), \tag{25}$$

where $\hat{\mathbf{r}}_{n,n'}$ is a unit vector directed from site n to site n'. In our model, the thermodynamic averages of such polarizations vanish in the absence of DM interactions, but non-vanishing in-plane vector components $\boldsymbol{d}^g_q$ of the d^g DM interaction parameter sets allow them to become finite. Tetramers with the rather low molecular group symmetries S_4 and D_{2d} have no overall center of inversion symmetry, and contain a complex set of DM interactions. Depending upon the polarizability of the attached ligand groups, this may lead to a combined spin-induced electric polarization

$$\boldsymbol{P}_s \;\propto\; \frac{1}{2} \sum_{n,n'=1}^{4} \hat{\boldsymbol{r}}_{n,n'} \times \langle \boldsymbol{S}_n \times \boldsymbol{S}_{n'} \rangle, \tag{26}$$

where $\langle \ldots \rangle$ represents the thermodynamic average in the presence of the full Hamiltonian, including the relevant DM interactions.

Besides the direct DM interactions, we predict the possibility of dual, or induced, DM interactions. Although $\boldsymbol{d}^g_q$ DM interactions between individual spin pairs are allowed in tetramers with the lowest C_{4h} and D_{4h} symmetries studied, the group symmetry causes the dipole moments on opposite sides of their square geometries to cancel one another. Although we have not studied this point in detail, tetramers with these symmetries can in

principle be made to exhibit additional effective DM interactions by application of an electric field $\boldsymbol{E} \neq 0$.[44, 45] Thus, in tetramers with S_4, D_{2d}, or lower symmetry, a multiferroic effect can occur,[45] in which both DM interactions and $\boldsymbol{P}_s \neq 0$. More generally, multiferroic effects arise in systems such as some dimers, trimers, and tetramers that generally do not have a center of inversion at the midpoints of the $\boldsymbol{r}_{n,n'}$.[5]

V. THE HAMILTONIAN IN THE MOLECULAR REPRESENTATION

A. The molecular single-ion Hamiltonian

To make contact with experiment, we use the group symmetries to rewrite $\mathcal{H}_{si}^{g,\ell}$ in the molecular $(\hat{\boldsymbol{x}}, \hat{\boldsymbol{y}}, \hat{\boldsymbol{z}})$ representation,

$$\mathcal{H}_{si}^{g} = -\sum_{n}\Big(J_z^g S_{n,z}^2 + (-1)^n J_{xy}^g (S_{n,x}^2 - S_{n,y}^2) + \sum_{\alpha\neq\beta} K_{\alpha\beta}^g(n) S_{n,\alpha} S_{n,\beta}\Big), \tag{27}$$

where $\alpha, \beta = x, y, z$, and we subtracted an irrelevant constant. $\mathcal{H}_{si}^g$ contains the site-independent interactions J_z^g and the site-dependent interactions $(-1)^n J_{xy}^g$ and $K_{\alpha\beta}^g(n)$, which are written in terms of the parameter sets μ_1^g in Subsection B of the Appendix. Most important is the result that for T_d symmetry,

$$J_z^{T_d} = 0. \tag{28}$$

The first-order contributions to the eigenstate energies from the site-dependent interactions $(-1)^n J_{xy}^g$ and $K_{\alpha\beta}^g(n)$ vanish. Hence, these interactions only contribute to the eigenstate energies to second and higher orders in the interactions J_a^g and J_e^g. For C_{4v}, D_{2d} and S_4, the effective axial site-independent interactions J_z^g arise from a combination of the local axial and azimuthal interactions J_a^g and J_e^g. For $g \neq T_d$, J_z^g can be large, even if the molecular structure is nearly T_d.

B. Symmetric anisotropic exchange in the molecular representation

We then construct the group-invariant symmetric anisotropic exchange Hamiltonian in the molecular coordinates for the six g symmetries. For $g = D_{2d}, S_4$, there are renormalizations of the isotropic exchange interactions, modifying $\mathcal{H}_0^g$ to

$$\mathcal{H}_0^{g,r} = -\frac{\tilde{J}_g}{2}\boldsymbol{S}^2 - \gamma \boldsymbol{B}\cdot\boldsymbol{S} - \frac{(\tilde{J}_g' - \tilde{J}_g)}{2}(\boldsymbol{S}_{13}^2 + \boldsymbol{S}_{24}^2), \tag{29}$$

where

$$\tilde{J}_g = J_g + \delta J_g, \tag{30}$$

$$\tilde{J}_g' = J_g' + \delta J_g', \tag{31}$$

where J_g, J_g' are given by Eqs. (5) and (6), and the δJ_g and $\delta J_g^{'}$ are given in in terms of the parameters sets μ_{1p}^g in Subsection C of the Appendix. For the three planar symmetries, $g = C_{4h}, D_{4h}$, and C_{4v}, $\delta J_g = \delta J_g^{'} = 0$. For T_d symmetry, there are no group-satisfying azimuthal symmetric exchange vectors, so $J_{c,q}^{T_d} = 0$ for $q = 1, 2$. However, the axial vectors parallel to $\boldsymbol{r}_{n,n'}$ satisfy all of the group symmetries, so that the $J_{f,q}^{T_d}$ could exist, provided that $J_{f,1}^{T_d} = J_{f,2}^{T_d}$. However, the requirement $\tilde{J}_{T_d} = \tilde{J}_{T_d}'$ to preserve the T_d symmetry of the renormalized Heisenberg interactions forces $J_{f,2}^{T_d} = J_{f,1}^{T_d}/2$. Hence, we must conclude that $J_{f,q}^{T_d} = 0$ for $q = 1, 2$ and $\delta J_{T_d} = \delta J_{T_d}' = 0$.

$\mathcal{H}_{ae}^{g,\ell}$ also leads to additional interactions $\delta\mathcal{H}_{ae}^g$ in the molecular frame,

$$\delta\mathcal{H}_{ae}^{g} = \sum_{q=1}^{2}\sum_{n=1}^{6-2q}\Big[J_{q,z}^g S_{n,z} S_{n+q,z} + (-1)^{n+1}\Big(J_{q,xy}^g \times\Big[S_{n,x}S_{n+q,x} - S_{n,y}S_{n+q,y}\Big] + \sum_{\alpha\neq\beta} K_{q,\alpha\beta}^g(n) S_{n,\alpha} S_{n+q,\beta}\Big)\Big], \tag{32}$$

where $\alpha, \beta = x, y, z$. As for the single-ion interactions in the molecular representation, the site-independent symmetric exchange interactions $J_{q,z}^g$ contribute to the eigenstate energies to first order, but the first-order contributions to the eigenstate energies from the site-dependent interactions vanish. Both the site-independent and site-dependent symmetric exchange interactions are given in terms of the parameter sets μ_{1p}^g in Subsection C of the Appendix.

C. Antisymmetric exchange Hamiltonian

In Secs. IV and V, we already evaluated the antisymmetric exchange Hamiltonians in the molecular representation, and the parameter sets are listed in Table III. These six $\mathcal{H}_{DM}^g$ may be combined as

$$\mathcal{H}_{DM}^{g} = \sum_{q=1}^{2}\sum_{n=1}^{6-2q}\big(\boldsymbol{S}_n \times \boldsymbol{S}_{n+q}\big)\cdot\Big(d_z^g(n)\delta_{q,1}\hat{\boldsymbol{z}} + \boldsymbol{d}_q^g \sin(n\pi/2) + (\hat{\boldsymbol{z}}\times\boldsymbol{d}_q^g)\cos(n\pi/2)\Big), \tag{33}$$

where the scalar $d_z^g(n)$ and the two two-vectors $\boldsymbol{d}_q^g$ all vanish for $g = C_{4v}, T_d$, but for the other four symmetries are given in Subsection C of the Appendix.

We note that both site-dependent and site-independent DM interactions give rise to second-order eigenstate energy corrections, and can only be neglected in fits to experiment for tetramers with symmetries very close to T_d, C_{4v}, or higher. In Subsection D of the Appendix, we give $\mathcal{H}^g_{DM}$ for the lower symmetry C^{13}_{2v} tetramers.

D. Biquadratic and three-center quartic isotropic exchange interactions

In the previous subsections, we listed the quadratic single-ion and anisotropic exchange interactions for the six high-symmetry tetramer groups under study. However, in the lower-symmetry AFM tetramers $\{Ni_4Mo_{12}\}$, with C_{1v} symmetry,[46] and Ni_4 and Co_4 [2×2] grids (or rhombuses), with approximate C^{13}_{2v} symmetry,[47, 48, 49] fits to magnetization data were facilitated by the inclusion of biquadratic interactions.[46, 47, 48] In the former case, the powder fits assumed field-dependent interaction parameters, but the single-ion interactions were assumed to have T_d symmetry, which vanish to first order in their strength, and the anisotropic exchange interactions were neglected. In the latter C^{13}_{2v} case, the authors neglected the NN DM interactions given in the Appendix. Subsequently, Kostyuchenko showed that three-center isotropic quartic interactions should be comparable in magnitude to the biquadratic interactions, and provided a fit to the midpoints of the level-crossing magnetization behavior on $\{Ni_4Mo_{12}\}$, without making the assumption of strong field dependence to the Heisenberg interactions.[50] Here we provide preliminary fits to the AFM $\{Ni_4Mo_{12}\}$ magnetization data, extending the treatment of Kostyuchenko to include the first order anisotropy interactions, which can fit the widths of the transitions, as well as the midpoints. More complete fits to those experiments and to experiments on the grid SMM's will be presented elsewhere.[51] Such fits are greatly aided by an analytic treatment of biquadratic and three-center isotropic quartic exchange.

For tetramers with the six g symmetries under study, the biquadratic interactions may be written as

$$\mathcal{H}^g_{\rm b} = \sum_{q=1}^{2} \mathcal{H}^g_{{\rm b},q} \tag{34}$$

$$\mathcal{H}^g_{{\rm b},q} = -J^g_{{\rm b},q} \sum_{n=1}^{6-2q} \big(\boldsymbol{S}_n \cdot \boldsymbol{S}_{n+q}\big)^2. \tag{35}$$

For $g = T_d$, we take $J^{T_d}_{{\rm b},1} = J^{T_d}_{{\rm b},2}$, but otherwise $J^g_{{\rm b},2} \neq J^g_{{\rm b},1}$. For the six g symmetries, $\mathcal{H}^g_{\rm b}$ is invariant under all of the appropriate symmetries.

The three-center quartic interactions for systems with the six g symmetries may be written as

$$\mathcal{H}^g_{\rm t} = \sum_{q=1}^{2} \mathcal{H}^g_{{\rm t},q} \tag{36}$$

$$\mathcal{H}^g_{{\rm t},1} = -J^g_{{\rm t},1} \sum_{\substack{n=1\\ \rm odd}}^{4} \sum_{\substack{n'=1\\ \rm even}}^{4} \big(\boldsymbol{S}_n \cdot \boldsymbol{S}_{n+1}\big)\big(\boldsymbol{S}_{n'} \cdot \boldsymbol{S}_{n'+1}\big), \tag{37}$$

$$\mathcal{H}^g_{{\rm t},2} = -J^g_{{\rm t},2} \sum_{n=1}^{4} \sum_{n'=1}^{2} \big(\boldsymbol{S}_n \cdot \boldsymbol{S}_{n+1}\big)\big(\boldsymbol{S}_{n'} \cdot \boldsymbol{S}_{n'+2}\big). \tag{38}$$

VI. EIGENSTATES OF THE FULL HAMILTONIAN

A. Induction representation

We assume a molecular Hamiltonian

$$\mathcal{H}^g = \mathcal{H}^{g,r}_0 + \mathcal{H}^g_{si} + \delta\mathcal{H}^g_{ae} + \mathcal{H}^g_{DM} + \mathcal{H}^g_{\rm b}. \tag{39}$$

To take proper account of $\boldsymbol{B}$ in $\mathcal{H}^{g,r}_0$, we construct our SMM eigenstates in the induction representation by

$$\begin{pmatrix} \hat{\boldsymbol{x}} \\ \hat{\boldsymbol{y}} \\ \hat{\boldsymbol{z}} \end{pmatrix} = \begin{pmatrix} \cos\theta\cos\phi & -\sin\phi & \sin\theta\cos\phi \\ \cos\theta\sin\phi & \cos\phi & \sin\theta\sin\phi \\ -\sin\theta & 0 & \cos\theta \end{pmatrix} \begin{pmatrix} \hat{\boldsymbol{x}}' \\ \hat{\boldsymbol{y}}' \\ \hat{\boldsymbol{z}}' \end{pmatrix}, \tag{40}$$

so that $\boldsymbol{B} = B\hat{\boldsymbol{z}}'$. A subsequent arbitrary rotation about $\hat{\boldsymbol{z}}'$ does not affect the eigenstates.[5] We then set $\hbar = 1$ and write

$$\boldsymbol{S}^2|\psi^{s_{13},s_{24}}_{s,m}\rangle = s(s+1)|\psi^{s_{13},s_{24}}_{s,m}\rangle, \tag{41}$$

$$\boldsymbol{S}^2_{13}|\psi^{s_{13},s_{24}}_{s,m}\rangle = s_{13}(s_{13}+1)|\psi^{s_{13},s_{24}}_{s,m}\rangle, \tag{42}$$

$$\boldsymbol{S}^2_{24}|\psi^{s_{13},s_{24}}_{s,m}\rangle = s_{24}(s_{24}+1)|\psi^{s_{13},s_{24}}_{s,m}\rangle, \tag{43}$$

$$S_{\tilde{z}}|\psi^{s_{13},s_{24}}_{s,m}\rangle = m|\psi^{s_{13},s_{24}}_{s,m}\rangle, \tag{44}$$

$$S_{\tilde{\sigma}}|\psi^{s_{13},s_{24}}_{s,m}\rangle = A^{\tilde{\sigma}m}_s|\psi^{s_{13},s_{24}}_{s,m+\tilde{\sigma}}\rangle, \tag{45}$$

$$A^m_s = \sqrt{(s-m)(s+m+1)}, \tag{46}$$

where $S_{\tilde{\sigma}} = S_{\tilde{x}} + i\tilde{\sigma}S_{\tilde{y}}$ with $\tilde{\sigma} = \pm$. For brevity, we define

$$\nu \equiv \{s, m, s_{13}, s_{24}, s_1\}, \tag{47}$$

$$\overline{\nu} \equiv \{s, s_{13}, s_{24}, s_1\}, \tag{48}$$

where $\overline{\nu}$ excludes m, and write $|\nu\rangle \equiv |\psi^{s_{13},s_{24}}_{s,m}\rangle$. $\mathcal{H}^g_{{\rm b},2}$ and $\mathcal{H}^{g,r}_0$ are both diagonal in this representation, but $\mathcal{H}^g_{si}, \delta\mathcal{H}^g_{ae}$, and $\mathcal{H}^g_{{\rm b},1}$ are not, and we therefore assume their interaction strengths to be small, relative to $\tilde{J}_g$ and $\tilde{J}'_g$. From Eqs. (41) to (44), $\langle\nu'|\mathcal{H}^{g,r}_0 + \mathcal{H}^g_{{\rm b},2}|\nu\rangle = E^g_{\nu,0}\delta_{\nu',\nu}$, where

$$E^g_{\nu,0} = -\frac{\tilde{J}_g}{2}s(s+1) - \gamma Bm + \delta E^g_{\overline{\nu},0} \tag{49}$$

$$\delta E^g_{\overline{\nu},0} = -\frac{1}{2}\sum_{n=1}^{2}\Big[(\tilde{J}'_g-\tilde{J}_g)s_{n,n+2}(s_{n,n+2}+1) + \frac{J^g_{\rm b,2}}{2}[-2s_1(s_1+1)+s_{n,n+2}(s_{n,n+2}+1)]^2 + \frac{J^g_{\rm t,2}}{2}[-2s_1(s_1+1)+s_{n,n+2}(s_{n,n+2}+1)] \times\Big(s(s+1)-\sum_{n'=1}^{2}s_{n',n'+2}(s_{n',n'+2}+1)\Big)\Big], \quad (50)$$

where the $\tilde{J}_g$ and $\tilde{J}'_g$ are given by Eqs. (5), (6), and (129)-(132). Since $\mathcal{H}^{g,r}_0$ and $\mathcal{H}^g_{\rm b,2}$ are invariant under all rotations, $E^g_{\nu,0}$ is independent of θ,ϕ.

B. First-order eigenstates

In the induction representation, we write $\mathcal{H}^g_{si}+\delta\mathcal{H}^g_{ae}+\mathcal{H}^g_{DM}$ as $\mathcal{H}'^{,g}_{si}+\mathcal{H}'^{,g}_{ae}+\mathcal{H}'^{,g}_{DM}$. $\mathcal{H}^g_{\rm b,1}$ is a scalar independent of the direction of $\boldsymbol{B}$. We then make a standard perturbation expansion for the seven remaining microscopic anisotropy energies $\{J^g_j\}\equiv\{J^g_a,J^g_e,J^g_{f,q},J^g_{c,q},J^g_{\rm b,1}\}$ for $q=1,2$ small relative to $|\tilde{J}_g|,|\tilde{J}'_g|$.[5] To do so, it is necessary to evaluate the single-ion matrix elements analytically, as they contain much of the interesting physics. Compact expressions for these matrix elements for general (s_1,s_2,s_3,s_4) are given in Subsection E of the Appendix.

At arbitrary $\boldsymbol{B}$ angles (θ,ϕ), the first order corrections $E^g_{\nu,1}=\langle\nu|\mathcal{H}'^{,g}_{si}+\mathcal{H}'^{,g}_{ae}+\mathcal{H}'^{,g}_{DM}+\mathcal{H}^g_{\rm b,1}+\mathcal{H}^g_{\rm t,1}|\nu\rangle$ to the eigenstate energies for $g=C_{4h}$, D_{4h}, C_{4v}, S_4, D_{2d}, and T_d symmetries are

$$E^g_{\nu,1} = \frac{\tilde{J}^{g,\overline{\nu}}_z}{2}[m^2-s(s+1)]-\delta\tilde{J}^{g,\overline{\nu}}_z - \frac{[3m^2-s(s+1)]}{2}\tilde{J}^{g,\overline{\nu}}_z\cos^2\theta, \quad (51)$$

$$\tilde{J}^{g,\overline{\nu}}_z = J^g_z a^+_{\overline{\nu}}-J^g_{1,z}c^-_{\overline{\nu}}-\frac{1}{2}J^g_{2,z}a^-_{\overline{\nu}}, \quad (52)$$

$$\delta\tilde{J}^{g,\overline{\nu}}_z = J^g_z b^+_{\overline{\nu}}-\frac{1}{4}J^g_{1,z}(b^+_{\overline{\nu}}+b^-_{\overline{\nu}})-\frac{1}{4}J^g_{2,z}b^-_{\overline{\nu}} + J^g_{\rm b,1}\mathcal{B}_{\overline{\nu}}+J^g_{\rm t,1}\mathcal{T}_{\overline{\nu}}, \quad (53)$$

where analytic expressions for the $a^\pm_{\overline{\nu}}$, $b^\pm_{\overline{\nu}}$, $c^\pm_{\overline{\nu}}$, $\mathcal{B}_{\overline{\nu}}$ and $\mathcal{T}_{\overline{\nu}}$ for general $\overline{\nu}$ are given in Subsection F of the Appendix, along with Tables IV-VII and VIII-XI of their simple analytic forms for the lowest four eigenstate manifolds of FM and AFM tetramers, respectively. We note that all of these interaction coefficients are invariant under $s_{13}\leftrightarrow s_{24}$, as expected. The DM and all site-dependent interactions vanish in this first-order perturbation. Second order corrections to the eigenstate energies will be presented elsewhere.[51]

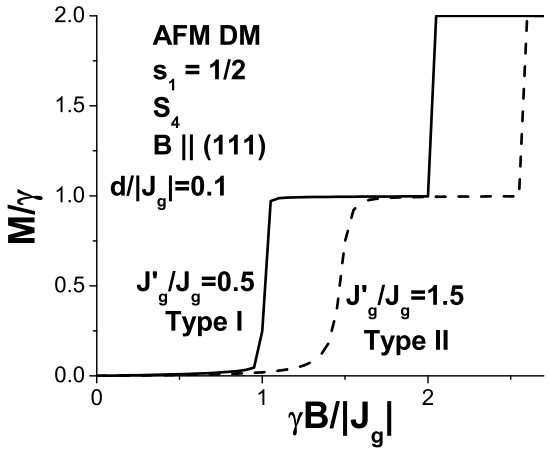

FIG. 4: Plots of the magnetization M/γ versus $\gamma B/|\tilde{J}_g|$ of an $s_1=1/2$ tetramer at $T=0$ with $c=a$, $g=S_4$, $d^g_z=d^g_{1y}=d^g_{2x}=d^g_{2y}=d$, $d^g_{1x}=0$, $d/|\tilde{J}_g|=0.1$, and $\boldsymbol{B}||(111)$. The solid and dashed curves are for the Type I ($\tilde{J}'_g/\tilde{J}_g=1.5$) and Type II ($\tilde{J}'_g/\tilde{J}_g=0.5$) tetramers, respectively.

For all six g symmetries, $E^g_{\nu,1}$ has a form analogous to that of the equal-spin dimer in the absence of azimuthal single-ion and symmetric anisotropic exchange interactions.[5] For these high-symmetry tetramers, to first order in the anisotropy interactions, the azimuthal single-ion and anisotropic exchange interactions merely renormalize the respective effective site-independent axial interactions. Thus, to first order, we only have two effective isotropic exchange, two biquadratic isotropic exchange, and three effective anisotropy interactions, $\tilde{J}_g$, $\tilde{J}'_g$, $J^g_{\rm b,1}$, $J^g_{\rm b,2}$, J^g_z, $J^g_{1,z}$, and $J^g_{2,z}$, which are fixed for a particular SMM. Nevertheless, the first-order eigenstate energies $E^g_\nu=E^g_{\nu,0}+E^g_{\nu,1}$, given by Eqs. (49) and (51), contain these seven effective interaction strengths in ways that depend strongly upon the quantum number set ν and upon θ. These different ν,θ dependencies can be employed to provide definitive measures of at least some of the seven $\overline{\nu}$-independent effective isotropic exchange and anisotropy interactions.

C. Type I and Type II tetramers

There are at least two types of FM and AFM tetramers. To the extent that single-ion, symmetric anisotropic exchange, and biquadratic exchange interactions are small relative to the Heisenberg interactions, there are just two types of tetramers. The criterion is simply based upon $\tilde{J}'_g-\tilde{J}_g$ in $\delta E^g_{\overline{\nu},0}$, which we assume to be larger in magnitude than all anisotropy and biquadratic interaction strengths. Type I tetramers have $\tilde{J}'_g-\tilde{J}_g>0$, which can occur for either sign of $\tilde{J}_g$, pro-

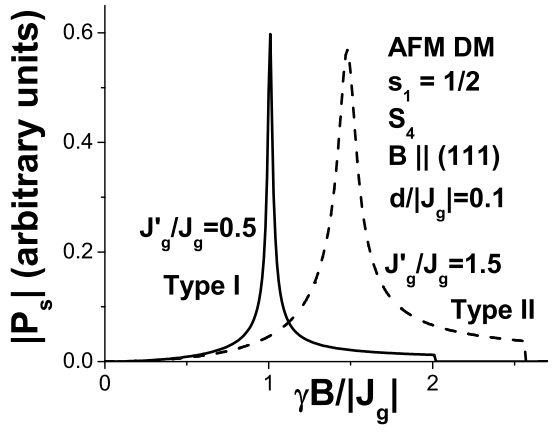

FIG. 5: Plots of the magnitude of the spin-derived polarization $|\mathbf{P}_s|$ in arbitrary units versus $\gamma B/|\tilde{J}_g|$ at $T = 0$ of an $s_1 = 1/2$ tetramer with $c = a$, $g = S_4$, $d^g_z = d^g_{1y} = d^g_{2x} = d^g_{2y} = d$, $d^g_{1x} = 0$, $d/|\tilde{J}_g| = 0.1$, and $\boldsymbol{B}||(111)$. The solid and dashed curves are for the Type I ($\tilde{J}'_g/\tilde{J}_g = 1.5$) and Type II ($\tilde{J}'_g/\tilde{J}_g = 0.5$) tetramers, respectively.

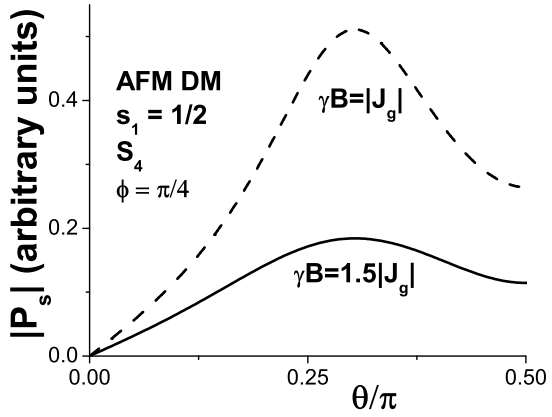

FIG. 6: Plots of the magnitude of the spin-derived polarization $|\mathbf{P}_s|$ in arbitrary units versus θ/π at $T = 0$ of an $s_1 = 1/2$ tetramer with $c = a$, $g = S_4$, $\tilde{J}'_g/\tilde{J}_g = 1$, $d^g_z = d^g_{1y} = d^g_{2x} = d^g_{2y} = d$, $d^g_{1x} = 0$, $d/J_g = 0.1$, and $\phi = \pi/4$. The solid and dashed curves are for $\gamma B/|\tilde{J}_g| = 1.5, 1$, respectively.

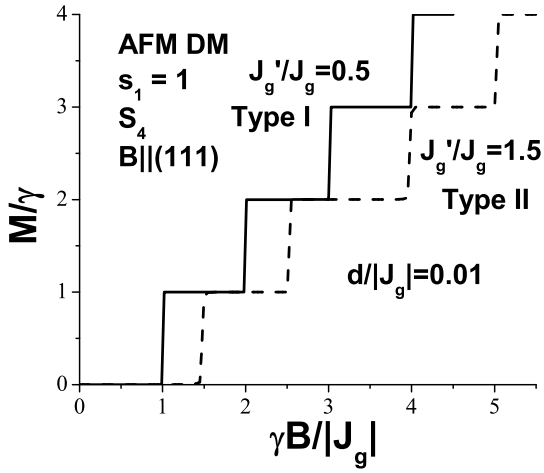

FIG. 7: Plots of the magnetization M/γ versus $\gamma B/|\tilde{J}_g|$ of an $s_1 = 1$ tetramer at $T = 0$ with $c = a$, $g = S_4$, $d^g_z = d^g_{1y} = d^g_{2x} = d^g_{2y} = d$, $d^g_{1x} = 0$, $d/|\tilde{J}_g| = 0.01$, and $\boldsymbol{B}||(111)$. The solid and dashed curves are for the Type I ($\tilde{J}'_g/\tilde{J}_g = 1.5$) and Type II ($\tilde{J}'_g/\tilde{J}_g = 0.5$) tetramers, respectively.

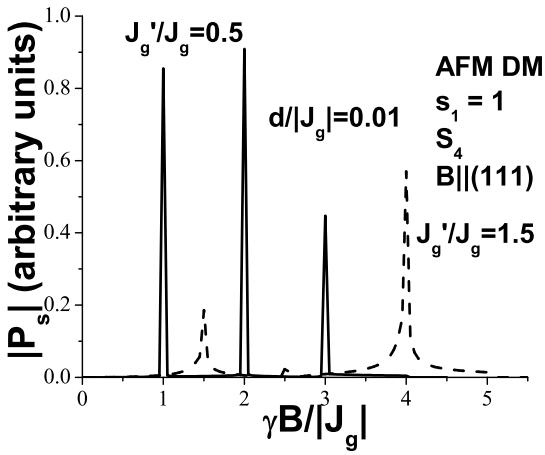

FIG. 8: Plots of the magnitude of the spin-derived polarization $|\mathbf{P}_s|$ in arbitrary units versus $\gamma B/|\tilde{J}_g|$ at $T = 0$ of an $s_1 = 1$ tetramer with $c = a$, $g = S_4$, $d^g_z = d^g_{1y} = d^g_{2x} = d^g_{2y} = d$, $d^g_{1x} = 0$, $d/|\tilde{J}_g| = 0.01$, and $\boldsymbol{B}||(111)$. The solid and dashed curves are for the Type I ($\tilde{J}'_g/\tilde{J}_g = 1.5$) and Type II ($\tilde{J}'_g/\tilde{J}_g = 0.5$) tetramers, respectively.

vided $g \neq T_d$. For Type I, the lowest energy state in each s manifold occurs for the maximum values $s_{13}, s_{24} = 2s_1$. Thus, at low T, Type I tetramers behave as pairs of spin $2s_1$ dimers. Type II tetramers with $\tilde{J}'_g - \tilde{J}_g < 0$ are frustrated, with the lowest energy state in each s manifold occurring for the minimal s_{13}, s_{24} values. For even s, these minima occur for $s_{13}, s_{24} = s/2$, but for odd s, the energy minimum is doubly degenerate, occurring at $s_{13}, s_{24} = (s \pm 1)/2, (s \mp 1)/2$. Hence, explicit formulas for first-order eigenstate energy parameters $a^{\pm}_{\overline{\nu}}$, $b^{\pm}_{\overline{\nu}}$, $c^{\pm}_{\overline{\nu}}$, and $\mathcal{B}_{\overline{\nu}}$ with arbitrary s in the three special cases of $(s_{13}, s_{24}) = (2s_1, 2s_1)$, $(s_{13}, s_{24}) = (s/2, s/2)$ for even s, and $(s_{13}, s_{24}) = [(s \pm 1)/2, (s \mp 1)/2)]$ for odd s are given in Subsections G and H of the Appendix. For sufficiently strong $\tilde{J}'_g - \tilde{J}_g$, these formulas can apply to the lowest energy eigenstate in each s manifold. When $\tilde{J}'_g - \tilde{J}_g$ is

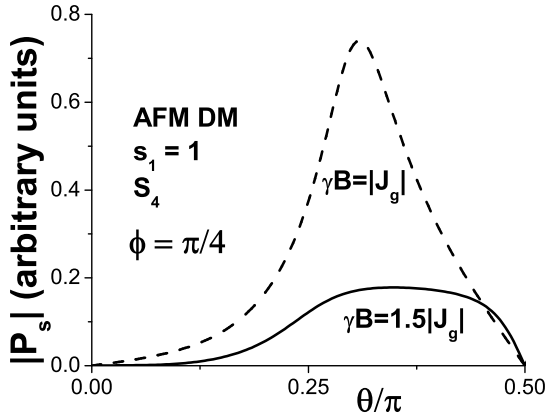

FIG. 9: Plots of the magnitude of the spin-derived polarization $|\boldsymbol{P}_s|$ in arbitrary units versus θ/π at $T = 0$ of an $s_1 = 1$ tetramer with $c = a$, $g = S_4$, $\tilde{J}'_g/\tilde{J}_g = 1$, $d^g_z = d^g_{1y} = d^g_{2x} = d^g_{2y} = d$, $d^g_{1x} = 0$, $d/J_g = 0.01$, and $\phi = \pi/4$. The solid and dashed curves are for $\gamma B/|\tilde{J}_g| = 1.5, 1$, respectively.

small relative to the other interactions, the situation becomes more complicated, as the lowest energy eigenstate for a particular $\boldsymbol{B}$ can depend upon more of the effective interaction values. Tables IV-XI in the Appendix are sufficient for full analyses of such cases for $s_1 \leq 3/2$, but such studies will be made subsequently.[51]

D. DM interactions and spin-induced polarizations

Although the first order correction to the energy arising from the DM interactions vanishes, for $s_1 = 1/2, 1$, it is not too difficult to diagonalize the Hamiltonian matrix exactly, and hence to take precise account of the effects of the DM interactions. To focus on the effects of DM interactions, in Figs. 4-9, we omit the single-ion, symmetric anisotropic exchange interactions, and biquadratic interactions, keeping only the AFM Heisenberg, Zeeman, and weak DM interactions. In Fig. 4, we plotted M/γ versus $\gamma B/|\tilde{J}_g|$ for $s_1 = 1/2$ AFM tetramers with S_4 symmetry with $\boldsymbol{B}||(111)$, $T = 0$, and $d/|\tilde{J}_g| = 0.1$, where $d^g_z = d^g_{1y} = d^g_{2x} = d^g_{2y} = d$, $d^g_{1x} = 0$, in the limit $c = a$. We note that for $\tilde{J}_g < 0$ and $\tilde{J}'_g/\tilde{J}_g = 0.5$ the magnetization exhibits sharp steps close to the integral values $s = 1, 2$ of $\gamma B/|\tilde{J}_g|$, characteristic of Type I AFM tetramers. For $\tilde{J}_g < 0$ and $\tilde{J}'_g/\tilde{J}_g = 1.5$, the two steps are shifted to higher B values, and the first step is broadened. This is Type II AFM tetramer behavior for the DM interaction. In Fig. 5, the corresponding curves for the spin-induced polarization $|\boldsymbol{P}_s|$ are shown. In both cases, there is a sharp peak at the inflection point of the first magnetization step, at which the total spin value s changes from 0 to 1. In addition, there is a discontinuity in slope at the positions of the second magnetization steps, at which $\boldsymbol{P}_s$ begins its rapid decrease to zero, which it reaches at the B value for which M just reaches saturation. Note that $\boldsymbol{P}_s \to 0$ at large B, since the large $\boldsymbol{B}$ aligns the spins at all sites, causing their vector products to vanish. Some results for the intermediate case $\tilde{J}'_g/\tilde{J}_g = 1$ are shown in Fig. 6. In this figure, we plotted $|\boldsymbol{P}_s|$ in arbitrary units versus θ/π for $s_1 = 1/2$ AFM tetramers with S_4 symmetry at $\phi = \pi/4$ with $d/|\tilde{J}_g| = 0.1$ with $\gamma B/|\tilde{J}_g| = 1.5, 1$, respectively. The curves are symmetric about $\theta = \pi/2$. We note that the curves exhibit broad maxima at $\theta/\pi \approx 0.3$ for both B values. These broad curves reflect the strong frustration of the spins with $\tilde{J}'_g = \tilde{J}_g$, for which no preferred s_{13}, s_{24} values exist.

In Figs. 7-9, we plotted analogous curves for $s_1 = 1$ tetramers, except that $d/|\tilde{J}_g| = 0.01$. Curves with $d/|\tilde{J}_g| = 0.1$ for $s_1 = 1$ exhibit steps or peaks which are much more broadened than the corresponding ones for $s_1 = 1/2$ pictured in Figs. 4-7. We note that in Fig. 7, the dashed curve for the Type II case $\tilde{J}'_g/\tilde{J}_g = 1.5$ has a wider steps at $M/\gamma = 0, 2$ than at 1,3. This low value of the DM strength $d/|\tilde{J}_g| = 0.01$ leads to very sharp peaks in $|\boldsymbol{P}_s|$ for both Type I and II tetramers, as shown in Fig. 8. However, the three peak tails are much broader for Type II tetramers with $\tilde{J}'_g/\tilde{J}_g = 1.5$ than for Type I tetramers with $\tilde{J}'_g/\tilde{J}_g = 0.5$. In each case, the peak positions correspond to the first three magnetization step $\gamma B/|\tilde{J}_g|$ values, and the polarization also vanishes at the $\gamma B/|\tilde{J}_g|$ value at which the fourth magnetization step is completed. Finally, in Fig. 9 we plotted $|\boldsymbol{P}_s|$ in arbitary units versus θ/π with the same parameters as in Fig. 6, except that $d/|\tilde{J}_g| = 0.01$. The curve with $\gamma B/|\tilde{J}_g| = 1$ has a peak at $\theta/\pi \approx 0.3$, as for the corresponding curve with $s_1 = 1/2$, but the solid curve for $\gamma B/|\tilde{J}_g| = 1.5$ has a flat region for θ/π between 0.3 and 0.45, and both curves become vanishingly small at $\theta = \pi/2$, which differs strongly from the behavior shown in Fig. 6 for $s_1 = 1/2$. This difference suggests an interesting parity effect at $\theta = \pi/2$, with $\boldsymbol{P}_s(\theta) \propto (\theta - \pi/2)^{2s_1+1}$.

E. First-order AFM level crossing inductions

For AFM tetramers, $\tilde{J}_g < 0$. There will be $2s_1+1$ level crossings, as exhibited by the magnetization steps in Figs. 4 and 7 for $s_1 = 1/2, 1$, respectively, provided that the lowest energy state in each s manifold does not exhibit level repulsion. In order to specify the level-crossing inductions, we first write $E^g_{s,m}(s_{13}, s_{24}, s_1) = E^g_{\nu,0} + E^g_{\nu,1}$. We then note that the s_{13}, s_{24} values involved in level crossings are those corresponding to the lowest energies for a particular s value. These are different for Type I and II tetramers. For Type I tetramers, the level crossing-

inductions occur for

$$E^g_{s,s}(2s_1, 2s_1, s_1) \;=\; E^g_{s-1,s-1}(2s_1, 2s_1, s_1). \quad (54)$$

and for Type II tetramers, they occur for

$$E^g_{s,s}(s/2, s/2, s_1) \;=\; E^g_{s-1,s-1}[(s-1\pm 1)/2, (s-1\mp 1)/2, s_1] \quad (55)$$

for even s, and

$$E^g_{s,s}[(s\pm 1)/2, (s\mp 1)/2, s_1] \;=\; E^g_{s-1,s-1}[(s-1)/2, (s-1)/2, s_1] \quad (56)$$

for odd s. In Subsections G and H of the Appendix, we presented the formulas for the level-crossing induction parameters for both Types I and II tetramers.

For Type I tetramers, the first-order level-crossing inductions $B^{g,\mathrm{lc}(1)}_{s_1,s}$ obtained from Eq. (54) have the remarkably simple form,

$$\gamma B^{g,\mathrm{lc}(1)}_{s_1,s}(\theta) \;=\; -s\tilde{J}_g - J^g_z\frac{b^+}{2} - J^g_{\mathrm{b},1}d - J^g_{\mathrm{t},1}e - 2J^g_{\mathrm{t},2}ss_1^2 - \frac{c_1^-}{3}\Big(J^g_{\mathrm{eff}} - \frac{(2s_1-1)}{(4s_1-1)}J^g_z\Big)(1-3\cos^2\theta), \quad (57)$$

$$J^g_{\mathrm{eff}} \;=\; \frac{J^g_{1,z}}{2} + \frac{s_1 J^g_{2,z}}{4s_1-1}, \quad (58)$$

where $b^+ = b_I^{s_1,+}(s), c_1^- = c_{I,1}^{s_1,-}(s)$, $d = d_I^{s_1}(s)$, and $e = e_I^{s_1}(s)$ are given in Subsection G of the Appendix. We note that this is independent of $\tilde{J}'_g$ and $J^g_{\mathrm{b},2}$, and that the NN and NNN symmetric anisotropic exchange interactions combine to yield the universal Type-I level crossing form J^g_{eff}. Furthermore, the θ-dependencies of the single-ion and symmetric anisotropic exchange contributions have the same s-dependencies for fixed s_1. However the θ-independent contributions from J^g_z, J^g_{eff}, and $J^g_{\mathrm{b},1}$ depend separately upon s for fixed s_1.

For the Type II AFM tetramer level-crossing inductions, the contributions from the near-neighbor anisotropic exchange interaction $J^g_{1,z}$ has a rather simple form. As shown in Subsection H of the Appendix, these contributions $\gamma B^{g,\mathrm{lc}(1)}_{1,z} = J^g_{1,z} f_{1,z}(s,\theta)$ to $\gamma B^{g,\mathrm{lc}(1)}_{s_1,s}(\theta)$ are independent of s_1, where

$$f_{1,z}(s,\theta) \;=\; \begin{cases} \frac{(s-1)}{4s}\Big(1+(2s-1)\cos^2\theta\Big), & s \text{ odd} \\ \frac{s}{4(s-1)}\Big(1+(2s-3)\cos^2\theta\Big), & s \text{ even.} \end{cases} \quad (59)$$

Note in particular that for $s = 1$, $f_{1,z}(1,\theta) = 0$. However, the single-ion and NNN symmetric anisotropic exchange contributions to the level crossing inductions depend upon both s and s_1 in different ways.

$s_1 = 1/2$ first-order AFM level crossings

For the simplest case $s_1 = 1/2$, as in AFM Cu_4 tetramers, the single-ion interaction J^g_z does not contribute to the level-crossing inductions, as for the dimer of equal $s_1 = 1/2$ spins.[5] Using the results given in Subsections G and H of the Appendix, the expressions for the $\gamma B^{g,\mathrm{lc}(1)}_{1/2,s}(\theta)$ functions are particularly simple. For $s_1 = 1/2$ effective-dimer Type I tetramers, $\tilde{J}'_g - \tilde{J}_g > 0$,

$$\gamma B^{g,\mathrm{lc}(1)}_{1/2,1}(\theta) \;=\; -\tilde{J}_g + \frac{1}{2}(J^g_{\mathrm{b},1} - J^g_{\mathrm{t},2}) + \frac{1}{6}J^g_{\mathrm{eff}}(1-3\cos^2\theta), \quad (60)$$

$$\gamma B^{g,\mathrm{lc}(1)}_{1/2,2}(\theta) \;=\; -2\tilde{J}_g + J^g_{\mathrm{b},1} - J^g_{\mathrm{t},2} - \frac{1}{2}J^g_{\mathrm{eff}}(1-3\cos^2\theta), \quad (61)$$

where J^g_{eff} is given by Eq. (58) with $s_1 = 1/2$. For frustrated Type II tetramers with $s_1 = 1/2$, $\tilde{J}_g - \tilde{J}'_g > 0$,

$$\gamma B^{g,\mathrm{lc}(1)}_{1/2,1}(\theta) \;=\; -\tilde{J}'_g - \frac{1}{4}(3J^g_{\mathrm{b},1} - J^g_{\mathrm{t},1}) + \frac{J^g_{\mathrm{b},2}}{2} + \frac{1}{4}J^g_{2,z}(1+\cos^2\theta), \quad (62)$$

$$\gamma B^{g,\mathrm{lc}(1)}_{1/2,2}(\theta) \;=\; -\tilde{J}_g - \tilde{J}'_g + \frac{5}{4}(J^g_{\mathrm{b},1} - J^g_{\mathrm{t},1}) + \frac{1}{2}(J^g_{\mathrm{b},2} - J^g_{\mathrm{t},2}) + \frac{1}{4}\Big(2J^g_{1,z} + J^g_{2,z}\Big)(1+\cos^2\theta). \quad (63)$$

Even in this simplest of all tetramer cases, there is still a qualitative difference between the level crossing inductions of Type I and Type II AFM $s_1 = 1/2$ tetramers. For Type I, there is only one effective anisotropic exchange interaction, $J^g_{\mathrm{eff}} = (J^g_{1,z} + J^g_{2,z})/2$ that affects the level crossing. However, for Type II $s_1 = 1/2$ tetramers, the level crossing is different for the NN and NNN anisotropic exchange interactions. The only effect of the group symmetry is to provide restrictions upon the values of the interactions. These expressions also show that Type II AFM tetramers have a more complex level-crossing induction variation than do Type I AFM tetramers, as the first-order Type I level-crossing behavior is fully described by three parameters, whereas the first-order Type II level-crossing behavior depends upon four independent parameters. On the other hand, for this special $s_1 = 1/2$ example, the θ dependencies of the first and second $\gamma B^{g,\mathrm{lc}(1)}_{1/2,s}$ are opposite in sign for Type I, but can have the same sign for Type II. In Fig. 10, we illustrate these $s_1 = 1/2$ behaviors for the Type I with $J^g_{\mathrm{eff}}/\tilde{J}_g = 0.2$ and for Type II with $J^g_{2,z}/\tilde{J}_g = 0.2$ and $\tilde{J}_g - \tilde{J}'_g = 0.5|\tilde{J}_g|$.

In the special case of T_d symmetry, we have $\tilde{J}_{T_d} = \tilde{J}'_{T_d} = J$, $J^{T_d}_{\mathrm{b},1} = J^{T_d}_{\mathrm{b},2} = J_b$, $J^{T_d}_{\mathrm{t},1} = J^{T_d}_{\mathrm{t},2} = J_b t$, and

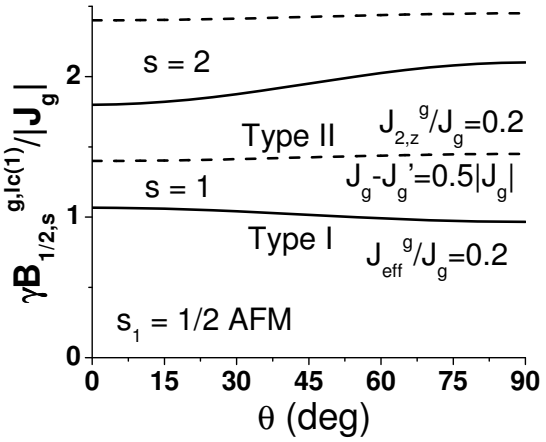

FIG. 10: Plots of the $s_1 = 1/2$ first-order level-crossing $\gamma B^{g,\mathrm{lc}(1)}_{1/2,s}(\theta)/|\tilde{J}_g|$, where θ is the angle between $\boldsymbol{B}$ and $\hat{\boldsymbol{z}}$, with $J^g_{\mathrm{b,q}} = 0$, $J^g_{\mathrm{eff}}/\tilde{J}_g = 0.2$, $\tilde{J}'_g - \tilde{J}_g > 0$ (solid, Type I) and $J^g_{2,z}/\tilde{J}_g = 0.2$, $\tilde{J}_g - \tilde{J}'_g = 0.5|\tilde{J}_g|$ (dashed, Type II).

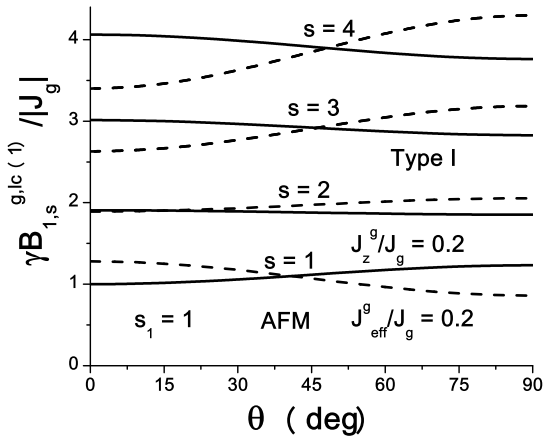

FIG. 11: Plots of the first-order level-crossing $B^{g,\mathrm{lc}(1)}_{1,s}(\theta)/|\tilde{J}_g|$ for Type I, $\tilde{J}_g - \tilde{J}'_g < 0$, $J^g_{\mathrm{b,q}} = 0$, and $s_1 = 1$. Solid curves: $J^g_z/\tilde{J}_g = 0.2$. Dashed curves: $J^g_{\mathrm{eff}}/\tilde{J}_g = 0.2$.

$J^{T_d}_{q,z} = 0$. Since for $s_1 = 1/2$, $\mathcal{H}^g_b$ and $\mathcal{H}^g_t$ are diagonal, the J_b and J_t dependencies of the eigenstate energies are exact. Hence, the only difference between Type I and Type II $s_1 = 1/2$ tetramers with T_d symmetry is determined by the sign of $J_b - J_t$, as is evident by comparing Eqs. (60)-(63). In any event, there is no θ dependence to the first-order level-crossing inductions for $s_1 = 1/2$ AFM tetramers with T_d symmetry.

$s_1 \geq 1$ *first-order AFM level crossings*

For $s_1 > 1/2$, the AFM level-crossings become much more complex than for the $s_1 = 1/2$ case, as single-ion anisotropies J^g_z are allowed, and the biquadratic interactions $J^g_{\mathrm{b},q}$ affect the various level-crossings differently. We first consider the simplest $s_1 > 1/2$ case, $s_1 = 1$, appropriate for AFM Ni_4 tetramers. Exact expressions for the $s = 1, 2, 3, 4$ first-order level-crossing inductions $B^{g,\mathrm{lc}(1)}_{1,s}(\theta)$ for Type I and II $s_1 = 1$ tetramers are given in Subsection F of the Appendix. In Figs. 11 and 12, we plotted the θ-dependence of the first-order level crossing induction $\gamma B^{g,\mathrm{lc}(1)}_{1,s}(\theta)/|\tilde{J}_g|$ for $g = C_{4h}, D_{4h}, C_{4v}, S_4$, and D_{2d}, for two AFM Type I examples and for three Type II examples with $\tilde{J}_g - \tilde{J}'_g = 0.5|\tilde{J}_g|$, respectively. In each curve, we allow only one of the anisotropy interactions (or effective interactions) to be non-vanishing. In Fig. 11, the solid and dashed curves are for $J^g_z/\tilde{J}_g = 0.2$ and $J^g_{\mathrm{eff}}/\tilde{J}_g = 0.2$, respectively, where $J^g_{\mathrm{eff}} = J^g_{1,z}/2 + J^g_{2,z}/3$ for $s_1 = 1$. We note from Eq. (57) and from Fig. 11 that for Type I, the single-ion and symmetric exchange anisotropies lead to opposite θ-dependencies, both having a change in sign just before the second level crossing, and the dependence of $\gamma B^{g,\mathrm{lc}(1)}_{1,s}$ upon $J^g_{\mathrm{b},1}$ decreases with increasing s.

In Fig. 12, we illustrate the $s_1 = 1$ Type II level crossings, setting $\tilde{J}_g - \tilde{J}'_g = 0.5|\tilde{J}_g|$. The solid curves are for $J^g_z/\tilde{J}_g = 0.2$ for $g = C_{4h}, D_{4h}, C_{4v}, S_4$, and D_{2d}, as in Fig. 11. The dashed and dotted curves are for $J^g_{1,z}/\tilde{J}_g = 0.4$ and $J^g_{2,z}/\tilde{J}_g = 0.4$, respectively. For each curve, the Type II isotropic exchange parameters lead to a larger gap between the $s = 2$ and $s = 3$ level crossings. The sign of the θ-dependencies of the single-ion (solid) curves changes between $s = 2$ and $s = 3$. The effects of the NN symmetric anisotropic exchange interactions vanish for $s = 1$, but increase in magnitude with increasing s for $s = 2, 3, 4$. The sign of the θ-dependence of the level crossing due to the NNN symmetric anisotropic exchange interactions does not change, but its magnitude increases monotonically. Thus, Type II AFM $s_1 = 1$ tetramers have a richer set of first-order level-crossing behaviors than do Type I AFM $s_1 = 1$ tetramers, and the unpictured biquadratic interactions increase this richness.

In Figs. 13 and 14, the analogous Type I and Type II first-order AFM level crossing inductions are plotted versus θ for $s_1 = 3/2$ equal-spin tetramers, such as Cr_4. The notation is the same as in Figs. 11 and 12. For Type I $s_1 = 3/2$ AFM tetramers, the single-ion and symmetric anisotropic exchange interactions lead to different θ-dependencies of the level-crossing inductions, each with a change in sign in the θ dependence at about the second level crossings, as seen in Fig. 13. For Type II $s_1 = 3/2$ AFM tetramers, the sign changes appear between the second and third level crossings, as shown in Fig. 14. Although not pictured, the contributions for $s_1 = 3/2$ to the level-crossing inductions from the $J^g_{\mathrm{b,q}}$ can be easily

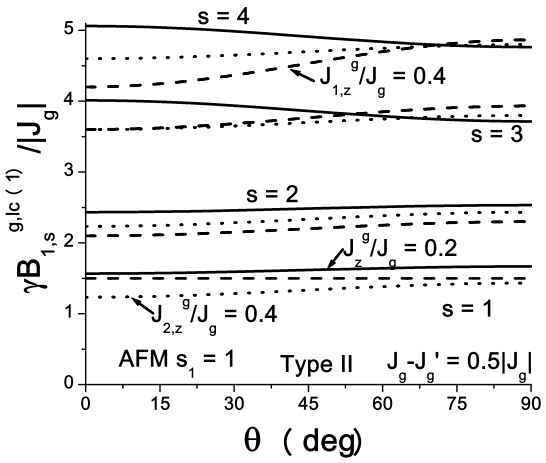

FIG. 12: Plots of the first-order level-crossing $\gamma B^{g,\mathrm{lc}(1)}_{1,s}(\theta)/|\tilde{J}_g|$ for Type II with $g = C_{4h}, D_{4h}, C_{4v}, S_4, D_{2d}$, $\tilde{J}_g - \tilde{J}'_g = 0.5|\tilde{J}_g|$, $J^g_{\mathrm{b,q}} = 0$, and $s_1 = 1$. Solid curves: $J^g_z/\tilde{J}_g = 0.2$. Dashed curves: $J^g_{1,z}/\tilde{J}_g = 0.4$. Dotted curves: $J^g_{2,z}/\tilde{J}_g = 0.4$.

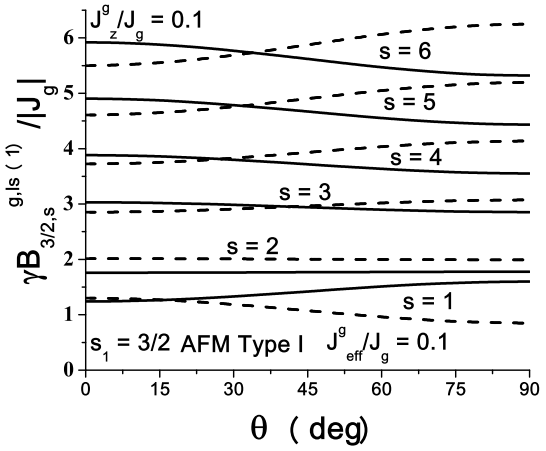

FIG. 13: Plots of the first-order level-crossing $\gamma B^{g,\mathrm{lc}(1)}_{3/2,s}(\theta)/|\tilde{J}_g|$ for Type I, $\tilde{J}_g - \tilde{J}'_g < 0$, $J^g_{\mathrm{b,q}} = 0$, and $s_1 = 3/2$. Solid curves: $J^g_z/\tilde{J}_g = 0.1$. Dashed curves: $J^g_{\mathrm{eff}}/\tilde{J}_g = 0.1$.

calculated from Eq. (50) and the expressions for $d^{3/2}_{IIo}(s)$ and $d^{3/2}_{IIe}(s)$ in Subsection H of the Appendix. They contribute to a more complex level-crossing pattern than for $s_1 = 1$.

For $g = T_d$ with $s_1 > 1/2$, we still have $J^g_{q,z} = J^g_z = 0$, so that the first-order level-crossing inductions $\gamma B^{T_d,\mathrm{lc}(1)}_{s_1,s}(\theta)/|\tilde{J}_{T_d}|$ vary from integral values only by θ-independent constants due to the biquadratic interaction

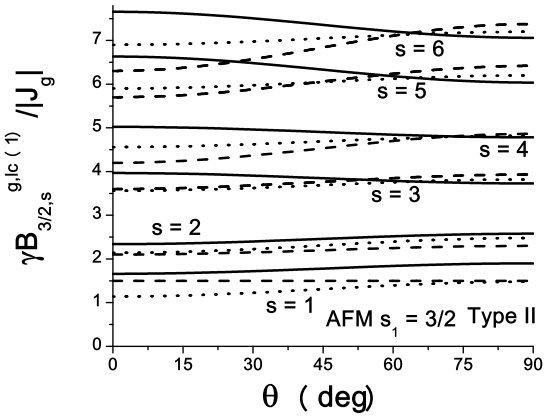

FIG. 14: Plots of the first-order level-crossing $\gamma B^{g,\mathrm{lc}(1)}_{3/2,s}(\theta)/|\tilde{J}_g|$ for Type II with $g = C_{4h}, D_{4h}, C_{4v}, S_4, D_{2d}$, $\tilde{J}_g - \tilde{J}'_g = 0.5|\tilde{J}_g|$, $J^g_{\mathrm{b,q}} = 0$, and $s_1 = 3/2$. Solid curves: $J^g_z/\tilde{J}_g = 0.2$. Dashed curves: $J^g_{1,z}/\tilde{J}_g = 0.4$. Dotted curves: $J^g_{2,z}/\tilde{J}_g = 0.4$.

$J^{T_d}_{\mathrm{b},1} = J^{T_d}_{\mathrm{b},2}$.

VII. THE SELF-CONSISTENT HARTREE APPROXIMATION

A. Partition function and thermodynamics

The self-consistent Hartree approximation, or strong exchange limit,[37] provides accurate results for the $\boldsymbol{B}$ dependence of the specific heat and magnetization at low $k_BT/|\tilde{J}_g|$ and $\gamma B/|\tilde{J}_g|$ not too small,[5] where k_B is Boltzmann's constant. In this approximation, $E^g_\nu = E^g_{\nu,0} + E^g_{\nu,1}$ is given by Eqs. (49) and (51), respectively. We shall present the self-consistent Hartree approximation of four measurable quantities in the induction representation. We first define the trace valid for our eiqenstate representation,

$$\mathrm{Tr}_\nu \equiv \sum_\nu = \sum_{s_{13},s_{24}=0}^{2s_1} \sum_{m=-s}^{s} \sum_{s=|s_{13}-s_{24}|}^{s_{13}+s_{24}}, \qquad (64)$$

The partition function in the self-consistent Hartree approximation may then be written

$$Z^{(1)}_g = \mathrm{Tr}_\nu e^{-\beta E^g_\nu}, \qquad (65)$$

where $\beta = 1/(k_BT)$. In this compact notation, the self-consistent Hartree magnetization $M^{(1)}_g(\boldsymbol{B},T)$ and specific heat $C^{(1)}_{g,V}(\boldsymbol{B},T)$ are given by

$$M^{(1)}_g(\boldsymbol{B},T) = \gamma \mathrm{Tr}_\nu \Big(m e^{-\beta E^g_\nu} \Big) / Z^{(1)}_g, \qquad (66)$$

$$\frac{C^{(1)}_{g,V}(\boldsymbol{B},T)}{k_B\beta^2} = \frac{\mathrm{Tr}_\nu\Big(\big(E^g_\nu\big)^2 e^{-\beta E^g_\nu}\Big)}{Z^{(1)}_g} - \Big[\frac{\mathrm{Tr}_\nu\Big(E^g_\nu e^{-\beta E^g_\nu}\Big)}{Z^{(1)}_g}\Big]^2. \quad (67)$$

We note that there are strong differences between the low-T behavior of FM and AFM tetramers. We assume $|\tilde{J}_g| > |\tilde{J}'_g - \tilde{J}_g|$. For FM tetramers with $\tilde{J}_g > 0$, the low-T thermodynamic behavior is dominated by the $s = 4s_1$, $m = -4s_1$ state, leading to

$$M^{(1)}_g(\boldsymbol{B},T) \overset{\approx}{_{T\to 0}} \gamma\hat{\boldsymbol{B}}\mathcal{B}_{4s_1}(\beta\gamma B), \quad (68)$$

where $\mathcal{B}_S(x)$ is the Brillouin function. The universality of this function renders thermodynamic studies useless for the determination of the microscopic parameters. For AFM tetramers with $\tilde{J}_g < 0$, however, there will be interesting level-crossing effects, which can be employed to measure the microscopic interaction parameters, as discussed in detail in Sec. V. As for dimers, $C_V(B,T)$ for AFM tetramers at sufficiently low T exhibit $2s_1$ central minima at the level-crossing inductions $B^{g,\mathrm{lc}}_{s_1,s}(\theta) \approx B^{g,\mathrm{lc}(1)}_{s_1,s}(\theta)$ that vanish as $T \to 0$, equally surrounded by peaks of equal height.[5] As for the magnetization, $C_V(B,T)$ for FM tetramers at low T reduces to that of a monomer with spin $4s_1$, yielding a rather uninteresting Schottky anomaly.

B. Electron paramagnetic resonance

However, the microscopic nature of FM tetramers can be better probed either by EPR or INS techniques. The self-consistent Hartree EPR absorption $\Im\chi^{g,(1)}_{-\sigma,\sigma}(\boldsymbol{B},\omega)$ for clockwise ($\sigma = 1$) or counterclockwise ($\sigma = -1$) circularly polarized oscillatory fields normal to $\boldsymbol{B}$ is

$$\Im\chi^{g,(1)}_{-\sigma,\sigma} = \frac{\gamma^2}{Z^{(1)}_g}\mathrm{Tr}_\nu\mathrm{Tr}_{\nu'}e^{-\beta E^g_\nu}\big|M_{\nu,\nu'}\big|^2 \times\big[\delta(E^g_\nu - E^g_{\nu'} + \omega) - \delta(E^g_{\nu'} - E^g_\nu + \omega)\big], \quad (69)$$

where $M_{\nu,\nu'} = A^{\sigma m}_s\delta_{m',m+\sigma}\delta_{s',s}\delta_{s'_{13},s_{13}}\delta_{s'_{24},s_{24}}$ and $\mathrm{Tr}_{\nu'} = \sum_{\nu'}$. The strong resonant inductions appear at

$$\gamma B^{g,(1)}_{\mathrm{res}} = \pm\omega + \frac{(2m+\sigma)}{2}(1 - 3\cos^2\theta)\tilde{J}^{g,\overline{\nu}}_z, \quad (70)$$

where $\tilde{J}^{g,\overline{\nu}}_z$ is given by Eq. (52) We note that $\tilde{J}^{g,\overline{\nu}}_z$ contains the three effective microscopic interactions, J^g_z, $J^g_{1,z}$, and $J^g_{2,z}$, multiplied by the constants $a^+_{\overline{\nu}}$, $-c^-_{\overline{\nu}}$, and $-a^-_{\overline{\nu}}/2$, respectively. In Tables IV and VI of Subsection F of the Appendix, the values of these parameters for the FM ground state and the first three excited state manifolds for arbitrary s_1 are given. We note that EPR measurements are insensitive to the Heisenberg and biquadratic exchange interactions, which preserve m.

For either FM or AFM $s_1 = 1/2$ tetramers, EPR measurements can only probe the two microscopic symmetric anisotropic exchange interaction parameters $J^g_{1,z}$ and $J^g_{2,z}$, and measurements of the two $s = 1$ excited states are sufficient to determine them. For FM tetramers with $s_1 \geq 1$, it is a bit more difficult. From Tables IV and VI and from Eq. (219) in Subsection G of the Appendix, it is easily seen that the $(s, s_{13}, s_{24}) = (s, 2s_1, 2s_1)$ states all provide measurements of the same combination of these three microscopic interactions. Hence, for FM tetramers with $s_1 > 1/2$, measurements of the ground $s = 4s_1$ and the first excited state manifold with $s = 4s_1 - 1$ are insufficient to completely determine the three microscopic interactions. In order to stay within a single s value for FM tetramers, one would need to study the second (or higher) excited state manifold with $s = 4s_1 - 2$ (or lower), in order to obtain sufficient information to determine the three microscopic interaction strengths. For AFM tetramers with $s_1 \geq 1$, EPR transitions in the ground state are not allowed, but measurements of the first excited $s = 1$ state manifold would suffice to determine J^g_z and the $J^g_{q,z}$, as seen from the formulas in Tables VIII and X in the Appendix.

C. Inelastic neutron scattering

The Hartree INS cross-section $S^{(1)}_g(\boldsymbol{B},\boldsymbol{q},\omega)$ is

$$S^{(1)}_g = \mathrm{Tr}_\nu\mathrm{Tr}_{\nu'}e^{-\beta E^g_\nu}\sum_{\tilde{\alpha},\tilde{\beta}}\big(\delta_{\tilde{\alpha},\tilde{\beta}} - \hat{q}_{\tilde{\alpha}}\hat{q}_{\tilde{\beta}}\big)\sum_{n,n'} \times e^{i\boldsymbol{q}\cdot(\boldsymbol{r}_n - \boldsymbol{r}_{n'})}\langle\nu|S^\dagger_{n',\tilde{\alpha}}|\nu'\rangle\langle\nu'|S_{n,\tilde{\beta}}|\nu\rangle \times\delta(\omega + E^g_\nu - E^g_{\nu'}), \quad (71)$$

where $\tilde{\alpha},\tilde{\beta} = \tilde{x},\tilde{y},\tilde{z}$, $\hat{q}_{\tilde{x}} = \sin\theta_{b,q}\cos\phi_{b,q}$, $\hat{q}_{\tilde{y}} = \sin\theta_{b,q}\sin\phi_{b,q}$, and $\hat{q}_{\tilde{z}} = \cos\theta_{b,q}$, $\theta_{b,q}$ and $\phi_{b,q}$ describe the relative orientations of $\boldsymbol{B}$ and $\boldsymbol{q}$,[5] the $\boldsymbol{r}_n$ are given by Eq. (1), and the $\langle\nu'|S_{n,\tilde{\alpha}}|\nu\rangle$ are given by Eqs. (164) and (165) in Subsection E of the Appendix. The scalar $\boldsymbol{q}\cdot(\boldsymbol{r}_n - \boldsymbol{r}_{n'})$ is invariant under the rotation, Eq. (40). After some algebra, we rewrite $S^{(1)}_g(\boldsymbol{q},\omega)$ as

$$S^{(1)}_g = \mathrm{Tr}_\nu e^{-\beta E^g_\nu}\sum_{\nu'}\delta(\omega + E^g_\nu - E^g_{\nu'}) \times\Big(\sin^2\theta_{b,q}L_{\nu,\nu'}(\boldsymbol{q}) + \frac{(2-\sin^2\theta_{b,q})}{4}M_{\nu,\nu'}(\boldsymbol{q})\Big), \quad (72)$$

where the Hartree functions $L_{\nu,\nu'}(\boldsymbol{q})$ and $M_{\nu,\nu'}(\boldsymbol{q})$ are given in Subsection I of the Appendix. They are independent of $\boldsymbol{B}$. Since E^g_ν is well-behaved as $\boldsymbol{B} \to 0$, Eq. (72) is accurate for all $\boldsymbol{B}$.

As for the dimer,[5] additional EPR and INS transitions with amplitudes higher order in the anisotropy parameters J_z^g, $J_{1,z}^g$, and $J_{2,z}^g$ relative to $\tilde{J}_g$ are obtained in the extended Hartree approximation, but will be presented elsewhere for brevity.[51]

VIII. DISCUSSION

The quadratic phenomenological total spin anisotropy model widely used in fitting experimental data on SMM's is

$$\mathcal{H}_p \;=\; \mathcal{A} - \mathcal{D}S_z^2 - \mathcal{E}(S_x^2 - S_y^2), \tag{73}$$

where $\mathcal{A}$ represents the isotropic total spin interactions, and $\mathcal{D}$ and $\mathcal{E}$ are measures of the axial and azimuthal total spin anisotropy, respectively.[1] Often, additional quartic terms are added.[22, 52] The anisotropy is defined relative to the total spin principal axes, which for equal spin, high-symmetry systems are the molecular axis vectors. It is easy to evaluate $E_\nu^p = \langle\nu|\tilde{\mathcal{H}}_p|\nu\rangle$ in the induction representation. One obtains Eqs. (49) and (51), provided that

$$\mathcal{A} \;=\; \mathcal{A}_0 + \delta\mathcal{A}, \tag{74}$$

$$\mathcal{A}_0 \;=\; -\tilde{J}_g s(s+1)/2 - \gamma B m, \tag{75}$$

$$\delta\mathcal{A} \;=\; \delta E_{\overline{\nu},0}^g - \delta\tilde{J}_z^{g,\overline{\nu}}, \tag{76}$$

$$\mathcal{D} \;=\; \tilde{J}_z^{g,\overline{\nu}}, \tag{77}$$

$$\mathcal{E} \;=\; 0, \tag{78}$$

where $\delta E_{\overline{\nu},0}^g$, $\tilde{J}_z^{g,\overline{\nu}}$ and $\delta\tilde{J}_z^{g,\overline{\nu}}$ are given by Eqs. (50), (52) and (53), respectively, which contain the constants $a_{\overline{\nu}}^{\pm}$, $b_{\overline{\nu}}^{\pm}$, $c_{\overline{\nu}}^{\pm}$, and $\mathcal{B}_{\overline{\nu}}$. Precise formulas for arbitrary $\overline{\nu}$ appear in Subsection F of the Appendix, along with Tables IV-XI of their values for arbitrary s_1 in the ground and lowest three excited state manifolds for FM and AFM tetramers, respectively. Usually, one assumes the strong exchange limit, so that the isotropic $\mathcal{A}_0$ is sufficiently large that it remains constant for $B = 0$, and can be neglected. A non-vanishing $\mathcal{E}$ would lead to a term in Eq. (51) proportional to $\sin^2\theta\cos(2\phi)$, as for the dimer,[5] which does not arise in the first-order calculation for the high-spin tetramers under consideration, based upon the microscopic parameters alone. Hence, the $\mathcal{D}$ term in $\mathcal{H}_p$ alone describes the θ and m dependencies of $E_{\nu,0}^g + E_{\nu,1}^g$ correctly, provided that the quantum numbers s_{13} and s_{24} remain constant.

More important, the additional constant term $\delta\mathcal{A}$ has generally been neglected. Even to zeroth order, the sign of $\tilde{J}_g - \tilde{J}_g'$ in $\delta E_{\overline{\nu},0}^g$ distinguishes between Type I and Type II tetramers, which distinction is absent in the phenomenological model. Moreover the different first-order dependencies of $\mathcal{A}$ and $\mathcal{D}$ upon the $\overline{\nu}$ are important in determining the level-crossing inductions for AFM tetramers, each of which involves two values of s and m, and hence different s_{13} and s_{24} values, as well. The zero-field energy spectrum is thus more complicated than that given by the usual phenomenological model, which could lead to substantially different fits to experiment.

For simplicity, the only higher order interactions we have considered are the isotropic NN and NNN biquadratic exchange interactions. These isotropic interactions are rotationally invariant, so they are independent of θ in the induction representation. Hence, they only contribute to δA. Thus they modify the positions but not the θ-dependencies of the AFM level-crossing inductions, and do not modify any EPR transitions.

In the ground state of FM tetramers, $\overline{\nu}$ is restricted to the single set of values, $(s, s_{13}, s_{24}) = (4s_1, 2s_1, 2s_1)$. In this high-spin case, $\mathcal{H}_p$ can provide a correct phenomenology of the ground state energy. However, if applied to the two low-lying excited states with $s = 4s_1 - 1$, for instance, one would infer two different $\mathcal{A}$ and $\mathcal{D}$ values from those obtained in the ground state. However, as noted above, since all states with $(s_{13}, s_{24}) = (2s_1, 2s_1)$ contain the same combination of $a_{\overline{\nu}}^{\pm}$ and $c_{\overline{\nu}}^{-}$, in order to exploit the $\overline{\nu}$ dependence of $\mathcal{D}$ to obtain an unambiguous EPR measurement of the three microscopic parameters $J_z^g, J_{1,z}^g$, and $J_{2,z}^g$, for $s_1 > 1/2$, one needs to examine higher state manifolds, such as the manifold with $s = 4s_1 - 2$. For AFM tetramers, $\mathcal{H}_p$ also correctly provides a vanishing first-order correction to the $s = 0$ manifold of states with $s_{13} = s_{24} = 0, 1, \ldots, 2s_1$. However, $\mathcal{H}_p$ also has problems describing the first excited manifold of AFM states with $s = 1$, because it leads to the choice of $\delta\mathcal{A}$ independent of the quantum numbers $\overline{\nu}$, which is unphysical except for tetramers with T_d symmetry. Hence, the phenomenological model works best in describing only a single state with fixed (s, s_{13}, s_{24}). This is more restrictive than the usual assumption of its applicability to all states with fixed s.[18, 52, 53, 54, 55]

We note that the FM Cu_4 tetramer $Cu_4OCl_6(TPPO)_6$ was claimed to have T_d symmetry and an $s = 2$ ground state.[12, 13, 14] It is noteworthy that those authors thought that anisotropic exchange interactions might be responsible for their observed zero-field energy splittings.[12, 15] Since tetramers with T_d symmetry do not have either symmetric or antisymmetric anisotropic exchange interactions, another explanation must be considered. From Tables IV-VII in the Appendix, it is evident that the FM ground state is non-degenerate for all s_1, even for those SMM's with lower symmetries allowing anisotropic exchange interactions. It therefore appears that the sample may not have been single-phase,[12, 13, 14] as in a nominally S_4 Ni_4 tetramer,[22] allowing for an apparent ground state splitting.

We note that for the FM Fe_4 SMM, $Fe_4(thme)_2(dpm)_6$, where H_3thme is 1,1,1-tris(hydroxymethyl)ethane and Hdpm is dipivaloylmethane,[52, 53, 54] the high D_3 symmetry also precludes the $\mathcal{E}$ term in $\mathcal{H}_p$. Nevertheless,

in fits to INS data, it was assumed that $\mathcal{E} \neq 0$,[52, 55] in order to obtain the appropriate anticrossing gaps, so that either the powdered sample did not have pure D_3 symmetry, or the phenomenological model they used, Eq. (73) plus two quartic terms obeying D_3 symmetry, was not appropriate. Since single-ion interactions appeared to be important,[52] the total spin might not have been a well-defined quantum number, as in at least one Fe_2 dimer and in Fe_8.[5, 6, 8, 9] However, we note that it might be interesting to investigate whether second-order DM effects might yield an effective finite $\mathcal{E}$ value.

Using a microscopic Hamiltonian, detailed fits to the four magnetization step data obtained in large pulsed fields on powder samples of the AFM Ni_4 tetramer $[Mo^V_{12}O_{30}(\mu_2\text{-OH})_{10}H_2\{Ni^{II}(H_2O)_3\}_4]$, or $\{Ni_4Mo_{12}\}$ were presented.[46] Although the molecule has C_{1v} symmetry, it is close to exhibiting C_{3v} symmetry. Since the steps were unevenly spaced, the authors assumed the molecule to have weak, but important biquadratic interactions. To limit the number of fitting parameters, they assumed C_{3v} symmetry for the Heisenberg and biquadratic interactions, and T_d symmetry for the single-ion and anisotropic exchange interactions. In addition, they allowed the two Heisenberg interaction strengths to have strong magnetic field dependencies. Subsequently, magnetoinfrared studies of that compound were made, revealing only very small differences in the responses at $B = 0$ and 14 T,[61] providing little, if any justification for such strong magnetic field dependencies of the Heisenberg interaction strengths.

More recently, a remarkably simple fit to the four level-crossing midpoints was made by Kostyuchenko.[50] In this fit, the $\{Ni_4Mo_{12}\}$ molecule was assumed to have T_d symmetry, so that $\tilde{J}_g = \tilde{J}'_g = -J$, and a convincing argument was presented that the strength $-J_3$ of the isotropic three-center quartic interactions ought to be comparable in magnitude to that $(-J_2)$ of the biquadratic interactions. Since each of these terms preserves the s quantum number, the Hamiltonian matrix in the absence of single-ion and anisotropic exchange interactions is block diagonal, and for $s_1 = 1$, it is possible to obtain the exact eigenvalues in terms of the three parameters J, J_2, J_3. However, in his fit to the magnetization level crossing midpoint data on $\{Ni_4Mo_{12}\}$, he found $J_2 = J_3$, which implies that he claimed to fit the four linear equations for the four level crossing midpoints with two parameters. Although two of those equations were nearly degenerate, three were clearly non-degenerate, rendering his two-parameter fit inappropriate.

In Subsection F of the Appendix, we extended the calculation of Kostyuchenko to the five lower symmetries, so that there are six isotropic interactions $\tilde{J}_g, \tilde{J}'_g, J^g_{\mathrm{b},q}$, and $J^g_{\mathrm{t},1q}$ for $q = 1, 2$. In the limit investigated by Kostyuchenko, $\tilde{J}_g = \tilde{J}'_g = -J$, $J^g_{\mathrm{b},1} = J^g_{\mathrm{b},2} = -J_2$, and $J^g_{\mathrm{t},1} = J^g_{\mathrm{t},2} = -J_3$, our results agree with those of Kostyuchenko for the $s = 4$ and $s = 0$ states, and one each of the $s = 2$ and $s = 3$ states. However, our results do not agree with his for the other $s = 1, 2, 3$ states, except for the special case $J_2 = J_3$, which is what he claimed to have obtained in his inappropriate fit.[50] Although Kostyuchenko presented no details of his calculations, and provided no reference to the matrix elements, in Subsection F of the Appendix, we provided the explicit details of our calculations. We note that his fit assumed no widths to each level crossings. Although this is essentially correct for the first two level crossings, it is certainly not true for the third and fourth level crossings.[46]

Even if one takes the correct forms for the eigenstate energies with T_d symmetry (neglecting the second order single-ion anisotropy contributions) given in the appendix, one still has to solve four equations with the three parameters J, J_2, and J_3. In the case that there might be an accidental remaining degeneracy, we have tried to do this. We first assumed $J_2 \geq J_3$, but no consistent solution to the four level-crossing equations could be found. We then assumed $J_3 > J_2$. In this case, the minimum energies are $E_0 = 16J_2 - 8J_3$, E_{1-}, $E_2 = 3J + \frac{39}{4}J_2 - \frac{31}{4}J_3$, $E_3 = 6J + \frac{61}{9}J_2 - \frac{7}{9}J_3$, and $E_4 = 10J + 6J_2 + 12J_3$, where $E_{1-} = J + \frac{87}{8}J_2 - \frac{31}{8}J_3 - \frac{1}{24}\sqrt{(91J_3 - 75J_2)^2 + 320(3J_2 - 4J_3)^2}$. In this case, the square root appears in the equations for the first and second level crossings, so that we add those two equations to obtain three linear equations in the three unknowns. Solving these three unknowns, we then find

$$J/k_B = 7.511\mathrm{K}, \tag{79}$$

$$J_2/k_B = 0.7637\mathrm{K}, \tag{80}$$

$$J_3/k_B = 0.9665\mathrm{K}. \tag{81}$$

These results necessarily fit the midpoints of the third and fourth level crossings precisely. Now, substituting these values into the equations for the first and second level crossings, we obtain 4.35 T and 9.05 T, which are in remarkably good agreement with the experimental values of 4.5 T and 8.9T, respectively. Hence, although Kostyuchenko didn't obtain a correct set of formulas or a correct fit, his idea that the three-center terms could be important is valid.[50] It is remarkable that one is able to a good fit to four level-crossings with only three parameters. Nevertheless, these parameters do not give rise to any widths to the transitions, unlike the experiments.[46]

In Subsection F of the Appendix, we listed the Type-I and Type-II first-order level crossing inductions for $s_1 = 1$ AFM tetramers quantization scheme is appropriate for C_{1v} symmetry, the number of independent parameters for that low symmetry is very large. Nevertheless, one can quantitatively fit the four experimental level-crossing induction midpoints at 4.5 T, 8.9 T, 20.1 T, and 32 T, by assuming some approximate symmetry such as D_{2d} or S_4, for which J^g_z is non-vanishing. The midpoint of the level crossings occur at $\theta = \pi/4$, and

the level-crossing widths are obtained from the differences between the values at $\theta = 0$ and $\theta = \pi/2$. We first tried to fit the data assuming a Type-I tetramer. In this case, the widths of the four level crossings are determined by the single parameter $|J^g_z - 3J^g_{\rm eff}|$, and are in the proportions $49 : 19 : 65 : 105$, respectively. Taking $|J^g_z - 3J^g_{\rm eff}| = 2.0{\rm T}\gamma$, we obtain the widths to be 1.4T, 0.54T, 1.85T, and 3.0T, which overestimates the width of the first level crossing, and underestimates the widths of the third and fourth level crossings. Nevertheless, it is interesting to try to fit the midpoint data with this assumption. We note that for Type-I, the level crossings do not depend upon $J^g_{\rm b,2}$ and $\tilde{J}'_g$, and $J^g_{\rm t,2}$ only enters the level-crossing equations via the combination $\tilde{J}_g + 2J^g_{\rm t,2}$. We first assumed $J^g_z - 3J^g_{\rm eff} = +2.0{\rm T}\gamma$. In this case we could fit the four equations with the remaining four parameters, and obtained $(\tilde{J}_g - 2J^g_{\rm t,2})/k_B = -11.02{\rm K}$, $J^g_z/k_B = -3.522{\rm K}$, $J^g_{\rm eff}/k_B = -2.069{\rm K}$, $J^g_{\rm b,1}/k_B = -2.752{\rm K}$, and $J^g_{\rm t,1}/k_B = -0.503{\rm K}$. This fit gives a large value to the symmetric anisotropic exchange $J^g_{\rm eff}$. We then assumed $J^g_z - 3J^g_{\rm eff} = -2.0{\rm T}\gamma$. This led to

$$(\tilde{J}_g - 2J^g_{\rm t,2})/k_B = -10.24{\rm K}, \quad (82)$$
$$J^g_z/k_B = -2.570{\rm K}, \quad (83)$$
$$J^g_{\rm eff}/k_B = +0.039{\rm K}, \quad (84)$$
$$J^g_{\rm b,1}/k_B = -1.861{\rm K}, \quad (85)$$
$$J^g_{\rm t,1}/k_B = -0.784{\rm K}, \quad (86)$$

which is a much smaller value of $J^g_{\rm eff} = J^g_{1,z}/2 + J^g_{2,z}/3$, and a smaller ratio of $J^g_{\rm b,1}$ to $J^g_{\rm t,1}$, which is reasonable. However, the fit to the four level-crossing widths is mediocre, at best.

It therefore seems that with the nine parameters in the four Type-II tetramer level-crossing inductions listed in the Appendix, one might do better by fitting not only the midpoints but also the widths of at least three of the level-crossing inductions. The four widths are governed by the three parameters $J^g_{q,z}$ and J^g_z for $q = 1, 2$. Setting $J^g_{1,z} = J^g_{2,z} = -J^g_z/2$, for instance, leaves the widths in the proportions $3 : 0 : 26 : 31$, and their magnitudes are then set by $|J^g_z|$. We then fit J^g_z to the half-width of the fourth transition, which is roughly 8.0T. The fit with more reasonable parameter values is obtained for $J^g_z < 0$. To limit the remaining parameters, we arbitrarily take $J^g_{\rm b,2} = J^g_{\rm t,2}$, and to insure Type-II behavior, choose $\tilde{J}'_g = 1.5\tilde{J}_g$. Then, we fit the midpoints of the four transitions with the remaining four parameters, and we find

$$\tilde{J}_g/k_B = -6.799\,{\rm K}, \quad (87)$$
$$\tilde{J}'_g/k_B = -10.198\,{\rm K}, \quad (88)$$
$$J^g_z/k_B = -4.17\,{\rm K}, \quad (89)$$
$$J^g_{1,z}/k_B = J^g_{2,z} = 2.08\,{\rm K}, \quad (90)$$
$$J^g_{\rm b,1}/k_B = 4.602\,{\rm K}, \quad (91)$$
$$J^g_{\rm t,1}/k_B = -2.529\,{\rm K}, \quad (92)$$
$$J^g_{\rm b,2}/k_B = J^g_{\rm t,2}/k_B = 0.614\,{\rm K}. \quad (93)$$

The resulting widths of the transitions are 0.8 T, 0, 6.7T, and 8.0T, respectively. These widths are in good agreement with experiment,[46] and the magnitudes of both Heisenberg interactions are larger than those of the other interactions, justifying the first-order perturbation fit.

While this is certainly not the best fit, it is quantitatively in agreement with experiment, and does not involve the assumption of strongly field-dependent Heisenberg interaction strengths.[46] We emphasize that this fit is not optimized, as we made the arbitrary choices $J^g_{\rm t,2} = J^g_{\rm b,2}$, and $J'_g = 1.5J_g$, although the only restrictions on those parameters were $\tilde{J}_g < 0$ and $\tilde{J}'_g - \tilde{J}_g < 0$. In addition, non-vanishing DM interactions (which vanish in first order) do give some additional widths to the level crossings, and these might provide an additional contribution to the broad third and fourth level crossings observed in experiment.[46] The best fit to experiment may not be either Type-I or Type-II, but may involve a more complicated analysis involving other states within some of the constant s manifolds.

However, with only polycrystalline data available, it is difficult to distinguish the different possible interactions uniquely. When single crystals of sufficient size for low-temperature magnetization measurements are made, we intend to fit the data using a more consistent set of parameters, neglecting any field dependencies, if possible.[51] To limit the number of parameters, we intend to make the assumption of C_{3v} symmetry, which will require a new quantization scheme, $|\nu\rangle = |s, m, s_{123}, s_{12}, s_1\rangle$ and the appropriate single-ion matrix elements, which are not yet in the literature.[31]

We note that our formulation of the single-ion matrix elements in terms of a pair of dimers is applicable to low-symmetry systems such as $Mo_{12}O_{30}(\mu_2\text{-}OH)_{10}H_2\{Ni(H_2O)_3\}_4$, abbreviated as $\{Ni_4Mo_{12}\}$,[46] systems such as Ni_4 tetramers obtained from salts of $[Ni_4(H_2O)_2(PW_9O_{34})_2]^{10-}$ with C_{2v} symmetry,[56] and the unequal-spin systems $Mn^{II}_2Mn^{III}_2$ and $Ni^{II}_2Mn^{III}_2$.[57, 58] In the first system with C_{1v} symmetry, one would expect many more single-ion, symmetric anisotropic exchange, and DM interactions, making definitive fits to the existing powder magnetization data problematic.[46] However, to improve the fits to C_{3v} or D_3 symmetry systems, such as the Fe_4 compound $Fe_4(thme)_2(dpm)_6$ and the $Cr^{III}Ni^{II}_3$ tetramer with an $s = 9/2$ ground state,[52, 59] would require a reformulation of the single-ion matrix elements as a trimer plus a monomer.[51] Even classical Heisenberg models of such systems show strongly different dynamics than of systems with T_d symmetry.[34, 60]

Unless they vanish identically, as for T_d and C_{4v} symmetries, DM interactions will appear in the second-order eigenstate energies. This is true even when the DM interactions are site-dependent and average to zero, just

as for the cases of site-dependent single-ion and symmetric anisotropic exchange interactions. Hence, although they have been neglected in many fits to experimental data, they should be included in subsequent fits. They are most prominent for systems with lower symmetry, such as S_4 or D_{2d}, and the effects become increasingly strong with increasing s_1 value. As an example, in the Appendix, we derived the symmetry-allowed DM interactions for the lower-symmetry C_{2v}^{13}, appropriate for the [2×2] grid tetramers.[47, 48]

Finally, the DM interactions also can give rise to an electric polarization, and hence to multiferroic behavior. Our results suggest that this behavior should apply for tetramers with all possible individual spin values, as long as there is no center of inversion symmetry connecting the interacting spin pairs. For tetramers with S_4 and D_{2d} or lower symmetry, this should be observable. Our results indicate that these effects should also occur for quantum spins. In addition, there is an interesting parity effect present in the systems we studied, with $|\boldsymbol{P}_s(\theta)| \propto (\theta - \pi/2)^{2s_1+1}$. This deserves further study to elucidate its generality.

IX. CONCLUSIONS

We presented a theory of high-symmetry single molecule magnets, including a compact form for the exact single-spin matrix elements for four general spins. We used the local axial and azimuthal vector groups to construct the invariant single-ion and symmetric anisotropic exchange Hamiltonians, and the molecular representation to obtain the Dzyaloshinskii-Moriya interactions, for equal-spin s_1 tetramers with site point group symmetries T_d, D_{4h}, D_{2d}, S_4, C_{4h}, or C_{4v}. Each vector group introduces site-dependent molecular single-ion and anisotropic exchange interactions. Assuming weak effective site-independent single-ion, symmetric exchange anisotropy, and isotropic biquadratic exchange interactions, we evaluated the first-order corrections to the eigenstate energies. Depending upon the relative strengths of the near-neighbor and next-nearest-neighbor Heisenberg exchange interactions, there are generally two types of high-symmetry tetramers. For the single-ion and symmetric exchange anisotropy interactions, we provided analytic results and illustrations of the antiferromagnetic level-crossing inductions. We also provided Hartree expressions for the magnetization, specific heat, EPR absorption, and INS cross-section, which are accurate at low temperatures and arbitrary magnetic fields. For ferromagnetic tetramers, we provided a procedure for a precise EPR determination of three of the microscopic anisotropy parameters. We predict that geometrically frustrated tetramers with symmetries S_4 and D_{2d}, as well as C_{2v}^{13}, are likely candidate materials for multiferroic states. Our procedure is extendable to more general systems.

We thank N. S. Dalal, D. Khomskii, and J. van den Brink for helpful comments and discussions. This work was supported in part by the NSF under contract NER-0304665.

APPENDIX

A. Symmetry operation matrices

Rotations by $\pm\pi/2$ about the z axis are represented by

$$\mathcal{O}_{1,2} = \begin{pmatrix} 0 & \pm 1 & 0 \\ \mp 1 & 0 & 0 \\ 0 & 0 & 1 \end{pmatrix}. \quad (94)$$

Rotations by π about the x and y axes are represented by

$$\mathcal{O}_{3,4} = \begin{pmatrix} \pm 1 & 0 & 0 \\ 0 & \mp 1 & 0 \\ 0 & 0 & -1 \end{pmatrix}. \quad (95)$$

Rotations by π about the z axis and reflections in the xy plane are respectively represented by

$$\mathcal{O}_{5,6} = \begin{pmatrix} \mp 1 & 0 & 0 \\ 0 & \mp 1 & 0 \\ 0 & 0 & \pm 1 \end{pmatrix}. \quad (96)$$

Rotations by π about the $y = \pm x$ diagonal axes are represented by

$$\mathcal{O}_{7,8} = \begin{pmatrix} 0 & \pm 1 & 0 \\ \pm 1 & 0 & 0 \\ 0 & 0 & -1 \end{pmatrix}. \quad (97)$$

Reflections in the xz and yz mirror planes are represented by

$$\mathcal{O}_{9,10} = \begin{pmatrix} \pm 1 & 0 & 0 \\ 0 & \mp 1 & 0 \\ 0 & 0 & 1 \end{pmatrix}. \quad (98)$$

Reflections in the mirror planes containing the z axis and the diagonals $y = \pm x$ are represented by

$$\mathcal{O}_{11,12} = \begin{pmatrix} 0 & \pm 1 & 0 \\ \pm 1 & 0 & 0 \\ 0 & 0 & 1 \end{pmatrix}. \quad (99)$$

Reflections in the mirror planes containing the y axis and the lines $z = \pm x$ are represented by

$$\mathcal{O}_{13,14} = \begin{pmatrix} 0 & 0 & \pm 1 \\ 0 & 1 & 0 \\ \pm 1 & 0 & 0 \end{pmatrix}. \quad (100)$$

Reflections in the mirror planes containing the x axis and the lines $y = \pm z$ are represented by

$$\mathcal{O}_{15,16} = \begin{pmatrix} 1 & 0 & 0 \\ 0 & 0 & \pm 1 \\ 0 & \pm 1 & 0 \end{pmatrix}. \quad (101)$$

For T_d, clockwise rotations by $2\pi/3$ about the cube diagonals are represented by

$$\mathcal{O}_{17,18} = \begin{pmatrix} 0 & \pm 1 & 0 \\ 0 & 0 & 1 \\ \pm 1 & 0 & 0 \end{pmatrix} \quad (102)$$

and

$$\mathcal{O}_{19,20} = \begin{pmatrix} 0 & \pm 1 & 0 \\ 0 & 0 & -1 \\ \mp 1 & 0 & 0 \end{pmatrix}. \quad (103)$$

Counterclockwise rotations by $2\pi/3$ about the cube diagonals are represented by $\mathcal{O}_\lambda^T = \mathcal{O}_\lambda^{-1}$ for $\lambda = 17, \ldots, 20$. Finally, there are the six S_4 improper rotations consisting of rotations about a high-symmetry axis by $\pm\pi/2$ followed by a reflection in the plane perpendicular to the rotation axis. For S_4 symmetry, z is the high symmetry axis, and the operations are represented by

$$\mathcal{O}_{21,22} = \begin{pmatrix} 0 & \pm 1 & 0 \\ \mp 1 & 0 & 0 \\ 0 & 0 & -1 \end{pmatrix}. \quad (104)$$

For T_d symmetry, we also have

$$\mathcal{O}_{23,24} = \begin{pmatrix} -1 & 0 & 0 \\ 0 & 0 & \pm 1 \\ 0 & \mp 1 & 0 \end{pmatrix} \quad (105)$$

and

$$\mathcal{O}_{25,26} = \begin{pmatrix} 0 & 0 & \pm 1 \\ 0 & -1 & 0 \\ \mp 1 & 0 & 0 \end{pmatrix}. \quad (106)$$

As described in the text, C_{4h} symmetry involves $\mathcal{O}_1 = (\mathcal{O}_2)^T$ and $\mathcal{O}_6$.

D_{4h} symmetry contains the same three symmetry operations of C_{4h} symmetry, rotations by $\pm\pi/2$ about the z axis, $\mathcal{O}_{1,2}$, and reflections in the xy plane, $\mathcal{O}_6$. In addition, it is also symmetric under the four rotations by π about the x and y axes, represented by $\mathcal{O}_{3,4}$, and about the $y = \pm x$ diagonals, represented by $\mathcal{O}_{7,8}$.[33]

For C_{4v} symmetry, there are six group operations. These are rotations by $\pm\pi/2$ about the z axis, $\mathcal{O}_{1,2}$, reflections in the xz and yz planes, represented respectively by $\mathcal{O}_{9,10}$, and reflections in the diagonal mirror planes containing the z axis and the lines $y = \pm x$, represented by $\mathcal{O}_{11,12}$.

For the lowest group symmetry under study, S_4, the only two group operations are clockwise and counterclockwise rotations by $\pi/4$ about the z axis, followed by a reflection in the xy plane.[33] These improper rotations are represented by $\mathcal{O}_{21,22}$.

Besides the identity operation, D_{2d} group symmetry has five operations. The first three are rotations by π about the x, y, and z axes, respectively represented by $\mathcal{O}_{3,4,6}$. In addition, there are two diagonal mirror planes associated with the principal axis, z. These are represented by $\mathcal{O}_{11,12}$.

Finally, the highest symmetry under study, T_d, has 23 operations besides the identity. The first five are the same as for D_{2d} symmetry: rotations by π about the x, y, and z axes, and reflections in the two diagonal mirror planes associated with the z axis. Then there are the four diagonal mirror planes associated with x and y axes, represented respectively by $\mathcal{O}_{13,14,15,16}$. Next, there are the four clockwise and four counterclockwise rotations by $2\pi/3$ about the cube diagonals. The four clockwise rotations are represented by $\mathcal{O}_{17,18,19,20}$, and the four counterclockwise rotations are represented respectively by $\mathcal{O}^T_{17,18,19,20} = \mathcal{O}^{-1}_{17,18,19,20}$. Finally, there are the six improper rotations by $\pm\pi/2$ about the x, y, and z axes, represented by $\mathcal{O}_{21,22,23,24,25,26}$.

B. Molecular single-ion interactions

The site-independent interactions in the molecular representation are

$$J_z^g = J_a^g \qquad \text{for } g = C_{4h}, D_{4h}, \quad (107)$$

$$J_z^g = \frac{1}{2}\Big(J_a^g(3\cos^2\theta_1^g - 1) + 3J_e^g \sin^2\theta_1^g\Big) \qquad \text{for } g = C_{4v}, D_{2d}, \quad (108)$$

$$J_z^{S_4} = \frac{J_a^{S_4}}{2}(3\cos^2\theta_1^{S_4} - 1) - \frac{3}{2}J_e^{S_4}\sin^2\theta_1^{S_4}\cos(2\psi_1^{S_4}), \quad (109)$$

$$J_z^{T_d} = 0. \quad (110)$$

For $g = D_{4h}$, the only non-vanishing site-dependent single-ion interaction is

$$K_{xy}^{D_{4h}}(n) = (-1)^{n+1}J_e^{D_{4h}}. \quad (111)$$

For $g = C_{4h}$, the two non-vanishing site-dependent single-ion interactions are

$$J_{xy}^{C_{4h}} = J_e^{C_{4h}}\cos(2\chi_1^{C_{4h}}), \quad (112)$$

$$K_{xy}^{C_{4h}}(n) = (-1)^{n+1}J_e^{C_{4h}}\sin(2\chi_1^{C_{4h}}). \quad (113)$$

For $g = C_{4v}, D_{2d}$, the three non-vanishing site-dependent single-ion interactions in Eq. (27) are

$$K^g_{xy}(n) = \frac{(-1)^{n+1}}{2}\Big(J^g_a \sin^2\theta^g_1 + J^g_e(1+\cos^2\theta^g_1)\Big), \quad (114)$$

$$K^g_{xz}(n) = \frac{1}{2}\cos[(2n-1)\pi/4]\sin(2\theta^g_1)(J^g_a - J^g_e), \quad (115)$$

$$K^g_{yz}(n) = \frac{1}{2}\sin[(2n-1)\pi/4]\sin(2\theta^g_1)(J^g_a - J^g_e). \quad (116)$$

For S_4, the single-ion site-dependent interactions are

$$J^{S_4}_{xy} = -J_1\cos(2\phi^{S_4}_1) + J_2\sin(2\phi^{S_4}_1), \quad (117)$$

$$K^{S_4}_{xy}(n) = (-1)^n\Big(J_1\sin(2\phi^{S_4}_1) + J_2\cos(2\phi^{S_4}_1)\Big), \quad (118)$$

$$K^{S_4}_{xz}(n) = (-1)^{n+1}\Big[J_3\cos\Big(\phi^{S_4}_1 - \frac{n\pi}{2}\Big) - J_4\sin\Big(\phi^{S_4}_1 - \frac{n\pi}{2}\Big)\Big], \quad (119)$$

$$K^{S_4}_{yz}(n) = (-1)^{n+1}\Big[J_3(\sin\Big(\phi^{S_4}_1 - \frac{n\pi}{2}\Big) + J_4\cos\Big(\phi^{S_4}_1 - \frac{n\pi}{2}\Big)\Big], \quad (120)$$

$$J_1 = \frac{1}{2}\Big(J^{S_4}_a\sin^2\theta^{S_4}_1 - J^{S_4}_e(1+\cos^2\theta^{S_4}_1)\cos(2\psi^{S_4}_1)\Big), \quad (121)$$

$$J_2 = J^{S_4}_e\cos\theta^{S_4}_1\sin(2\psi^{S_4}_1), \quad (122)$$

$$J_3 = \frac{1}{2}\sin(2\theta^{S_4}_1)[J^{S_4}_a + J^{S_4}_e\cos(2\psi^{S_4}_1)], \quad (123)$$

$$J_4 = J^{S_4}_e\sin\theta^{S_4}_1\sin(2\psi^{S_4}_1). \quad (124)$$

The site-dependent single-ion interactions for T_d symmetry are easily obtained from those Eqs. (114)-(116) by setting $\theta^{D_{2d}}_1 \to \tan^{-1}(\sqrt{2})$ and $J^{T_d}_e \to 0$,

$$K^{T_d}_{xy}(n) = \frac{(-1)^n}{3}J^{T_d}_a, \quad (125)$$

$$K^{T_d}_{xz}(n) = \frac{\sqrt{2}}{3}\cos[(2n-1)\pi/4]J^{T_d}_a, \quad (126)$$

$$K^{T_d}_{yz}(n) = \frac{\sqrt{2}}{3}\sin[(2n-1)\pi/4]J^{T_d}_a. \quad (127)$$

C. Molecular anisotropic exchange interactions

We first consider the symmetric anisotropic exchange interactions, letting $q = 1, 2$ and $p = q+1$. For simplicity of presentation, we write

$$J^g_{q,\pm} = \frac{1}{2}(J^g_{c,q} \pm J^g_{f,q}). \quad (128)$$

Then, the isotropic exchange renormalizations may be written as

$$\delta J_g = \delta J'_g = 0 \text{ for } g = C_{4h}, D_{4h}, C_{4v}, T_d \quad (129)$$

$$\delta J_{D_{2d}} = -J^{D_{2d}}_{1,-}\sin^2\theta^{D_{2d}}_{12}, \quad (130)$$

$$\delta J'_{D_{2d}} = -J^{D_{2d}}_{2,-}, \quad (131)$$

$$\delta J_{S_4}, \delta J'_{S_4} = \frac{\sin^2\theta^{S_4}_{1p}}{2}[J^{S_4}_{f,q} + J^{S_4}_{c,q}\cos(2\psi^{S_4}_{1p})]. \quad (132)$$

In Eq. (132), $q = 1, 2$ corresponds to $\delta J_{S_4}, \delta J'_{s_4}$, respectively.

The non-vanishing site-independent symmetric anisotropic exchange interactions in the molecular representation are

$$J^g_{q,z} = -J^g_{f,q} \text{ for } g = C_{4h}, D_{4h}, C_{4v}, \quad (133)$$

$$J^{D_{2d}}_{1,z} = \frac{J^{D_{2d}}_{f,1}}{2}(1-3\cos^2\theta^{D_{2d}}_{12}) - \frac{3J^{D_{2d}}_{c,1}}{2}\sin^2\theta^{D_{2d}}_{12}, \quad (134)$$

$$J^{D_{2d}}_{2,z} = -J^{D_{2d}}_{2,-} - J^{D_{2d}}_{c,2}, \quad (135)$$

$$J^{S_4}_{q,z} = \frac{J^{S_4}_{f,q}}{2}(1-3\cos^2\theta^{S_4}_{1p}) + \frac{3J^{S_4}_{c,q}}{2}\sin^2\theta^{S_4}_{1p}\cos(2\psi^{S_4}_{1p}). \quad (136)$$

For $g = C_{4h}$, the non-vanishing site-dependent symmetric anisotropic exchange interactions in Eq. (32) have strengths

$$K^{C_{4h}}_{q,xy} = J^{C_{4h}}_{c,q}\sin(2\chi^{C_{4h}}_{1p}), \quad (137)$$

$$J^{C_{4h}}_{q,xy} = -J^{C_{4h}}_{c,q}\cos(2\chi^{C_{4h}}_{1p}), \quad (138)$$

where $\chi^g_{1p} = \phi^g_{1p} + \psi^g_{1p}$. For $g = D_{4h}, C_{4v}$, the non-vanishing site-dependent symmetric anisotropic exchange interaction strengths are

$$J^g_{1,xy} = -J^g_{c,1}, \quad (139)$$

$$K^g_{2,xy} = -J^g_{c,2}. \quad (140)$$

Again, the more interesting group is $g = S_4$. We find

$$J^{S_4}_{q,xy} = -\tilde{J}_1\cos(2\phi^{S_4}_{1p}) + \tilde{J}_2\sin(2\phi^{S_4}_{1p}), \quad (141)$$

$$K^{S_4}_{q,xy} = \tilde{J}_1\sin(2\phi^{S_4}_{1p}) + \tilde{J}_2\cos(2\phi^{S_4}_{1p}), \quad (142)$$

$$K^{S_4}_{q,xz}(n) = -\tilde{J}_3\cos\Big(\phi^{S_4}_{1p} - \frac{n\pi}{2}\Big)$$

$$+\tilde{J}_4 \sin\Big(\phi_{1p}^{S_4} - \frac{n\pi}{2}\Big), \quad (143)$$

$$K_{q,yz}^{S_4}(n) = -\tilde{J}_3 \sin\Big(\phi_{1p}^{S_4} - \frac{n\pi}{2}\Big) - \tilde{J}_4 \cos\Big(\phi_{1p}^{S_4} - \frac{n\pi}{2}\Big), \quad (144)$$

$$\tilde{J}_1 = \frac{1}{2}\Big(J_{f,q}^{S_4} \sin^2\theta_{1p}^{S_4} - J_{c,q}^{S_4}(1+\cos^2\theta_{1p}^{S_4})\cos(2\psi_{1p}^{S_4})\Big), \quad (145)$$

$$\tilde{J}_2 = J_{c,q}^{S_4} \cos\theta_{1p}^{S_4} \sin(2\psi_{1p}^{S_4}), \quad (146)$$

$$\tilde{J}_3 = \frac{1}{2}\sin(2\theta_{1p}^{S_4})[J_{f,m}^{S_4} + J_{c,m}^{S_4}\cos(2\psi_{1p}^{S_4})], \quad (147)$$

$$\tilde{J}_4 = J_{c,q}^{S_4} \sin\theta_{1p}^{S_4} \sin(2\psi_{1p}^{S_4}). \quad (148)$$

For $g = D_{2d}$, the non-vanishing site-dependent anisotropic exchange interaction strengths are

$$J_{1,xy}^{D_{2d}} = -\frac{J_{f,1}^{D_{2d}}}{2}\sin^2\theta_{12}^{D_{2d}} - \frac{J_{c,1}^{D_{2d}}}{2}(1+\cos^2\theta_{12}^{D_{2d}}), \quad (149)$$

$$K_{1,xz}^{D_{2d}}(n) = \cos(n\pi/2) J_{1,+}^{D_{2d}} \sin 2\theta_{12}^{D_{2d}}, \quad (150)$$

$$K_{1,yz}^{D_{2d}}(n) = -\sin(n\pi/2) J_{1,+}^{D_{2d}} \sin 2\theta_{12}^{D_{2d}}, \quad (151)$$

$$K_{2,xy}^{D_{2d}} = -J_{2,+}^{D_{2d}}. \quad (152)$$

For $g = T_d$, there are no symmetric or antisymmetric anisotropic exchange interactions.

The antisymmetric anisotropic exchange interactions in the molecular representation are given for $g = C_{4h}, D_{4h}, S_4$, and D_{2d} by

$$d_z^g(n) = d_z^g \quad \text{for } g = C_{4h}, D_{4h}, \quad (153)$$

$$\boldsymbol{d}_q^g = 0 \quad \text{for } g = C_{4h}, D_{4h}, \quad (154)$$

$$d_z^g(n) = d_z^g(-1)^{n+1} \quad \text{for } g = S_4, D_{2d}, \quad (155)$$

$$\boldsymbol{d}_1^{D_{2d}} = d_{y1}^{D_{2d}}\hat{\boldsymbol{y}}, \quad (156)$$

$$\boldsymbol{d}_2^{D_{2d}} = d_{x2}^{D_{2d}}(\hat{\boldsymbol{x}} + \hat{\boldsymbol{y}}), \quad (157)$$

$$\boldsymbol{d}_1^{S_4} = d_{x1}^{S_4}\hat{\boldsymbol{x}} + d_{y1}^{S_4}\hat{\boldsymbol{y}}, \quad (158)$$

$$\boldsymbol{d}_2^{S_4} = d_{x2}^{S_4}\hat{\boldsymbol{x}} + d_{y2}^{S_4}\hat{\boldsymbol{y}}. \quad (159)$$

Tetramers with the lowest-symmetry S_4 require five parameters to describe the full DM interactions, those with D_{2d} symmetry require three parameters, those with either C_{4h} or D_{4h} symmetry require just one parameter, and tetramers with T_d or C_{4v} symmetry have no DM interactions.

D. C_{2v}^{13} DM interactions

For the [2×2] grid compounds with approximate C_{2v}^{13} symmetry, the four spins lie on the corners of a rhombus of side a with the position vectors relative to the origin given by

$$\boldsymbol{r}_n = \frac{a}{\sqrt{2}}\Big[\hat{\boldsymbol{x}}\Big(\sin[(2n-1)\pi/4] + \cos[(2n-1)\pi/4]\cos\theta_0\Big) + \hat{\boldsymbol{y}}\cos[(2n-1)\pi/4]\sin\theta_0\Big], \quad (160)$$

where the acute angle θ_0 satisfies $\pi/2 > \theta_0 > \pi/3$ for the [2×2] grid compounds.[47, 48] There are three C_{2v}^{13} symmetry operations $\mathcal{O}_\lambda^{C_{2v}^{13}}$. The first describes rotations about the z axis by π, equivalent to $\mathcal{O}_3^{D_{2d}}$. The other two are mirror planes containing the z axis and the diagonals of the rhombus,[49] which are described by

$$\mathcal{O}_{2,3}^{C_{2v}^{13}} = \begin{pmatrix} \pm\cos\theta_0 & \pm\sin\theta_0 & 0 \\ \pm\sin\theta_0 & \mp\cos\theta_0 & 0 \\ 0 & 0 & 1 \end{pmatrix}. \quad (161)$$

For the NNN and next-next-nearest-neighbor DM interactions, corresponding to pairs across the diagonals, vanish due to Moriya rule (3) and invariance under $\mathcal{O}_{2,3}^{C_{2v}^{13}}$. However, as for C_{4h} and D_{4h} symmetries, the DM interactions between NN spins do not vanish for C_{2v}^{13} symmetry, but are given by

$$\mathcal{H}_{DM}^{C_{2v}^{13}} = \sum_{n=1}^{4}\Big[d_z(-1)^{n+1}\hat{\boldsymbol{z}} + \boldsymbol{d}\sin(n\pi/2) - \tilde{\boldsymbol{d}}\cos(n\pi/2)\Big]\cdot\Big(\boldsymbol{S}_n \times \boldsymbol{S}_{n+1}\Big), \quad (162)$$

$$\tilde{\boldsymbol{d}} = \mathcal{O}_2^{C_{2v}^{13}}\cdot\boldsymbol{d}, \quad (163)$$

for a general two-vector $\boldsymbol{d}$ in the xy plane. We note that Eq. (162) is invariant under all three symmetries of C_{2v}^{13}.

E. Compact single-ion matrix elements

By using the Schwinger boson technique of representing a spin by two non-interacting bosons, and checking our results using the standard Clebsch-Gordan algebra with the assistance of symbolic manipulation software, we find the single-spin matrix elements with general $\{s_n\} = (s_1, s_2, s_3, s_4)$ to be

$$\langle\nu'|S_{n,\tilde{z}}|\nu\rangle = \delta_{m',m}\Big(m\delta_{s',s}\Gamma_{s_{13},s'_{13},s_{24},s'_{24}}^{\{s_n\},s,n} + \delta_{s',s+1}C_{-s-1}^{m}\Delta_{s_{13},s'_{13},s_{24},s'_{24}}^{\{s_n\},-s-1,n} + \delta_{s',s-1}C_{s}^{m}\Delta_{s_{13},s'_{13},s_{24},s'_{24}}^{\{s_n\},s,n}\Big), \quad (164)$$

$$\langle\nu'|S_{n,\tilde{\sigma}}|\nu\rangle = \delta_{m',m+\tilde{\sigma}}\Big(A_s^{\tilde{\sigma}m}\delta_{s',s}\Gamma_{s_{13},s'_{13},s_{24},s'_{24}}^{\{s_n\},s,n} - \delta_{s',s+1}D_{-s-1}^{\tilde{\sigma},m}\Delta_{s_{13},s'_{13},s_{24},s'_{24}}^{\{s_n\},-s-1,n} + \delta_{s',s-1}D_{s}^{\tilde{\sigma},m}\Delta_{s_{13},s'_{13},s_{24},s'_{24}}^{\{s_n\},s,n}\Big), \quad (165)$$

$$C_s^m = \sqrt{s^2-m^2}, \tag{166}$$

$$D_s^{\tilde\sigma,m} = \tilde\sigma\sqrt{(s-\tilde\sigma m)(s-\tilde\sigma m-1)}, \tag{167}$$

$$\Gamma^{\{s_n\},s,n}_{s_{13},s'_{13},s_{24},s'_{24}} = \delta_{s'_{24},s_{24}}\epsilon_n^-\alpha^{s_{24},s,n}_{s_1,s_3}(s_{13},s'_{13}) + \delta_{s'_{13},s_{13}}\epsilon_n^+\alpha^{s_{13},s,n}_{s_2,s_4}(s_{24},s'_{24}), \tag{168}$$

$$\Delta^{\{s_n\},s,n}_{s_{13},s'_{13},s_{24},s'_{24}} = \delta_{s'_{24},s_{24}}\epsilon_n^-\beta^{s_{24},s,n}_{s_1,s_3}(s_{13},s'_{13}) + \delta_{s'_{13},s_{13}}\epsilon_n^+\beta^{s_{13},s,n}_{s_2,s_4}(s_{24},s'_{24}), \tag{169}$$

$$\alpha^{s_{24},s,n}_{s_1,s_3}(s_{13},s'_{13}) = \frac{1}{4}(1+\xi_{s,s_{13},s_{24}})\delta_{s'_{13},s_{13}} - \sqrt{2}\sin[(2n-1)\pi/4]\Big(F^{s_{13},s_{24}}_{s_1,s_3,s}\delta_{s'_{13},s_{13}-1} + F^{s_{13}+1,s_{24}}_{s_1,s_3,s}\delta_{s'_{13},s_{13}+1}\Big), \tag{170}$$

$$\beta^{s_{24},s,n}_{s_1,s_3}(s_{13},s'_{13}) = -\frac{(-1)^n}{4}\eta_{s,s_{13},s_{24}}\delta_{s'_{13},s_{13}} + \sqrt{2}\sin[(2n-1)\pi/4]\Big(G^{s_{13},s_{24}}_{s_1,s_3,s}\delta_{s'_{13},s_{13}-1} + G^{s_{13}+1,s_{24}}_{s_1,s_3,-s}\delta_{s'_{13},s_{13}+1}\Big), \tag{171}$$

$$F^{s_{13},s_{24}}_{s_1,s_3,s} = \frac{\eta_{s_{13},s_1,s_3}A^{s_{24}}_{s+s_{13}}A^{s-s_{13}}_{s_{24}}}{4s(s+1)}, \tag{172}$$

$$G^{s_{13},s_{24}}_{s_1,s_3,s} = \frac{\eta_{s_{13},s_1,s_3}A^{s_{24}}_{s+s_{13}}A^{s_{24}}_{s+s_{13}-1}}{4s\sqrt{4s^2-1}}, \tag{173}$$

$$\eta_{z,x,y} = \frac{A^y_{x+z}A^{x-z}_y}{\sqrt{z^2(4z^2-1)}}, \tag{174}$$

$$\xi_{z,x,y} = \frac{x(x+1)-y(y+1)}{z(z+1)}, \tag{175}$$

$$\epsilon_n^\pm = \frac{1}{2}[1\pm(-1)^n], \tag{176}$$

where A_s^m is given by Eq. (46). The prefactors m, $A_s^{\tilde\sigma m}$, C_s^m, C_{-s-1}^m, $D_s^{\tilde\sigma,m}$, and $D_{-s-1}^{\tilde\sigma,m}$ are consequences of the Wigner-Eckart theorem for a vector operator.[33] The challenge was to obtain the coefficients $\Gamma^{\{s_n\},s,n}_{s_{13},s'_{13},s_{24},s'_{24}}$ and $\Delta^{\{s_n\},s,n}_{s_{13},s'_{13},s_{24},s'_{24}}$. Their hierarchical structure based upon the unequal-spin dimer suggests that analogous coefficients with $n>4$ may be obtainable.[5] Details will be presented elsewhere.[51]

F. First-order eigenstate energy constants

The constants appearing in the first-order eigenstate energies (51) are

$$c_{\overline{\nu}}^\pm = \frac{1}{4}\Big(1\pm\xi^2_{s,s_{13},s_{24}}-\eta^2_{s,s_{13},s_{24}}-\eta^2_{s+1,s_{13},s_{24}}\Big)$$

$$a_{\overline{\nu}}^\pm = c_{\overline{\nu}}^\pm \pm 2\Bigg(\sum_{\sigma=\pm1}\Big[\Big(F^{s_{13}+(\sigma+1)/2,s_{24}}_{s_1,s_1,s}\Big)^2 - \sum_{\sigma'=\pm1}\Big(G^{s_{13}+(1+\sigma)/2,s_{24}}_{s_1,s_1,\sigma\sigma' s+\sigma(1+\sigma')/2}\Big)^2\Big] + (s_{13}\leftrightarrow s_{24})\Bigg), \tag{177}$$

$$b_{\overline{\nu}}^\pm = \frac{1}{8}\sum_{\sigma'=\pm1}(2s+1+\sigma')^2\Bigg(\eta^2_{s+(1+\sigma')/2,s_{13},s_{24}} \pm 8\sum_{\sigma=\pm1}\Big[\Big(G^{s_{13}+(1+\sigma)/2,s_{24}}_{s_1,s_1,\sigma\sigma' s+\sigma(1+\sigma')/2}\Big)^2 + (s_{13}\leftrightarrow s_{24})\Big]\Bigg), \tag{178}$$

where the $F^{s_{13},s_{24}}_{s_1,s_3,s}$, $G^{s_{13},s_{24}}_{s_1,s_3,s}$, $\eta_{z,x,y}$, and $\xi_{z,x,y}$, are given by Eqs. (172)-(175), respectively.

In order to calculate the $\langle\nu|\mathcal{H}^g_{\rm b,1}|\nu\rangle$ we first write it as

$$\langle\nu|\mathcal{H}^g_{\rm b,1}|\nu\rangle = -\frac{J^g_{\rm b,1}}{4}\sum_{n,\nu'}\Big|\langle\nu'|\boldsymbol{S}_n\cdot\boldsymbol{S}_{n+1}+\boldsymbol{S}_{n+1}\cdot\boldsymbol{S}_n|\nu\rangle\Big|^2. \tag{179}$$

We note that for general n, $\boldsymbol{S}_n\cdot\boldsymbol{S}_{n\pm1}$ commutes with the isotropic part of the Hamiltonian, which includes the Heisenberg, biquadratic, and isotropic three-center interactions. Thus, we expect $\langle\nu'|\boldsymbol{S}_n\cdot\boldsymbol{S}_{n+1}+\boldsymbol{S}_{n+1}\cdot\boldsymbol{S}_n|\nu\rangle$ to vanish unless $m'=m$ and $s'=s$. It is easy to see that $m'=m$ by inspection. The matrix elements for $s'=s\pm1$ and $s'=s\pm2$ can then easily be shown from their s,m dependencies to vanish. For example, the $s'=s-2$ terms are proportional to $C_s^mC_{s-1}^m+\frac{1}{2}\sum_{\tilde\sigma}D_s^{-\tilde\sigma,m}D_{s-1}^{\tilde\sigma,m-\tilde\sigma}=0$. There are three non-vanishing $s'=s$ terms, corresponding to the intermediate states $s''=s,s+1$, and $s-1$. These are respectively proportional to $m^2+\frac{1}{2}\sum_{\tilde\sigma}A_s^{-\tilde\sigma m}A_s^{\tilde\sigma(m+\tilde\sigma)}=s(s+1)$, $C_{-s-1}^mC_{s+1}^m-\frac{1}{2}\sum_{\tilde\sigma}D_{-s-1}^{-\tilde\sigma,m}D_{s+1}^{\tilde\sigma,m-\tilde\sigma}=(s+1)(2s+3)$, and $C_s^mC_{-s}^m-\frac{1}{2}\sum_{\tilde\sigma}D_s^{-\tilde\sigma,m}D_{-s}^{\tilde\sigma,m-\tilde\sigma}=s(2s-1)$. Hence, the Wigner-Eckart theorem guarantees that these are independent of m. We first performed two checks of our matrix element forms. First, we evaluated

$$\begin{aligned}\langle\nu'|\boldsymbol{S}_1\cdot\boldsymbol{S}_3|\nu\rangle &= \delta_{\nu,\nu'}\Bigg(s(s+1)\Big[\frac{1}{16}(1+\xi_{s,s_{13},s_{24}})^2 - \Big(F^{s_{13},s_{24}}_{s_1,s_1,s}\Big)^2-\Big(F^{s_{13}+1,s_{24}}_{s_1,s_1,s}\Big)^2\Big] \\ &\quad +s(2s-1)\Big[\frac{1}{16}\eta^2_{s,s_{13},s_{24}} - \Big(G^{s_{13},s_{24}}_{s_1,s_1,-s}\Big)^2-\Big(G^{s_{13}+1,s_{24}}_{s_1,s_1,-s}\Big)^2\Big] \\ &\quad +(s+1)(2s+3)\Big[\frac{1}{16}\eta^2_{s+1,s_{13},s_{24}} - \Big(G^{s_{13},s_{24}}_{s_1,s_1,s+1}\Big)^2-\Big(G^{s_{13}+1,s_{24}}_{s_1,s_1,s+1}\Big)^2\Big]\Bigg) \\ &= \Big(\frac{1}{2}s_{13}(s_{13}+1)-s_1(s_1+1)\Big)\delta_{\nu,\nu'},\end{aligned} \tag{180}$$

$$\delta_{\nu,\nu'} = \delta_{s,s'}\delta_{m,m'}\delta_{s_{13},s'_{13}}\delta_{s_{24},s'_{24}}, \tag{181}$$

as required. Similarly, $\langle\nu'|\boldsymbol{S}_2\cdot\boldsymbol{S}_4|\nu\rangle$ is found from the above by setting $s_{13}\leftrightarrow s_{24}$, as required. Then, we found

$$\sum_{n=1}^{4}\langle\nu'|\boldsymbol{S}_n\cdot\boldsymbol{S}_{n+1}|\nu\rangle \;=\; \frac{g_0(\overline{\nu})}{4}\delta_{\nu,\nu'}, \tag{182}$$

where

$$\begin{aligned} g_0(\overline{\nu}) \;&=\; s(s+1)(1-\xi^2_{s,s_{13},s_{24}})-s(2s-1)\eta^2_{s,s_{13},s_{24}} \\ &\quad -(s+1)(2s+3)\eta^2_{s+1,s_{13},s_{24}} \\ &=\; 2\Big[s(s+1)-s_{13}(s_{13}+1)-s_{24}(s_{24}+1)\Big], \end{aligned} \tag{183}$$

as required. We then may write

$$\langle\nu'|\boldsymbol{S}_n\cdot\boldsymbol{S}_{n+1}+\boldsymbol{S}_{n+1}\cdot\boldsymbol{S}_n|\nu\rangle \;=\; \delta_{s,s'}\delta_{m,m'}M^{s_{24},s'_{24}}_{s_{13},s'_{13}}(\overline{\nu},n), \tag{184}$$

where

$$\begin{aligned} M^{s_{24},s'_{24}}_{s_{13},s'_{13}}(\overline{\nu},n) \;&=\; \delta_{s'_{13},s_{13}}\delta_{s'_{24},s_{24}}\frac{g_0(\overline{\nu})}{8} \\ &\quad +(-1)^{n+1}\sum_{\sigma,\sigma'=\pm1}\delta_{s'_{24},s_{24}+\sigma}\delta_{s'_{13},s_{13}+\sigma'} \\ &\quad \times h_{\sigma,\sigma'}(\overline{\nu}) \\ &\quad -\sqrt{2}\sin[(2n-1)\pi/4] \\ &\quad \times\sum_{\sigma=\pm1}\delta_{s'_{13},s_{13}}\delta_{s'_{24},s_{24}+\sigma}\frac{g_\sigma(\overline{\nu})}{4} \\ &\quad -\sqrt{2}\sin[(2n+1)\pi/4] \\ &\quad \times\sum_{\sigma=\pm1}\delta_{s'_{13},s_{13}+\sigma}\delta_{s'_{24},s_{24}}\frac{\tilde{g}_\sigma(\overline{\nu})}{4}, \end{aligned} \tag{185}$$

where

$$\begin{aligned} g_\sigma \;&=\; \sum_{\sigma_1=\pm1}\Big[s(s+1)(1+\xi_{s,s_{13},s_{24}+\sigma(1+\sigma_1)/2}) \\ &\quad \times F^{s_{24}+(1+\sigma)/2,s_{13}}_{s_1,s_1,s} \\ &\quad +\frac{1}{2}\sum_{\sigma_2=\pm1}(2s+1+\sigma_1)(2s+1+2\sigma_1) \\ &\quad \times\eta_{s+(\sigma_1+1)/2,s_{13},s_{24}+(\sigma+\sigma_2)/2} \\ &\quad \times G^{s_{24}+(1+\sigma)/2,s_{13}}_{s_1,s_1,\sigma_1\sigma_2 s+\sigma_2(1+\sigma_1)/2}, \end{aligned} \tag{186}$$

$$\begin{aligned} h_{\sigma,\sigma} \;&=\; s(s+1)F^{s_{13}+(\sigma+1)/2,s_{24}}_{s_1,s_1,s}F^{s_{24}+(1+\sigma)/2,s_{13}+\sigma}_{s_1,s_1,s} \\ &\quad +\frac{1}{2}\sum_{\sigma_1=\pm1}(2s+1+\sigma_1)(2s+1+2\sigma_1) \\ &\quad \times G^{s_{13}+(1+\sigma)/2,s_{24}}_{s_1,s_1,\sigma_1\sigma s+\sigma(1+\sigma_1)/2}G^{s_{24}+(1+\sigma)/2,s_{13}+\sigma}_{s_1,s_1,-\sigma_1\sigma s-\sigma(1+\sigma_1)/2} \\ &\quad +(s_{13}\leftrightarrow s_{24}), \end{aligned} \tag{187}$$

$$\begin{aligned} h_{+,-} \;&=\; \sum_{\sigma=\pm1}s(s+1)F^{s_{13}+1,s_{24}-(1-\sigma)/2}_{s_1,s_1,s}F^{s_{24},s_{13}+(1+\sigma)/2}_{s_1,s_1,s} \\ &\quad +\frac{1}{2}\sum_{\sigma_1=\pm1}(2s+\sigma_1+1)(2s+2\sigma_1+1) \\ &\quad \times G^{s_{13}+1,s_{24}-(1-\sigma)/2}_{s_1,s_1,\sigma\sigma_1 s+\sigma(1+\sigma_1)/2}G^{s_{24},s_{13}+(1+\sigma)/2}_{s_1,s_1,\sigma\sigma_1 s+\sigma(1+\sigma_1)/2}, \end{aligned} \tag{188}$$

and where $\tilde{g}_\sigma(\overline{\nu})$ and $h_{-,+}(\overline{\nu})=\tilde{h}_{+,-}(\overline{\nu})$ are respectively obtained from $g_\sigma(\overline{\nu})$ and the $h_{+,-}(\overline{\nu})$ by setting $s_{13}\leftrightarrow s_{24}$.

Letting $x=s_{13}$ and $y=s_{24}$, these expressions may be simplified to yield

$$\begin{aligned} h_{\sigma,\sigma}(0,x,x) \;&=\; -\sqrt{(2x+2+\sigma)(2x+\sigma)}\eta^2_{x+(1+\sigma)/2,s_1,s_1} \\ &\quad \times\frac{(2x+1+\sigma)}{2}, \end{aligned} \tag{189}$$

$$\begin{aligned} h_{\sigma,\sigma}(s,x,y) \;&=\; -\frac{(x-y)^2}{s(s+1)}\eta_{x+(1+\sigma)/2,s_1,s_1}\eta_{y+(1+\sigma)/2,s_1,s_1} \\ &\quad \times\sqrt{(x+y+1+\sigma)^2-s^2} \\ &\quad \times\sqrt{(x+y+1+\sigma)^2-(s+1)^2}, \\ &\qquad \text{for } s\geq1, \end{aligned} \tag{190}$$

$$\begin{aligned} h_{+,-}(s,x,y) \;&=\; \frac{(x+y+1)^2}{s(s+1)}\eta_{x,s_1,s_1}\eta_{y+1,s_1,s_1} \\ &\quad \times\sqrt{(s+1)^2-(x-y-1)^2} \\ &\quad \times\sqrt{s^2-(x-y-1)^2}, \end{aligned} \tag{191}$$

$$\begin{aligned} g_\sigma(s,x,y) \;&=\; \eta_{x+(1+\sigma)/2,s_1,s_1} \\ &\quad \times\sqrt{[x+(1+\sigma)/2]^2-(y-s)^2} \\ &\quad \times\sqrt{(y+s+1)^2-[x+(1+\sigma)/2]^2}. \end{aligned} \tag{192}$$

The diagonal matrix elements of $\mathcal{H}^g_{\rm b,1}$ are then easily found to be

$$\langle\nu|\mathcal{H}^g_{\rm b,1}|\nu\rangle \;=\; -J^g_{\rm b,1}\mathcal{B}_{\overline{\nu}}, \tag{193}$$

where

$$\begin{aligned} \mathcal{B}_{\overline{\nu}} \;&=\; \sum_{\sigma=\pm1}\left(h^2_{\sigma,\sigma}(\overline{\nu})+\frac{1}{16}\Big[g^2_\sigma(\overline{\nu})+\tilde{g}^2_\sigma(\overline{\nu})\Big]\right) \\ &\quad +h^2_{+,-}(\overline{\nu})+\tilde{h}^2_{+,-}(\overline{\nu})+\frac{1}{64}g^2_0(\overline{\nu}). \end{aligned} \tag{194}$$

The three-center isotropic quartic spin-spin interactions proposed by Kostyuchenko may be written for the six g symmetries as

$$\mathcal{H}^g_{\rm t} \;=\; \mathcal{H}^g_{\rm t,1}+\mathcal{H}^g_{\rm t,2}, \tag{195}$$

$$\begin{aligned} \mathcal{H}^g_{\rm t,1} \;&=\; -\frac{1}{8}J^g_{\rm t,1}\sum_{n=1,3}\Big(\boldsymbol{S}_n\cdot\boldsymbol{S}_{n+1}+\boldsymbol{S}_{n+1}\cdot\boldsymbol{S}_n\Big) \\ &\quad \times\sum_{n'=2,4}\Big(\boldsymbol{S}_{n'}\cdot\boldsymbol{S}_{n'+1}+\boldsymbol{S}_{n'+1}\cdot\boldsymbol{S}_{n'}\Big) \\ &\quad +H.c., \end{aligned} \tag{196}$$

$$\mathcal{H}^g_{\rm t,2} \;=\; -\frac{1}{2}J^g_{\rm t,2}\Big(\boldsymbol{S}_1\cdot\boldsymbol{S}_3+\boldsymbol{S}_2\cdot\boldsymbol{S}_4\Big)$$

s	s_{13}	s_{24}	$a^+_{\overline{\nu}}$	$a^-_{\overline{\nu}}$	$b^+_{\overline{\nu}}$	$b^-_{\overline{\nu}}$	$c^+_{\overline{\nu}}$	$c^-_{\overline{\nu}}$	$\mathcal{B}_{\overline{\nu}}$	$\mathcal{T}_{\overline{\nu}}$
2	1	1	0	$\frac{1}{3}$	2	$-\frac{2}{3}$	$\frac{1}{6}$	$\frac{1}{6}$	$\frac{1}{4}$	$\frac{1}{4}$
1	1	1	0	-1	2	2	$-\frac{1}{2}$	$-\frac{1}{2}$	$\frac{5}{4}$	$\frac{1}{4}$
1	1	0	0	1	2	-2	$\frac{1}{2}$	0	$\frac{3}{2}$	-1
0	1	1	0	$\frac{11}{3}$	2	$\frac{2}{3}$	$\frac{11}{6}$	$\frac{11}{6}$	$\frac{7}{4}$	$\frac{1}{4}$
0	0	0	2	-1	2	-2	$\frac{1}{2}$	$\frac{1}{2}$	$\frac{3}{4}$	$-\frac{3}{4}$

TABLE IV: Values of $a^\pm_{\overline{\nu}}$, $b^\pm_{\overline{\nu}}$, $c^\pm_{\overline{\nu}}$, $\mathcal{B}_{\overline{\nu}}$, and $\mathcal{T}_{\overline{\nu}}$ for $s_1 = 1/2$.

$$\times \sum_{n=1}^{4} \Big(\boldsymbol{S}_n \cdot \boldsymbol{S}_{n+1} + \boldsymbol{S}_{n+1} \cdot \boldsymbol{S}_n \Big), \tag{197}$$

where for $g = T_d$, we have $J^{T_d}_{\mathrm{t},1} = J^{T_d}_{\mathrm{t},2} = -J_3$ in the notation of Kostyuchenko.[50] From our matrix elements above, it is then easy to see that

$$\begin{aligned} \langle \nu' | \mathcal{H}^g_{\mathrm{t},2} | \nu \rangle &= -\frac{g_0(\overline{\nu}) \delta_{\nu,\nu'}}{8} J^g_{\mathrm{t},2} \Big(s_{13}(s_{13}+1) \\ &\quad + s_{24}(s_{24}+1) - 4 s_1 (s_1+1) \Big), \end{aligned} \tag{198}$$

where $g_0(\overline{\nu})$ is given by Eq. (183). With regard to the matrix elements $\langle \nu' | \mathcal{H}^g_{\mathrm{t},1} | \nu \rangle$, we first note that

$$\sum_{n=2,4} \sin[(2n \pm 1)\pi/4] = \sum_{n=1,3} \sin[(2n \pm 1)\pi/4] = 0, \tag{199}$$

so that there are no contributions from g_σ and $\tilde{g}_\sigma$. The diagonal matrix elements $\langle \nu | \mathcal{H}^g_{\mathrm{t},1} | \nu \rangle$ is then easily found to be

$$\langle \nu | \mathcal{H}^g_{\mathrm{t},1} | \nu \rangle = -J^g_{\mathrm{t},1} \mathcal{T}_{\overline{\nu}}, \tag{200}$$

$$\begin{aligned} \mathcal{T}_{\overline{\nu}} &= \frac{g_0^2(\overline{\nu})}{64} - h^2_{+,-}(\overline{\nu}) - \tilde{h}^2_{+,-}(\overline{\nu}) \\ &\quad - \sum_{\sigma=\pm 1} h^2_{\sigma,\sigma}(\overline{\nu}). \end{aligned} \tag{201}$$

For $s_1 = 1/2$, the matrix $\langle \nu' | \mathcal{H}^g_{\mathrm{b},1} + \mathcal{H}^g_{\mathrm{t},1} | \nu \rangle$ is diagonal, so these interactions can be treated exactly. For $s_1 \geq 1$, since these quartic interactions preserve s, the resulting matrix is block diagonal, as noted by Kostyuchenko.[50] To the extent that the single-ion and exchange anisotropy interactions can be neglected or treated in first order only, the matrix of the resulting Hamiltonian is block diagonal. Kostyuchenko compiled a table of the diagonalized eigenstates for T_d symmetry with $s_1 = 1$, neglecting the anisotropy interactions. In Table IV, we calculated the exact eigenstates for $s_1 = 1$ of the above Hamiltonian for the six symmetries under consideration.

In Tables IV-VII, and VII-XI, we have listed analytic formulas for the coefficients $a^\pm_{\overline{\nu}}$, $b^\pm_{\overline{\nu}}$, and $c^\pm_{\overline{\nu}}$, and $\mathcal{B}_{\overline{\nu}}$ for the lowest four eigenstate manifolds of FM and AFM tetramers, respectively. In both cases, the manifolds are

s	s_{13}	s_{24}	$a^+_{\overline{\nu}}$	$a^-_{\overline{\nu}}$	$b^+_{\overline{\nu}}$	$b^-_{\overline{\nu}}$	$c^+_{\overline{\nu}}$	$c^-_{\overline{\nu}}$	$\mathcal{B}_{\overline{\nu}}$	$\mathcal{T}_{\overline{\nu}}$
4	2	2	$\frac{1}{7}$	$\frac{2}{7}$	$\frac{24}{7}$	$-\frac{8}{7}$	$\frac{3}{14}$	$\frac{3}{14}$	4	4
3	2	2	$\frac{1}{15}$	$\frac{2}{15}$	$\frac{24}{5}$	$\frac{8}{5}$	$\frac{1}{10}$	$\frac{1}{10}$	4	0
3	2	1	$\frac{1}{15}$	$\frac{2}{5}$	$\frac{24}{5}$	$-\frac{16}{5}$	$\frac{7}{30}$	$\frac{8}{45}$	$\frac{43}{9}$	$-\frac{7}{9}$
2	2	2	$-\frac{1}{7}$	$-\frac{2}{7}$	$\frac{124}{21}$	$\frac{80}{21}$	$-\frac{3}{14}$	$-\frac{3}{14}$	$\frac{23}{4}$	$\frac{9}{4}$
2	2	1	$\frac{1}{3}$	0	4	0	$\frac{1}{6}$	$-\frac{1}{18}$	$\frac{307}{36}$	$-\frac{55}{36}$
2	2	0	$\frac{1}{3}$	$\frac{2}{3}$	4	-4	$\frac{1}{2}$	0	7	-3
2	1	1	$-\frac{1}{3}$	$\frac{2}{3}$	$\frac{20}{3}$	$-\frac{16}{3}$	$\frac{1}{6}$	$\frac{1}{6}$	$\frac{31}{4}$	$-\frac{23}{4}$
1	2	2	$-\frac{7}{5}$	$-\frac{14}{5}$	$\frac{36}{5}$	$\frac{32}{5}$	$-\frac{21}{10}$	$-\frac{21}{10}$	$\frac{31}{4}$	$\frac{25}{4}$
1	2	1	$\frac{3}{5}$	$\frac{8}{5}$	$\frac{68}{15}$	$-\frac{32}{15}$	$\frac{11}{10}$	$-\frac{9}{10}$	$\frac{23}{4}$	$-\frac{1}{12}$
1	1	1	1	-2	4	0	$-\frac{1}{2}$	$-\frac{1}{2}$	$\frac{15}{4}$	$\frac{1}{4}$
1	1	0	-1	2	$\frac{20}{3}$	$-\frac{20}{3}$	$\frac{1}{2}$	0	9	$-\frac{23}{3}$
0	2	2	3	6	$\frac{16}{3}$	$\frac{8}{3}$	$\frac{9}{2}$	$\frac{9}{2}$	$\frac{32}{3}$	$\frac{22}{3}$
0	1	1	$-\frac{11}{3}$	$\frac{22}{3}$	$\frac{16}{3}$	$-\frac{8}{3}$	$\frac{11}{6}$	$\frac{11}{6}$	8	-6
0	0	0	$\frac{11}{3}$	$-\frac{8}{3}$	$\frac{16}{3}$	$-\frac{16}{3}$	$\frac{1}{2}$	$\frac{1}{2}$	$\frac{16}{3}$	$-\frac{16}{3}$

TABLE V: Values of $a^\pm_{\overline{\nu}}$, $b^\pm_{\overline{\nu}}$, $c^\pm_{\overline{\nu}}$, $\mathcal{B}_{\overline{\nu}}$ and $\mathcal{T}_{\overline{\nu}}$ for $s_1 = 1$.

$\overline{\nu} = s s_{13} s_{24}$	$E_{\overline{\nu}}$
422	$-4\tilde{J}_g - 6\tilde{J}'_g - 4J^g_{\mathrm{b},1} - 2J^g_{\mathrm{b},2} - 4J^g_{\mathrm{t},1} - 8J^g_{\mathrm{t},2}$
322	$-6\tilde{J}'_g - 4J^g_{\mathrm{b},1} - 2J^g_{\mathrm{b},2}$
312,321	$-2\tilde{J}_g - 4\tilde{J}'_g - \frac{43}{9}J^g_{\mathrm{b},1} - 2J^g_{\mathrm{b},2} + \frac{7}{9}J^g_{\mathrm{t},1}$
212,221	$\tilde{J}_g - 4\tilde{J}'_g - \frac{307}{36}J^g_{\mathrm{b},1} - 2J^g_{\mathrm{b},2} + \frac{55}{36}J^g_{\mathrm{t},1}$
211	$-\tilde{J}_g - 2\tilde{J}'_g - \frac{31}{4}J^g_{\mathrm{b},1} - 2J^g_{\mathrm{b},2} + \frac{23}{4}J^g_{\mathrm{t},1} + 2J^g_{\mathrm{t},2}$
222,202,220	$-3\tilde{J}'_g - 4J^g_{\mathrm{b},1} - 5J^g_{\mathrm{b},2}$, $E_{2\pm}$
122	$2\tilde{J}_g - 3\tilde{J}'_g - \frac{31}{4}J^g_{\mathrm{b},1} - 2J^g_{\mathrm{b},2} - \frac{25}{4}J^g_{\mathrm{t},1} + 10J^g_{\mathrm{t},2}$
111	$\tilde{J}_g - 2\tilde{J}'_g - \frac{15}{4}J^g_{\mathrm{b},1} - 2J^g_{\mathrm{b},2} - \frac{1}{4}J^g_{\mathrm{t},1} - 2J^g_{\mathrm{t},2}$
121,101	$E_{1\pm}$
112,110	$E_{1\pm}$
011	$-2\tilde{J}_g + 2\tilde{J}'_g - 8J^g_{\mathrm{b},1} - 2J^g_{\mathrm{b},2} + 6J^g_{\mathrm{t},1} - 4J^g_{\mathrm{t},2}$
022,000	$E_{0\pm}$

TABLE VI: Eigenstate energies $E_{\overline{\nu}}$ for $s_1 = 1$ as a function of the quantum numbers $\overline{\nu} = s, s_{13}, s_{24}$ in the absence of anisotropy interactions. The two additional $s = 2$ eigenstate energies $E_{2\pm} = \frac{1}{2}[a \pm \sqrt{b^2 + 56(J^g_{\mathrm{b},1})^2}]$, where $a = 3\tilde{J}_g - 9\tilde{J}'_g - \frac{63}{4}J^g_{\mathrm{b},1} - 7J^g_{\mathrm{b},2} + \frac{15}{4}J^g_{\mathrm{t},1} + 6J^g_{\mathrm{t},2}$ and $b = 3\tilde{J}_g - 3\tilde{J}'_g + \frac{17}{4}J^g_{\mathrm{b},1} + 3J^g_{\mathrm{b},2} - \frac{33}{4}J^g_{\mathrm{t},1} + 6J^g_{\mathrm{t},2}$. The two sets of doubly-degenerate $s = 1$ eigenstates have $E_{1\pm} = \frac{1}{2}[A + B \pm \sqrt{(A-B)^2 + 4C^2}]$, where $A = 3\tilde{J}_g - 4\tilde{J}'_g - \frac{23}{4}J^g_{\mathrm{b},1} - 2J^g_{\mathrm{b},2} + \frac{1}{12}J^g_{\mathrm{t},1}$, $B = -\tilde{J}'_g - 9J^g_{\mathrm{b},1} - 5J^g_{\mathrm{b},2} + \frac{23}{3}J^g_{\mathrm{t},1}$, and $C = \frac{\sqrt{5}}{3}(3J^g_{\mathrm{b},1} - 4J^g_{\mathrm{t},1})$, and $E_{0\pm} = \frac{1}{2}[\alpha + \beta \pm \sqrt{(\alpha-\beta)^2 + 4\gamma^2}]$, where $\alpha = -6\tilde{J}_g + 6\tilde{J}'_g - \frac{32}{3}J^g_{\mathrm{b},1} - 2J^g_{\mathrm{b},2} - \frac{22}{3}J^g_{\mathrm{t},1} + 12J^g_{\mathrm{t},2}$, $\beta = \frac{16}{3}(J^g_{\mathrm{t},1} - J^g_{\mathrm{b},1}) - 8J^g_{\mathrm{b},2}$, and $\gamma = \frac{4\sqrt{5}}{3}(J^g_{\mathrm{t},1} - J^g_{\mathrm{b},1})$.

s, s_{13}, s_{24}	a_ν^+	a_ν^-
$4s_1, 2s_1, 2s_1$	$\frac{2s_1-1}{8s_1-1}$	$\frac{2s_1}{8s_1-1}$
$4s_1-1, 2s_1, 2s_1$	$\frac{(2s_1-1)(4s_1-3)}{(4s_1-1)(8s_1-3)}$	$\frac{2s_1(4s_1-3)}{(4s_1-1)(8s_1-3)}$
$4s_1-1, 2s_1, 2s_1-1$	$\frac{(2s_1-1)(4s_1-3)}{(4s_1-1)(8s_1-3)}$	$\frac{2s_1}{8s_1-3}$
$4s_1-2, 2s_1, 2s_1$	$\frac{(2s_1-1)a_1(s_1)}{(4s_1-1)(8s_1-1)}$	$\frac{2s_1a_1(s_1)}{(4s_1-1)(8s_1-1)}$
	$\times\frac{1}{(8s_1-5)}$	$\times\frac{1}{(8s_1-5)}$
$4s_1-2, 2s_1, 2s_1-1$	$\frac{a_2(s_1)}{(2s_1-1)(4s_1-1)}$	$\frac{4s_1(s_1-1)}{(2s_1-1)(8s_1-5)}$
	$\times\frac{1}{(8s_1-5)}$	
$4s_1-2, 2s_1, 2s_1-2$	$\frac{a_2(s_1)}{(2s_1-1)(4s_1-1)}$	$\frac{2a_3(s_1)}{(2s_1-1)(4s_1-1)}$
	$\times\frac{1}{(8s_1-5)}$	$\times\frac{1}{(8s_1-5)}$
$4s_1-2, 2s_1-1, 2s_1-1$	$\frac{2s_1-3}{8s_1-5}$	$\frac{2s_1}{8s_1-5}$
$4s_1-3, 2s_1, 2s_1$	$\frac{(2s_1-1)(8s_1-15)}{(8s_1-3)(8s_1-7)}$	$\frac{2s_1(8s_1-15)}{(8s_1-3)(8s_1-7)}$
$4s_1-3, 2s_1, 2s_1-1$	$\frac{a_4(s_1)}{(4s_1-3)^2(2s_1-1)}$	$\frac{4s_1a_5(s_1)}{(4s_1-3)^2(2s_1-1)}$
	$\times\frac{1}{(4s_1-1)(8s_1-3)}$	$\times\frac{1}{(4s_1-1)(8s_1-3)}$
	$\times\frac{1}{(8s_1-7)}$	$\times\frac{1}{(8s_1-7)}$
$4s_1-3, 2s_1, 2s_1-2$	$\frac{a_6(s_1)}{(2s_1-1)(4s_1-3)}$	$\frac{a_7(s_1)}{(2s_1-1)(4s_1-3)}$
	$\times\frac{1}{(8s_1-7)}$	$\times\frac{1}{(8s_1-7)}$
$4s_1-3, 2s_1, 2s_1-3$	$\frac{(2s_1-1)a_8(s_1)}{(4s_1-3)^2(8s_1-7)}$	$\frac{2a_9(s_1)}{(4s_1-3)^2(8s_1-7)}$
$4s_1-3, 2s_1-1, 2s_1-1$	$\frac{(2s_1-3)((4s_1-5)}{(4s_1-3)(8s_1-7)}$	$\frac{2s_1(4s_1-5)}{(4s_1-3)(8s_1-7)}$
$4s_1-3, 2s_1-1, 2s_1-2$	$\frac{a_{10}(s_1)}{(4s_1-1)(4s_1-3)}$	$\frac{2a_{11}(s_1)}{(4s_1-1)(4s_1-3)}$
	$\times\frac{1}{(8s_1-7)}$	$\times\frac{1}{(8s_1-7)}$

TABLE VII: Values of $a_\nu^\pm$ for the ground and first three excited state manifolds for FM tetramers (or the highest four excited state manifolds of AFM tetramers), where $a_1(x) = 32x^2-44x+3$, $a_2(x) = 16x^3-36x^2+26x-3$, and $a_3(x) = 8x^3-6x^2+2x-1$, $a_4(x) = 2048x^6-9472x^5+17344x^4-15440x^3+6924x^2-1530x+135$, $a_5(x) = 512x^5-1856x^4+2416x^3-1420x^2+399x-45$ $a_6(x) = 16x^3-52x^2+58x-9$, $a_7(x) = 4x^3-7x^2+3x-1$, $a_8(x) = 16x^2-48x+45$, $a_9(x) = 16x^3-24x^2+15x-9$, $a_{10}(x) = 32x^3-96x^2+70x-9$, and $a_{11}(x) = 16x^3-16x^2+5x-2$.

restricted by $0 \le s_{13}, s_{24} \le 2s_1$ and $|s_{13}-s_{24}| \le s \le s_{13}+s_{24}$. In addition, the coefficients are symmetric under $s_{13} \leftrightarrow s_{24}$. Hence, for $s_1 = 1/2$, the five distinct allowed (s, s_{13}, s_{24}) states are (0,0,0), (0,1,1), (1,1,0), (1,1,1), and (2,1,1). For $s_1 = 1$, the fourteen distinct allowed (s, s_{13}, s_{24}) states are (0,0,0), (0,1,1), (0,2,2), (1,1,0), (1,1,1), (1,2,1), (1,2,2), (2,1,1), (2,2,0), (2,2,1), (2,2,2), (3,2,1), (3,2,2), and (4,2,2). From these tables, the coefficients $a_\nu^\pm$, $b_\nu^\pm$, and $c_\nu^\pm$, and $\mathcal{B}_\nu$ for all of the allowed eigenstates of tetramers with $s_1 \le 3/2$ are given. For $s_1 = 2$, the values for the nine states with $s = 4$ cannot be obtained from these formulas, but the values for the other 46 eigenstates with $0 \le s \le 3$ and $4 \le s \le 8$ are given.

s, s_{13}, s_{24}	b_ν^+	b_ν^-
$4s_1, 2s_1, 2s_1$	$\frac{24s_1^2}{8s_1-1}$	$-\frac{8s_1^2}{8s_1-1}$
$4s_1-1, 2s_1, 2s_1$	$\frac{8s_1(5s_1-2)}{8s_1-3}$	$\frac{8s_1^2}{8s_1-3}$
$4s_1-1, 2s_1, 2s_1-1$	$\frac{8s_1(5s_1-2)}{8s_1-3}$	$-\frac{8s_1(3s_1-1)}{8s_1-3}$
$4s_1-2, 2s_1, 2s_1$	$\frac{4(112s_1^3-102s_1^2+22s_1-1)}{(8s_1-1)(8s_1-5)}$	$\frac{8s_1(24s_1^2-15s_1+1)}{(8s_1-1)(8s_1-5)}$
$4s_1-2, 2s_1, 2s_1-1$	$\frac{4(14s_1^2-12s_1+1)}{8s_1-5}$	$-\frac{8s_1(s_1-1)}{8s_1-5}$
$4s_1-2, 2s_1, 2s_1-2$	$\frac{4(14s_1^2-12s_1+1)}{8s_1-5}$	$-\frac{4(10s_1^2-8s_1+1)}{8s_1-5}$
$4s_1-2, 2s_1-1, 2s_1-1$	$\frac{4(14s_1^2-10s_1+1)}{8s_1-5}$	$-\frac{8s_1(5s_1-3)}{8s_1-5}$
$4s_1-3, 2s_1, 2s_1$	$\frac{12(48s_1^3-74s_1^2+34s_1-5)}{(8s_1-3)(8s_1-7)}$	$\frac{8s_1(40s_1^2-51s_1+15)}{(8s_1-3)(8s_1-7)}$
$4s_1-3, 2s_1, 2s_1-1$	$\frac{4b_1(s_1)}{(4s_1-1)(4s_1-3)}$	$\frac{8s_1b_2(s_1)}{(4s_1-1)(4s_1-3)}$
	$\times\frac{1}{(8s_1-3)(8s_1-7)}$	$\times\frac{1}{(8s_1-3)(8s_1-7)}$
$4s_1-3, 2s_1, 2s_1-2$	$\frac{12(6s_1^2-8s_1+1)}{8s_1-7}$	$-\frac{4(6s_1^2-8s_1+1)}{8s_1-7}$
$4s_1-3, 2s_1, 2s_1-3$	$\frac{12(24s_1^2-50s_1^2+30s_1-5)}{(4s_1-3)(8s_1-7)}$	$-\frac{4b_3(s_1)}{(4s_1-3)(8s_1-7)}$
$4s_1-3, 2s_1-1, 2s_1-1$	$\frac{4(18s_162-22s_1+5)}{8s_1-7}$	$-\frac{24s_1(s_1-1)}{8s_1-7}$
$4s_1-3, 2s_1-1, 2s_1-2$	$\frac{4(72s_1^3-98s_1^2+34s_1-3)}{(4s_1-1)(8s_1-7)}$	$-\frac{4b_4(s_1)}{(4s_1-1)(8s_1-7)}$

TABLE VIII: Values of $b_\nu^\pm$ for the ground and first three excited state manifolds for FM tetramers (or the highest four excited state manifolds of AFM tetramers), where $b_1(x) = 2304x^5-6112x^4+5968x^3-2650x^2+552x-45$, $b_2(x) = 1024x^4-2304x^3+1808x^2-576x+63$, $b_3(x) = 56x^3-114x^2+72x-15$, $b_4(x) = 56x^3-70x^2+20x-1$.

For Types I and II tetramers, the sth AFM level-crossing induction in the first-order approximation may be written as

$$\begin{aligned}
\gamma B_{s_1,s}^{g,\mathrm{lc}(1)}(\theta) \;=\; & -\tilde{J}_g s - \Theta(\tilde{J}'_g-\tilde{J}_g)2ss_1^2J_{\mathrm{t},2}^g \\
& +\Theta(\tilde{J}_g-\tilde{J}'_g)\Big(\Big(\tilde{J}_g-\tilde{J}'_g \\
& +2s_1(s_1+1)J_{\mathrm{b},2}^g\Big)E\Big(\frac{s+1}{2}\Big) \\
& -J_{\mathrm{b},2}^g\Big[E\Big(\frac{s+1}{2}\Big)\Big]^3 \\
& -J_{\mathrm{t},2}^g E\Big(\frac{s}{2}\Big)\Big[sE\Big(\frac{s+1}{2}\Big)-2s_1(s_1+1)\Big]\Big) \\
& -\frac{J_z^g}{2}(a_2^+ + 2b^+ + a_1^+\cos^2\theta) \\
& +\frac{J_{1,z}^g}{2}[c_2^- + \frac{1}{2}(b^+ + b^-) + c_1^-\cos^2\theta)] \\
& +\frac{J_{2,z}^g}{4}(a_2^- + b^- + a_1^-\cos^2\theta) \\
& -J_{\mathrm{b},1}^g d - J_{\mathrm{t},1}^g e, \qquad (202)
\end{aligned}$$

$\Theta(s)$ is the standard Heaviside step function, $E(x)$ is the largest integer in x and the level-crossing parameters $a_j^\pm$, $b^\pm$, and c_j^- for $j = 1, 2$ and d are functions of s, s_1 and the tetramer type. For Type II, the functions are different

s, s_{13}, s_{24}	c_ν^+	c_ν^-
$4s_1, 2s_1, 2s_1$	$\frac{4s_1-1}{2(8s_1-1)}$	$\frac{4s_1-1}{2(8s_1-1)}$
$4s_1-1, 2s_1, 2s_1$	$\frac{4s_1-3}{2(8s_1-3)}$	$\frac{4s_1-3}{2(8s_1-3)}$
$4s_1-1, 2s_1, 2s_1-1$	$\frac{16s_1^2-12s_1+3}{2(4s_1-1)(8s_1-3)}$	$\frac{8s_1(2s_1-1)^2}{(4s_1-1)^2(8s_1-3)}$
$4s_1-2, 2s_1, 2s_1$	$\frac{32s_1^2-44s_1+3}{2(8s_1-1)(8s_1-5)}$	$\frac{32s_1^2-44s_1+3}{2(8s_1-1)(8s_1-5)}$
$4s_1-2, 2s_1, 2s_1-1$	$\frac{c_1(s_1)}{2(2s_1-1)(4s_1-1)}$	$\frac{c_2(s_1)}{2(2s_1-1)^2(4s_1-1)^2}$
	$\times\frac{1}{(8s_1-5)}$	$\times\frac{1}{(8s_1-5)}$
$4s_1-2, 2s_1, 2s_1-2$	$\frac{8s_1^2-10s_1+5}{2(2s_1-1)(8s_1-5)}$	$\frac{2s_1(4s_1^2-7s_1+3)}{(2s_1-1)^2(8s_1-5)}$
$4s_1-2, 2s_1-1, 2s_1-1$	$\frac{4s_1-3}{2(8s_1-5)}$	$\frac{4s_1-3}{2(8s_1-5)}$
$4s_1-3, 2s_1, 2s_1$	$\frac{(4s_1-1)(8s_1-15)}{2(8s_1-3)(8s_1-7)}$	$\frac{(4s_1-1)(8s_1-15)}{2(8s_1-3)(8s_1-7)}$
$4s_1-3, 2s_1, 2s_1-1$	$\frac{c_3(s_1)}{2(2s_1-1)(4s_1-3)}$	$\frac{c_4(s_1)}{2(2s_1-1)^2(4s_1-3)^2}$
	$\times\frac{1}{(8s_1-3)(8s_1-7)}$	$\times\frac{1}{(8s_1-3)(8s_1-7)}$
$4s_1-3, 2s_1, 2s_1-2$	$\frac{(4s_1-1)}{2(2s_1-1)(4s_1-3)}$	$\frac{2(s_1-1)(4s_1-1)}{(2s_1-1)^2(4s_1-3)^2}$
	$\times\frac{(8s_1^2-18s_1+3)}{(8s_1-7)}$	$\times\frac{(16s_1^3-40s_1^2+29s_1-8)}{(8s_1-7)}$
$4s_1-3, 2s_1, 2s_1-3$	$\frac{16s_1^2-28s_1+21}{2(4s_1-3)(8s_1-7)}$	$\frac{16s_1(s_1-1)(2s_1-3)}{(4s_1-3)^2(8s_1-7)}$
$4s_1-3, 2s_1-1, 2s_1-1$	$\frac{4s_1-5}{2(8s_1-7)}$	$\frac{4s_1-5}{2(8s_1-7)}$
$4s_1-3, 2s_1-1, 2s_1-2$	$\frac{16s_1^2-28s_1+13}{2(4s_1-3)(8s_1-7)}$	$\frac{16(s_1-1)^2(2s_1-1)}{(4s_1-3)^2(8s_1-7)}$

TABLE IX: Values of $c_\nu^\pm$ for the ground and first three excited state manifolds for FM tetramers (or the highest four excited state manifolds of AFM tetramers), where $c_1(x) = 32x^3 - 56x^2 + 30x - 3$ and $c_2(x) = 256x^5 - 640x^4 + 576x^3 - 240x^2 + 48x - 3$, $c_3(x) = 256x^4 - 800x^3 + 840x^2 - 330x + 45$, $c_4(x) = 2048x^6 - 8960x^5 + 15232x^4 - 13120x^3 + 6096x^2 - 1440x + 135$.

for even and odd s.

The AFM level-crossing parameters are defined according to

$$\begin{aligned}
a_1^\pm &= s(2s-1)a^{s_1,\pm}_{s,s_{13},s_{24}} \\
&\quad -(s-1)(2s-3)a^{s_1,\pm}_{s-1,s'_{13},s'_{24}}, && (203)\\
a_2^\pm &= sa^{s_1,\pm}_{s,s_{13},s_{24}} - (s-1)a^{s_1,\pm}_{s-1,s'_{13},s'_{24}}, && (204)\\
b^\pm &= b^{s_1,\pm}_{s,s_{13},s_{24}} - b^{s_1,\pm}_{s-1,s'_{13},s'_{24}}, && (205)\\
c_1^- &= s(2s-1)c^{s_1,-}_{s,s_{13},s_{24}} \\
&\quad -(s-1)(2s-3)c^{s_1,-}_{s-1,s'_{13},s'_{24}}, && (206)\\
c_2^- &= sc^{s_1,-}_{s,s_{13},s_{24}} - (s-1)c^{s_1,-}_{s-1,s'_{13},s'_{24}}, && (207)\\
d &= \mathcal{B}_{\overline{\nu}} - \mathcal{B}_{\overline{\nu}'}, && (208)\\
e &= \mathcal{T}_{\overline{\nu}} - \mathcal{T}_{\overline{\nu}'}, && (209)
\end{aligned}$$

where

$$\overline{\nu}' = \{s-1, s'_{13}, s'_{24}, s_1\} \qquad (210)$$

and the s'_{13}, s'_{24} values depend upon the tetramer type. In the next two sections, we evaluate the $a_j^\pm$, $b^\pm$ and

s, s_{13}, s_{24}	a_ν^+	a_ν^-
$0, x, x$	$\frac{\tilde{a}_1(x)[\tilde{a}_2(x)-4s_1(s_1+1)]}{3(2x+3)(2x-1)}$	$\frac{\tilde{a}_1(x)[x+x^2+4s_1(s_1+1)]}{3(2x+3)(2x-1)}$
$1, x, x$	$\frac{-\tilde{a}_2(x)+4s_1(s_1+1)}{5}$	$-\frac{x+x^2+4s_1(s_1+1)}{5}$
$1, x, x-1$	$\frac{\tilde{a}_3(x)-4s_1(s_1+1)(1+2x^2)}{5(4x^2-1)}$	$\frac{4x^2+2x^4+4s_1(s_1+1)(1+2x^2)}{5(4x^2-1)}$
$2, x, x$	$\frac{\tilde{a}_4(x)[\tilde{a}_5(x)+4s_1(s_1+1)]}{21(2x+3)(2x-1)}$	$-\frac{\tilde{a}_4(x)[x^2+x+4s_1(s_1+1)]}{21(2x+3)(2x-1)}$
$2, x, x-1$	$\frac{\tilde{a}_6(x)-4s_1(s_1+1)(5-2x^2)}{21(4x^2-1)}$	$\frac{\tilde{a}_7(x)+4s_1(s_1+1)(5-2x^2)}{21(4x^2-1)}$
$2, x, x-2$	$-\frac{3(-3+x+x^2)+4s_1(s_1+1)}{21}$	$\frac{4-x+x^2+4s_1(s_1+1)}{21}$
$3, x, x$	$\frac{\tilde{a}_8(x)[-3\tilde{a}_2(x)+4s_1(s_1+1)]}{45(2x+3)(2x-1)}$	$-\frac{\tilde{a}_8(x)[x+x^2+4s_1(s_1+1)]}{45(2x+3)(2x-1)}$
$3, x, x-1$	$\frac{\tilde{a}_9(x)+8s_1(s_1+1)\tilde{a}_{10}(x)}{30(4x^2-1)(4x^2-9)}$	$-\frac{\tilde{a}_{11}(x)+8s_1(s_1+1)\tilde{a}_{10}(x)}{30(4x^2-1)(4x^2-9)}$
$3, x, x-2$	$\frac{1}{2}$	$\frac{1}{6}$
$3, x, x-3$	$\frac{\tilde{a}_{12}(x)-8s_1(s_1+1)x(x-2)}{18(2x-1)(2x-3)}$	$\frac{\tilde{a}_{13}(x)+8s_1(s_1+1)x(x-2)}{18(2x-1)(2x-3)}$

TABLE X: Values of $a_\nu^\pm$ for the ground and first three excited state manifolds for AFM tetramers (or the highest four excited state manifolds of FM tetramers), where x represents any value of s_{13} that satisfies $0 \le s_{13}, s_{24} \le 2s_1$ and $|s_{13} - s_{24}| \le s \le s_{13} + s_{24}$, and $\tilde{a}_1(x) = 3 + 4x + 4x^2$, $\tilde{a}_2(x) = 3(-1 + x + x^2)$, $\tilde{a}_3(x) = -3 + 6x^2 + 6x^4$, $\tilde{a}_4(x) = (2x+5)(2x-3)$, $\tilde{a}_5(x) = 3(1 - x - x^2)$, $\tilde{a}_6(x) = 3(5 - 16x^2 + 2x^4)$, $\tilde{a}_7(x) = 2x^2(7 - x^2)$, $\tilde{a}_8(x) = -33 + 4x + 4x^2$, $\tilde{a}_9(x) = 198 - 729x^2 + 330x^4 - 24x^6$, $\tilde{a}_{10}(x) = 33 - 37x^2 + 4x^4$, $\tilde{a}_{11}(x) = 169x^2 - 102x^4$, $\tilde{a}_{12}(x) = 27 - 78x + 63x^2 - 24x^3 + 6x^4$, and $\tilde{a}_{13}(x) = 9 - 30x + 23x^2 - 8x^3 + 2x^4$.

$c_j^\pm$ for Type I and Type II AFM tetramers. The NN biquadratic exchange level-crossing parameter d has differently complicated forms for Type I and Type II AFM tetramers, the general forms of which are not given for brevity.

For $s_1 = 1/2$, the Types I and II first-order level-crossing inductions $\gamma B^{g,\mathrm{lc}(1)}_{1/2,s}(\theta)$ are given in the text. In that simple example, there are no effects of single-ion anisotropy. Hence to illustrate the full dependencies on all of the microscopic parameters, we list the $s_1 = 1$ first-order level-crossing inductions. For Type I, we have

$$\begin{aligned}
\gamma B^{g,\mathrm{lc}(1)}_{1,1}(\theta) &= -\tilde{J}_g + \frac{1}{12}(35J^g_{\mathrm{b},1} + 13J^g_{\mathrm{t},1}) - 2J^g_{\mathrm{t},2} \\
&\quad -J^g_z\Big(\frac{7}{6} - \frac{7}{10}\cos^2\theta\Big) \\
&\quad +\frac{7}{10}J^g_{\mathrm{eff}}(1 - 3\cos^2\theta), && (211)\\
\gamma B^{g,\mathrm{lc}(1)}_{1,2}(\theta) &= -2\tilde{J}_g + 2J^g_{\mathrm{b},1} + J^g_z\Big(\frac{31}{42} - \frac{19}{70}\cos^2\theta\Big) \\
&\quad +4J^g_{\mathrm{t},1} - 4J^g_{\mathrm{t},2} - \frac{19}{70}J^g_{\mathrm{eff}}(1 - 3\cos^2\theta), && (212)\\
\gamma B^{g,\mathrm{lc}(1)}_{1,3}(\theta) &= -3\tilde{J}_g + \frac{1}{4}(7J^g_{\mathrm{b},1} - 9J^g_{\mathrm{t},1}) - 6J^g_{\mathrm{t},2} \\
&\quad +J^g_z\Big(\frac{181}{210} - \frac{13}{14}\cos^2\theta\Big)
\end{aligned}$$

s, s_{13}, s_{24}	b_{ν}^{+}	b_{ν}^{-}
$0, x, x$	$\frac{8s_1(s_1+1)}{3}$	$\frac{4x(x+1)-8s_1(s_1+1)}{3}$
$1, x, x$	$\frac{4[-1+x+x^2+2s_1(s_1+1)]}{5}$	$\frac{8[x(x+1)-s_1(s_1+1)]}{5}$
$1, x, x-1$	$\frac{4[\tilde{b}_1(x)-2s_1(s_1+1)(1-8x^2)]}{5(4x^2-1)}$	$\frac{4[\tilde{b}_2(x)+2s_1(s_1+1)(1-8x^2)]}{5(4x^2-1)}$
$2, x, x$	$\frac{\tilde{b}_3(x)+8s_1(s_1+1)\tilde{b}_4(x)}{21(2x+3)(2x-1)}$	$\frac{\tilde{b}_5(x)-8s_1(s_1+1)\tilde{b}_4(x)}{21(2x+3)(2x-1)}$
$2, x, x-1$	$\frac{4[\tilde{b}_6(x)+2s_1(s_1+1)(1+8x^2)]}{7(4x^2-1)}$	$-\frac{4[\tilde{b}_7(x)+2s_1(s_1+1)(1+8x^2)]}{7(4x^2-1)}$
$2, x, x-2$	$\frac{4[-3+x-x^2+6s_1(s_1+1)]}{7}$	$\frac{4[1-2x+2x^2-6s_1(s_1+1)]}{7}$
$3, x, x$	$\frac{8[\tilde{b}_8(x)+s_1(s_1+1)\tilde{b}_9(x)]}{45(2x+3)(2x-1)}$	$-\frac{4[\tilde{b}_{10}(x)+2s_1(s_1+1)\tilde{b}_9(x)]}{45(2x+3)(2x-1)}$
$3, x, x-1$	$\frac{4[\tilde{b}_{11}(x)-2s_1(s_1+1)\tilde{b}_{12}(x)]}{15(4x^2-1)(4x^2-9)}$	$\frac{8[\tilde{b}_{13}(x)+s_1(s_1+1)\tilde{b}_{12}(x)]}{15(4x^2-1)(4x^2-9)}$
$3, x, x-2$	$\frac{4[-3+2s_1(s_1+1)]}{3}$	$-\frac{4[x(1-x)+2s_1(s_1+1)]}{3}$
$3, x, x-3$	$\frac{4[\tilde{b}_{14}(x)+2s_1(s_1+1)\tilde{b}_{15}(x)]}{9(2x-3)(2x-1)}$	$-\frac{8[\tilde{b}_{16}(x)+s_1(s_1+1)\tilde{b}_{15}(x)]}{9(2x-3)(2x-1)}$

TABLE XI: Values of $b_{\nu}^{\pm}$ for the ground and first three excited state manifolds for AFM tetramers (or the highest four excited state manifolds of FM tetramers), where $\tilde{b}_1(x) = 1 - 2x^2 - 2x^4$, $\tilde{b}_2(x) = -3x^2(1-2x^2)$, $\tilde{b}_3(x)12(15 - 19x - 15x^2 + 8x^3 + 4x^4)$, $\tilde{b}_4(x) = 9 + 20x + 20x^2$, $\tilde{b}_5(x) = -16x(9 + x - 16x^2 - 8x^3)$, $\tilde{b}_6(x) = 5 - 16x^2 + 2x^4$, $\tilde{b}_7(x) = 7x^2 - 10x^4$, $\tilde{b}_8(x) = 3(33 - 37x - 33x^2 + 8x^3 + 4x^4)$, $\tilde{b}_9(x) = 87 + 44x + 44x^2$, $\tilde{b}_{10}(x) = x(111 + 43x - 136x^2 - 68x^3)$, $\tilde{b}_{11}(x) = 3(-66 + 243x^2 - 110x^4 + 8x^6)$, $\tilde{b}_{12}(x) = 87 + 52x^2 - 64x^4$, $\tilde{b}_{13}(x) = x^2(107 - 151x^2 + 44x^4)$, $\tilde{b}_{14}(x) = -3(9 - 26x + 21x^2 - 8x^3 + 2x^4)$, $\tilde{b}_{15}(x) = 9 - 32x + 16x^2$, and $\tilde{b}_{16}(x) = -9 + 30x - 35x^2 + 20x^3 - 5x^4$.

s, s_{13}, s_{24}	c_{ν}^{+}	c_{ν}^{-}
$0, x, x$	$\frac{3+4x+4x^2}{6}$	$\frac{3+4x+4x^2}{6}$
$1, x, x$	$\frac{3-4x-4x^2}{6}$	$\frac{3-4x-4x^2}{6}$
$1, x, x-1$	$\frac{3+2x^2}{10}$	$\frac{3(1-x^2)}{10}$
$2, x, x$	$\frac{15-4x-4x^2}{42}$	$\frac{15-4x-4x^2}{42}$
$2, x, x-1$	$\frac{15-2x^2}{42}$	$\frac{15+x^2}{42}$
$2, x, x-2$	$\frac{13-4x+4x^2}{42}$	$\frac{8(2+x-x^2)}{63}$
$3, x, x$	$\frac{33-4x-4x^2}{90}$	$\frac{33-4x-4x^2}{90}$
$3, x, x-1$	$\frac{11-x^2}{30}$	$\frac{132-17x^2}{360}$
$3, x, x-2$	$\frac{1}{3}$	$\frac{23+4x-4x^2}{72}$
$3, x, x-3$	$\frac{6-2x+x^2}{18}$	$\frac{5(3+2x-x^2)}{72}$

TABLE XII: Values of $c_{\nu}^{\pm}$ for the ground and first three excited state manifolds for AFM tetramers (or the highest four excited state manifolds of FM tetramers).

$$-\frac{13}{14}J^g_{\rm eff}(1-3\cos^2\theta), \tag{213}$$

$$\begin{aligned}\gamma B^{g,{\rm lc}(1)}_{1,4}(\theta) &= -4\tilde{J}_g - 4J^g_{\rm t,1} + J^g_z\Big(\frac{83}{70} - \frac{3}{2}\cos^2\theta\Big)\\ &\quad -8J^g_{\rm t,2} - \frac{3}{2}J^g_{\rm eff}(1-3\cos^2\theta).\end{aligned} \tag{214}$$

The Type II first-order level-crossing inductions for $s_1 = 1$ are

$$\begin{aligned}\gamma B^{g,{\rm lc}(1)}_{1,1}(\theta) &= -\tilde{J}'_g - \frac{1}{3}(11J^g_{\rm b,1} + 9J^g_{\rm t,1}) + 3J^g_{\rm b,2}\\ &\quad -\frac{J^g_z}{6}(5-3\cos^2\theta) + \frac{J^g_{2,z}}{6}(1+3\cos^2\theta),\end{aligned} \tag{215}$$

$$\begin{aligned}\gamma B^{g,{\rm lc}(1)}_{1,2}(\theta) &= -\tilde{J}_g - \tilde{J}'_g + \frac{1}{12}(15J^g_{\rm b,1} + 23J^g_{\rm t,1})\\ &\quad +\frac{J^g_z}{2}(5+\cos^2\theta) + \frac{J^g_{1,z}}{2}(1+\cos^2\theta)\\ &\quad +3J^g_{\rm b,2} + 2J^g_{\rm t,2} + \frac{J^g_{2,z}}{6}(1+3\cos^2\theta),\end{aligned} \tag{216}$$

$$\begin{aligned}\gamma B^{g,{\rm lc}(1)}_{1,3}(\theta) &= -\tilde{J}_g - 2\tilde{J}'_g + \frac{1}{36}(107J^g_{\rm b,1} + 179J^g_{\rm t,1})\\ &\quad +J^g_z\Big(\frac{43}{30} - \frac{3}{2}\cos^2\theta\Big) + \frac{J^g_{1,z}}{6}(1+5\cos^2\theta)\\ &\quad -2J^g_{\rm t,2} + \frac{J^g_{2,z}}{2}(1+\cos^2\theta),\end{aligned} \tag{217}$$

$$\begin{aligned}\gamma B^{g,{\rm lc}(1)}_{1,4}(\theta) &= -2\tilde{J}_g - 2\tilde{J}'_g + \frac{1}{9}(7J^g_{\rm b,1} - 29J_{\rm t,1}) - 8J^g_{\rm t,2}\\ &\quad +J^g_z\Big(\frac{83}{70} - \frac{3}{2}\cos^2\theta\Big) + \frac{J^g_{1,z}}{3}(1+5\cos^2\theta)\\ &\quad +\frac{J^g_{2,z}}{2}(1+\cos^2\theta).\end{aligned} \tag{218}$$

G. Type I First-order AFM level-crossing constants

The Type I constants are relevant for both $\tilde{J}'_g - \tilde{J}_g > 0$ AFM level-crossing inductions and for some low energy FM manifold states (with $\tilde{J}'_g > \tilde{J}_g > 0$). The low-energy states within an arbitrary s manifold have $s_{13} = s_{24} = 2s_1$. We let $a^{s_1,\pm}_{s,s_{13},s_{24}} \equiv a^{\pm}_{\nu}$, etc. For general s, s_1, we have

$$a^{s_1,\pm}_{s,2s_1,2s_1} = c^{s_1,-}_{s,2s_1,2s_1}\Big(1 \mp \frac{1}{4s_1-1}\Big), \tag{219}$$

$$\begin{aligned}b^{s_1,\pm}_{s,2s_1,2s_1} &= \frac{1}{2(2s+3)(2s-1)}\Big[s(s+1)\\ &\quad +[2s(s+1)-1][8s_1(2s_1+1) - s(s+1)]\\ &\quad \pm\frac{1}{4s_1-1}\Big(2[16s_1^2 + s(s+1)][s(s+1)-1]\\ &\quad -8s_1[2s(s+1)-1]\Big)\Big],\end{aligned} \tag{220}$$

$$c^{s_1,\pm}_{s,2s_1,2s_1} = \frac{3[s(s+1)-1] - 8s_1(2s_1+1)}{2(2s-1)(2s+3)}, \tag{221}$$

$$\begin{aligned}\mathcal{B}^{s_1}_{s,2s_1,2s_1} &= \frac{1}{16}[s(s+1) - 4s_1(2s_1+1)]^2\\ &\quad +\frac{s(s+1)(4s_1-s)(s+4s_1+1)}{8(4s_1-1)}\\ &\quad +\frac{s_1^2(4s_1+1)}{(4s_1-1)}\delta_{s,0},\end{aligned} \tag{222}$$

$$\mathcal{T}^{s_1}_{s,2s_1,2s_1} = \frac{1}{16}[s(s+1)-4s_1(2s_1+1)]^2 - \frac{s_1^2(4s_1+1)}{(4s_1-1)}\delta_{s,0}, \quad (223)$$

From these expressions, we may evaluate the Type I first-order level-crossing inductions for AFM tetramers. From the definitions of the level-crossing constants in Eqs. (203)-(207), we rewrite them to explicitly indicate the s_1, s and type dependencies, and for Type I, it is easy to show that

$$a^{s_1,\pm}_{I,j}(s) = c^{s_1,-}_{I,j}(s)\Big(1 \mp \frac{1}{4s_1-1}\Big), \quad (224)$$

$$b^{s_1,\pm}_{I}(s) = -\frac{2s[8s_1(2s_1+1)+4s^4-10s^2+3]}{(4s^2-1)(4s^2-9)} \times\Big(1 \mp \frac{1}{4s_1-1}\Big), \quad (225)$$

$$c^{s_1,-}_{I,1}(s) = \frac{3[4s^3+5s^2-3s-3-8s_1(2s_1+1)]}{2(2s+1)(2s+3)}, \quad (226)$$

$$c^{s_1,-}_{I,2}(s) = \frac{c_{20}(s)+(4s^2-4s+3)8s_1(2s_1+1)}{2(4s^2-1)(4s^2-9)}, \quad (227)$$

$$c_{20}(s) = 3(4s^4-9s^2-s+3), \quad (228)$$

$$d^{s_1}_{I}(s) = \frac{s[s^2(4s_1-3)+8s_1(s_1+1-4s_1^2)]}{4(4s_1-1)} - \frac{s_1^2(4s_1+1)}{(4s_1-1)}\delta_{s,1}, \quad (229)$$

$$e^{s_1}_{I}(s) = \frac{s}{4}[s^2-4s_1(2s_1+1)] + \frac{s_1^2(4s_1+1)}{(4s_1-1)}\delta_{s,1}, \quad (230)$$

for $j = 1, 2$. For $s_1 = 1/2$, it is easy to see that $a^{1/2,+}_{I,j}(s) = b^{1/2,+}_{I}(s) = 0$ for $s = 1, 2$, as expected.

Letting $a^{s_1,\pm}_{I,j}(s) = a^{\pm}_j$, $b^{s_1,\pm}_{I}(s) = b^{\pm}$, and $c^{s_1,\pm}_{I,j}(s) = c^{\pm}_j$, it is easy to show that for Type I tetramers,

$$c^-_2 + \frac{1}{2}(b^+ + b^-) = -\frac{1}{3}c^-_1, \quad (231)$$

$$a^-_2 + b^- = -\frac{1}{3}a^-_1 = -\frac{4s_1}{3(4s_1-1)}c^-_1, \quad (232)$$

where $c^-_1 = c^{s_1,-}_{I,1}$.

This implies that for Type I, the axial NN and NNN axial anisotropic exchange interactions may be combined to yield an effective axial anisotropic exchange interaction given by Eq. (58).

For the single-ion contributions to the level-crossing inductions, no such simple relation can be found. We note that

$$a^+_2 + b^+ = -\frac{1}{3}a^+_1, \quad (233)$$

but the overall quantity $a^+_2 + 2b^+ + a^+_1\cos^2\theta$ in Eq. (202) contains the extra quantity b^+, which depends upon s, s_1.

H. Type II First-order AFM level-crossing constants

For AFM tetramers with $\tilde{J}_g < 0, \tilde{J}'_g - \tilde{J}_g < 0$, Type II, there are two classes of minimum energy configurations for each s manifold, depending upon whether s is even or odd. For even s, the relevant states have $s_{13} = s_{24} = s/2$, and for s odd, they are $s_{13}, s_{24} = (s\pm1)/2, (s\mp1)/2$. This type is also relevant for FM tetramers with $\tilde{J}_g > \tilde{J}'_g > 0$, especially for the first excited manifold of states with $s = 4s_1 - 1$. For even s the relevant parameters are

$$a^{s_1,\pm}_{s,s/2,s/2} = \frac{1}{2(2s-1)}\Big[s-1 \mp \frac{f_1(s,s_1)}{2(s+3)}\Big], \quad (234)$$

$$f_1(s,s_1) = 16s_1(s_1+1)-s^2-2s+6, \quad (235)$$

$$b^{s_1,\pm}_{s,s/2,s/2} = \frac{1}{2(2s-1)}\Big[s^2 \pm \frac{f_2(s,s_1)}{s+3}\Big], \quad (236)$$

$$f_2(s,s_1) = 16s_1(s_1+1)(s^2+2s-1) - s(s^3+4s^2+s-4), \quad (237)$$

$$c^{\pm}_{s,s/2,s/2} = \frac{s-1}{2(2s-1)}, \quad (238)$$

$$\mathcal{B}^{s_1}_{s,s/2,s/2} = \frac{s^4}{64} + \frac{s(s+1)[16s_1(s_1+1)-s(s+4)]}{16(s+3)} + (1-\delta_{s,0})\frac{(s+1)[16s_1(s_1+1)-s^2+4]}{128s(s+3)} \times(s+2)[16s_1(s_1+1)-s(s+4)] + \delta_{s,0}\frac{4s_1^2(s_1+1)^2}{3}, \quad (239)$$

$$\mathcal{T}^{s_1}_{s,s/2,s/2} = \frac{s^4}{64} - \delta_{s,0}\frac{4s_1^2(s_1+1)^2}{3} - (1-\delta_{s,0})\frac{(s+1)[16s_1(s_1+1)-s^2+4]}{128s(s+3)} \times(s+2)[16s_1(s_1+1)-s(s+4)]. \quad (240)$$

For odd s, the relevant parameters are

$$a^{s_1,\pm}_{s,(s+1)/2,(s-1)/2} = \frac{1}{2s(2s-1)}\Big[s^2-s+1 \mp \frac{f_3(s,s_1)}{2(s+2)(s+4)}\Big], \quad (241)$$

$$f_3(s,s_1) = 16s_1(s_1+1)(s^2+3s-1) - s^4-5s^3+11s-11, \quad (242)$$

$$b^{s_1,\pm}_{s,(s+1)/2,(s-1)/2} = \frac{1}{2(2s-1)}\Big[s^2-1 \pm \frac{f_4(s,s_1)}{(s+2)(s+4)}\Big], \quad (243)$$

$$f_4(s,s_1) = 16s_1(s_1+1)(s^3+5s^2+4s-3) - (s+1)(s^4+6s^3+7s^2-3s+1),$$

$$c^{+}_{s,(s+1)/2,(s-1)/2} = \frac{s^2-s+1}{2s(2s-1)}, \quad (244)$$

$$c^{-}_{s,(s+1)/2,(s-1)/2} = \frac{(s+1)(s-1)^2}{2s^2(2s-1)}, \quad (245)$$

$$\begin{aligned}\mathcal{B}^{s_1}_{s,(s+1)/2,(s-1)/2} &= \frac{(s^2-1)^2}{64}+\frac{(s+1)^2}{32(s+2)}\\ &\times[16s_1(s_1+1)-(s+3)(s-1)]\\ &+[16s_1(s_1+1)-(s+3)(s-1)]^2\\ &\times\frac{(s+1)^4}{256s^2(s+2)^2}\\ &+[16s_1(s_1+1)-(s+3)(s-1)]\\ &\times[16s_1(s_1+1)-(s+5)(s+1)]\\ &\times\frac{(2s+3)(s^2-2s-1)^2}{256s^3(s+1)(s+4)(2s+1)^2},\end{aligned} \quad (246)$$

$$\begin{aligned}\mathcal{T}^{s_1}_{s,(s+1)/2,(s-1)/2} &= \frac{(s^2-1)^2}{64}-\frac{(s+1)^4}{256s^2(s+2)^2}\\ &\times[16s_1(s_1+1)-(s+3)(s-1)]^2\\ &-[16s_1(s_1+1)-(s+3)(s-1)]\\ &\times[16s_1(s_1+1)-(s+5)(s+1)]\\ &\times\frac{(2s+3)(s^2-2s-1)^2}{256s^3(s+1)(s+4)(2s+1)^2}.\end{aligned} \quad (247)$$

From these expressions, we obtain the level-crossing inductions for the AFM type $\tilde{J}_g<0$ and $\tilde{J}'_g-\tilde{J}_g<0$.

For s even, we have

$$\begin{aligned}a^{s_1,\pm}_{IIe,1}(s) &= s(2s-1)a^{s_1,\pm}_{s,s/2,s/2}\\ &-(s-1)(2s-3)a^{s_1,\pm}_{s-1,s/2,(s-2)/2},\end{aligned} \quad (248)$$

$$\begin{aligned}a^{s_1,\pm}_{IIe,2}(s) &= sa^{s_1,\pm}_{s,s/2,s/2}\\ &-(s-1)a^{s_1,\pm}_{s-1,s/2,(s-2)/2},\end{aligned} \quad (249)$$

$$b^{s_1,\pm}_{IIe}(s) = b^{s_1,\pm}_{s,s/2,s/2}-b^{s_1,\pm}_{s-1,s/2,(s-2)/2}, \quad (250)$$

$$\begin{aligned}c^{s_1,\pm}_{IIe,1}(s) &= s(2s-1)c^{\pm}_{s,s/2,s/2}\\ &-(s-1)(2s-3)c^{\pm}_{s-1,s/2,(s-2)/2},\end{aligned} \quad (251)$$

$$\begin{aligned}c^{\pm}_{IIe,2}(s) &= sc^{\pm}_{s,s/2,s/2}\\ &-(s-1)c^{\pm}_{s-1,s/2,(s-2)/2},\end{aligned} \quad (252)$$

$$d^{s_1}_{IIe}(s) = \mathcal{B}^{s_1}_{s,s/2,s/2}-\mathcal{B}^{s_1}_{s-1,s/2,(s-2)/s}, \quad (253)$$

$$e^{s_1}_{IIe}(s) = \mathcal{T}^{s_1}_{s,s/2,s/2}-\mathcal{T}^{s_1}_{s-1,s/2,(s-2)/s}. \quad (254)$$

For s odd, we have

$$\begin{aligned}a^{s_1,\pm}_{IIo,1}(s) &= s(2s-1)a^{s_1,\pm}_{s,(s+1)/2,(s-1)/2}\\ &-(s-1)(2s-3)a^{s_1,\pm}_{s-1,(s-1)/2,(s-1)/2},\end{aligned} \quad (255)$$

$$\begin{aligned}a^{s_1,\pm}_{IIo,2}(s) &= sa^{s_1,\pm}_{s,(s+1)/2,(s-1)/2}\\ &-(s-1)a^{s_1,\pm}_{s-1,(s-1)/2,(s-1)/2},\end{aligned} \quad (256)$$

$$b^{s_1,\pm}_{IIo}(s) = b^{s_1,\pm}_{s,(s+1)/2,(s-1)/2}-b^{s_1,\pm}_{s-1,(s-1)/2,(s-1)/2}, \quad (257)$$

$$\begin{aligned}c^{s_1,\pm}_{IIo,1}(s) &= s(2s-1)c^{\pm}_{s,(s+1)/2,(s-1)/2}\\ &-(s-1)(2s-3)c^{\pm}_{s-1,(s-1)/2,(s-1)/2},\end{aligned} \quad (258)$$

$$\begin{aligned}c^{s_1,\pm}_{IIo,2}(s) &= sc^{\pm}_{s,(s+1)/2,(s-1)/2}\\ &-(s-1)c^{\pm}_{s-1,(s-1)/2,(s-1)/2},\end{aligned} \quad (259)$$

$$\begin{aligned}d^{s_1}_{IIo}(s) &= \mathcal{B}^{s_1}_{s,(s+1)/2,(s-1)/2}\\ &-\mathcal{B}^{s_1}_{s-1,(s-1)/2,(s-1)/2},\end{aligned} \quad (260)$$

$$\begin{aligned}e^{s_1}_{IIo}(s) &= \mathcal{T}^{s_1}_{s,(s+1)/2,(s-1)/2}\\ &-\mathcal{T}^{s_1}_{s-1,(s-1)/2,(s-1)/2}.\end{aligned} \quad (261)$$

From these expressions, we may obtain the Type II AFM level-crossing induction parameters. For even s, we find

$$a^{s_1,\pm}_{IIe,1}(s) = \frac{2s-3}{2}\mp\frac{48s_1(s_1+1)+a^{e}_{10}(s)}{4(s+1)(s+3)}, \quad (262)$$

$$a^{e}_{10}(s) = -2s^3-5s^2+6s+18, \quad (263)$$

$$\begin{aligned}a^{s_1,\pm}_{IIe,2}(s) &= \frac{1}{2(2s-1)(2s-3)}\Bigg[2s^2-6s+3\\ &\pm\frac{16s_1(s_1+1)(2s^2-4s+3)+a^{e}_{20}(s)}{2(s+1)(s+3)}\Bigg],\end{aligned} \quad (264)$$

$$a^{e}_{20}(s) = 2s^4+2s^3-9s^2-18s+18, \quad (265)$$

$$\begin{aligned}b^{s_1,\pm}_{IIe}(s) &= \frac{s}{(2s-1)(2s-3)}\Bigg[s-1\\ &\pm\frac{16s_1(s_1+1)(s-2)+b^{e}_{0}(s)}{2(s+1)(s+3)}\Bigg],\end{aligned} \quad (266)$$

$$b^{e}_{0}(s) = -4s^4-7s^3+20s^2+14s-18, \quad (267)$$

$$c^{-}_{IIe,1}(s) = \frac{s(2s-3)}{2(s-1)}, \quad (268)$$

$$c^{-}_{IIe,2}(s) = \frac{s(2s^2-4s+1)}{2(s-1)(2s-1)(2s-3)}, \quad (269)$$

(270)

and $d^{s_1}_{IIe}(s)$ and $e^{s_1}_{IIe}(s)$ are given by Eqs. (253) and (254). Combining $a^{s_1,-}_{IIe,2}(s)$ and $b^{s_1,-}_{IIe}(s)$, we find

$$a^{s_1,-}_{IIe,2}+b^{s_1,-}_{IIe} = \frac{1}{2}-\frac{16s_1(s_1+1)-d^{e}_{0}(s)}{4(s+1)(s+3)}, \quad (271)$$

$$d^{e}_{0}(s) = 2s^3+7s^2+2s-6. \quad (272)$$

We note that this expression differs substantially from that for $a^{s_1,-}_{IIe,1}(s)$, except for $s_1=1/2$ and $s=2$. Similarly, it is elementary to combine $c^{-}_{IIe,2}(s)$ and $[b^{s_1,+}_{IIe}(s)+b^{s_1,-}_{IIe}(s)]/2$. We find

$$c^{-}_{IIe,2}(s)+\frac{1}{2}\Big(b^{s_1,+}_{IIe}(s)+b^{s_1,-}_{IIe}(s)\Big) = \frac{s}{2(s-1)} \quad (273)$$

This simple expression differs from that for $c^{-}_{IIe,1}(s)$ by the factor $2s-3$. However, at $s=2$, the only even s value for $s_1=1/2$, they are equivalent. In addition, as for Type I, there is no simple relation between the single-ion parameters $a^{s_1,+}_{IIe,2}(s)+2b^{s_1,+}_{IIe}(s)$ and $a^{s_1,+}_{IIe,1}(s)$.

For odd s, the Type II level-crossing induction parameters are

$$a^{s_1,\pm}_{IIo,1}(s) = \frac{2s-1}{2} \mp \frac{48s_1(s_1+1)+a^{o}_{10}(s)}{4(s+2)(s+4)}, \quad (274)$$

$$a^{o}_{10}(s) = -2s^3-11s^2-10s+17, \quad (275)$$

$$a^{s_1,\pm}_{IIo,2}(s) = \frac{1}{2(2s-1)(2s-3)}\Bigg[2s^2-2s-1 \pm\frac{16s_1(s_1+1)(2s^2+1)+a^{o}_{20}(s)}{2(s+2)(s+4)}\Bigg], \quad (276)$$

$$a^{o}_{20}(s) = 2s^4+10s^3+9s^2-22s-5, \quad (277)$$

$$b^{s_1,\pm}_{IIo}(s) = \frac{1}{(2s-1)(2s-3)}\Bigg[(s-1)(s-2) \pm\frac{16s_1(s_1+1)(s^2-4s+1)+b^{o}_{0}(s)}{2(s+2)(s+4)}\Bigg], \quad (278)$$

$$b^{o}_{0}(s) = -4s^5-19s^4+54s^2-2s-5, \quad (279)$$

$$c^{-}_{IIo,1}(s) = \frac{(s-1)(2s-1)}{2s}, \quad (280)$$

$$c^{-}_{IIo,2}(s) = \frac{(s-1)(2s^2-4s+3)}{2s(2s-1)(2s-3)}, \quad (281)$$

$$d^{s_1}_{IIo}(1) = \frac{s_1}{6}(4s_1^3+8s_1^2+7s_1+3), \quad (282)$$

$$e^{s_1}_{IIo}(1) = -\frac{s_1}{6}(4s_1^3+8s_1^2+3s_1-1), \quad (283)$$

and the other $d^{s_1}_{IIo}(s)$ and $e^{s_1}_{IIo}(s)$ values are found from Eqs. (260) and (261).

We note that $a^{1/2,+}_{IIe,j}(2)=a^{1/2,+}_{IIo,j}(1)=b^{1/2,+}_{IIe}(2)=b^{1/2,+}_{IIo}(1)=0$ for $j=1,2$, as expected. However, by combining $a^{s_1,-}_{IIo,2}(s)$ and $b^{s_1,-}_{IIo}(s)$, we have

$$a^{s_1,-}_{IIo,2}+b^{s_1,-}_{IIo} = \frac{1}{2}-\frac{16s_1(s_1+1)-d^{o}_{0}(s)}{4(s+2)(s+4)}, \quad (284)$$

$$d^{o}_{o}(s) = 2s^3+13s^2+22s+5, \quad (285)$$

which differs substantially from the version with $s_1=1/2$. In addition, it is elementary to combine $c^{-}_{IIo,2}(s)+[b^{s_1,+}_{IIo}(s)+b^{s_1,-}_{IIo}(s)]/2$. We find

$$c^{-}_{IIo,2}(s)+\frac{1}{2}\Big(b^{s_1,+}_{IIo}(s)+b^{s_1,-}_{IIo}(s)\Big) = \frac{(s-1)}{2s}, \quad (286)$$

which differs from $c^{-}_{IIo,1}(s)$ by the factor $2s-1$. At $s=1$, the only relevant odd s value for $s_1=1/2$, these are equivalent. In addition, as for Type I and the even crossings of Type II, there is no simple relation between the single-ion parameters $a^{s_1,+}_{IIo,2}(s)+2b^{s_1,+}_{IIo}(s)$ and $a^{s_1,+}_{IIo,1}(s)$.

I. Hartree INS functions

The functions $L_{\nu,\nu'}(\boldsymbol{q})$ and $M_{\nu,\nu'}(\boldsymbol{q})$ in the self-consistent Hartree INS $S^{(1)}_{g}(\boldsymbol{q},\omega)$ in the induction representation are given by

$$\begin{aligned} L_{\nu,\nu'}(\boldsymbol{q}) &= \delta_{m',m}\delta_{s'_{24},s_{24}}\Big[m^2\delta_{s',s} \\ &\times\Big(\delta_{s'_{13},s_{13}}f_{\overline{\nu},0}(\boldsymbol{q})+\sum_{\sigma''=\pm1}\delta_{s'_{13},s_{13}+\sigma''}f^{\sigma''}_{\overline{\nu},1}(\boldsymbol{q})\Big) \\ &+\sum_{\sigma'=\pm1}\delta_{s',s+\sigma'}\Big(C^{m}_{-\sigma' s-(\sigma'+1)/2}\Big)^2 \\ &\times\Big(\delta_{s'_{13},s_{13}}f^{\sigma'}_{\overline{\nu},2}(\boldsymbol{q}) \\ &\quad+\sum_{\sigma''=\pm1}\delta_{s'_{13},s_{13}+\sigma''}f^{\sigma',\sigma''}_{\overline{\nu},3}(\boldsymbol{q})\Big)\Big] \\ &+\begin{pmatrix} s_{13}\leftrightarrow s_{24}\\ s'_{13}\leftrightarrow s'_{24}\\ q_y\to -q_y\end{pmatrix}, \end{aligned} \quad (287)$$

$$\begin{aligned} M_{\nu,\nu'}(\boldsymbol{q}) &= \sum_{\sigma=\pm1}\delta_{m',m+\sigma}\delta_{s'_{24},s_{24}}\Big[\Big(A^{\sigma m}_{s}\Big)^2\delta_{s',s} \\ &\times\Big(\delta_{s'_{13},s_{13}}f_{\overline{\nu},0}(\boldsymbol{q})+\sum_{\sigma''=\pm1}\delta_{s'_{13},s_{13}+\sigma''}f^{\sigma''}_{\overline{\nu},1}(\boldsymbol{q})\Big) \\ &+\sum_{\sigma'=\pm1}\delta_{s',s+\sigma'}\Big(D^{\sigma,m}_{-\sigma' s-(\sigma'+1)/2}\Big)^2 \\ &\times\Big(\delta_{s'_{13},s_{13}}f^{\sigma'}_{\overline{\nu},2}(\boldsymbol{q}) \\ &\quad+\sum_{\sigma''=\pm1}\delta_{s'_{13},s_{13}+\sigma''}f^{\sigma',\sigma''}_{\overline{\nu},3}(\boldsymbol{q})\Big)\Big] \\ &+\begin{pmatrix} s_{13}\leftrightarrow s_{24}\\ s'_{13}\leftrightarrow s'_{24}\\ q_y\to -q_y\end{pmatrix}, \end{aligned} \quad (288)$$

$$f_{\overline{\nu},0}(\boldsymbol{q}) = \frac{1}{8}\Big(f_{+}(\boldsymbol{q})+\xi^2_{s,s_{13},s_{24}}f_{-}(\boldsymbol{q}) -2\xi_{s,s_{13},s_{24}}\sin(q_x a)\sin(q_y a)\Big), \quad (289)$$

$$f^{\sigma''}_{\overline{\nu},1}(\boldsymbol{q}) = 2\Big(1-\cos[a(q_x+q_y)]\Big) \times\Big(F^{s_{13}+(\sigma''+1)/2,s_{24}}_{s_1,s_1,s}\Big)^2 \quad (290)$$

$$f^{\sigma'}_{\overline{\nu},2}(\boldsymbol{q}) = \frac{1}{8}f_{-}(\boldsymbol{q})\eta^2_{s+(\sigma'+1)/2,s_{13},s_{24}}, \quad (291)$$

$$f^{\sigma',\sigma''}_{\overline{\nu},3}(\boldsymbol{q}) = 2\Big(1-\cos[a(q_x+q_y)]\Big) \times\Big(G^{s_{13}+(\sigma''+1)/2,s_{24}}_{s_1,s_1,\sigma'\sigma''s+\sigma''(\sigma'+1)/2}\Big)^2, \quad (292)$$

$$f_{\pm}(\boldsymbol{q}) = 1+\cos(q_x a)\cos(q_y a) \pm\cos(q_z c)[\cos(q_x a)+\cos(q_y a)], \quad (293)$$

where the A_s^m, C_s^m, $D_s^{\tilde{\sigma},m}$, $F_{s_1,s_3,s}^{s_{13},s_{24}}$, $G_{s_1,s_3,s}^{s_{13},s_{24}}$, $\eta_{z,x,y}$, $\xi_{z,x,y}$, are given by Eqs. (46), (166), (167), and (172)-(175), respectively.

* Electronic address: klemm@physics.ucf.edu
† Electronic address: efremov@theory.phy.tu-dresden.de

[1] R. Sessoli, D. Gatteschi, A. Caneschi, and M. Novak, Nature (London), **365**, 141 (1993); W. Wernsdorfer and R. Sessoli, Science **284**, 133 (1999).
[2] M. N. Leuenberger and D. Loss, Nature (London), **410**, 789 (2001).
[3] D. V. Efremov and R. A. Klemm, Phys. Rev. B **66**, 174427 (2002).
[4] R. A. Klemm and D. V. Efremov, AIP Conf. Proc. **850**, 1151 (2006).
[5] D. V. Efremov and R. A. Klemm, Phys. Rev. B **74**, 064408 (2006)(cond-mat/0601591).
[6] Y. Shapira, M. T. Liu, S. Foner, C. E. Dubé, and P. J. Bonitatebus, Jr., Phys. Rev. B **59**, 1046 (1999).
[7] C. Mennerich, H.-H. Klauss, M. Broekelmann, F. J. Litterst, C. Golze, R. Klingeler, V. Kataev, B. Büchner, S.-N. Grossjohann, W. Brenig, M. Goiran, H. Rakoto, J.-M. Broto, O. Kataeva, and D. J. Price, Phys. Rev. B **73**, 174415 (2006).
[8] D. Zipse, J. M. North, N. S. Dalal, S. Hill, and R. S. Edwards, Phys. Rev. B **68**, 184408 (2003).
[9] S. Carretta, E. Liviotti, N. Magnani, P. Santini, and G. Amoretti, Phys. Rev. Lett. **92**, 207205 (2004).
[10] D. Zipse, N. S. Dalal, R. M. Achey, J. M. North, S. Hill, and R. S. Edwards, Appl. Magn. Reson. **27**, 151 (2004).
[11] S. Hill, R. S. Edwards, J. M. North, S. Maccagnano, and N. S. dalal, Polyhedron **22**, 1897 (2003).
[12] R. S. Rubins, T. D. Black, and J. Barak, J. Chem. Phys. **85**, 3770 (1985).
[13] T. D. Black. R. S. Rubins, D. K. De, R. C. Dickinson, and W. A. Baker, Jr., J. Chem. Phys. **80-**, 4620 (2984).
[14] R. C. Dickinson, W. A. Baker, Jr., T. D. Black, and R. S. Rubins, J. Chem. Phys. **79**, 2609 (1983).
[15] E. Buluggiu, J. Chem. Phys. **84**, 1243 (1986)
[16] A. Bino, D. C. Johnston, D. P. Goshorn, T. R. Halbert, and E. I. Stiefel, Science **241**, 1479 (1988).
[17] E.-C. Yang, D. N. Hendrickson, W. Wernsdorfer, M. Nakano, L. N. Zakharov, R. D. Sommer, A. L. Rheingold, M. Ledezma-Gairaud, and G. Christou, J. Appl. Phys. **91**, 7382 (2002).
[18] A. Sieber, C. Boskovic, R. Bircher, O. Waldmann, W. T. Ochsenbein, G. Chaboussant, H. U. Güdel, N. Kirchner, J. van Slageren, W. Wernsdorfer, A. Neels, H. Stoeckli-Evans, S. Jannsen, F. Juranyi, and H. Mutka, Inor. Chem. **44**, 4315 (2005), and references therein.
[19] M. Moragues-Cánovas, M. Helliwell, L. Ricard, Éric Rivière. W. Wernsdorfer, E. Brechin, and T. Mallah, Eur. J. Inorg. Chem. **2004**, 2219.
[20] R. S. Edwards, S. Maccagnano, E.-C. Yang, S. Hill, W. Wernsdorfer, D. Hendrickson, and G. Christou, J. Appl. Phys. **93**, 7807 (2003).
[21] E. del Barco, A. D. Kent, E.-C. Yang, and D. N. Hendrickson, Polyhedron **24**, 2695 (2005).
[22] D. N. Hendrickson, E.-C. Yang, R. M. Isidro, C. Kirman, J. Lawrence, R. S. Edwards, S. Hill, A. Yamaguchi, H. Ishimoto, W. Wernsdorfer, C. Ramsey, N. Dalal, and M. M. Olmstead, Polyhedron **24**, 2280 (2005).
[23] C. Boskovic, R. Bircher, P. L. W. Tregenna-Piggott, H. U. Güdel, C. Paulsen, W. Wernsdorfer, A.-L. Barra, E. Khatsko, A. Neels, and H. Stoeckli-Evans, J. Am. Chem. Soc. **125**, 14046 (2003).
[24] K. Park, M. R. Pederson, and C. S. Hellberg, Phys. Rev. B **69**, 014416 (2004).
[25] J. Ribas-Arino, T. Baruah, and M. R. Pederson, J. Chem. Phys. **123**, 044303 (2005).
[26] A. V. Postnikov, J. Kortus, and M. R. Pederson, Phys. Stat. Solidi B: Basic Research **243**, 2533 (2006).
[27] S. Stolbov, R. A. Klemm, and T. S. Rahman, cond-mat/0501178 (unpublished).
[28] K. Park, M. R. Pederson, and N. Bernstein, J. Phys. Chem. Solids **65**, 805 (2004).
[29] M. R. Pederson, private communications.
[30] D. W. Boukhvalov, M. Al-Sager, E. Z. Kurmaev, A. Moewes, V. R. Galakhov, L. D. Finkelstein, S. Chiuzbaian, M. Neumann, V. V. Dobrovitskii, M. I. Katsnelson, A. I. Lichtenstein, B. N. Harmon, K. Endo, J. M. North, and N. S. Dalal, Phys. Rev. B **75**, 014419 (2007).
[31] R. Boča, *Theoretical Foundations of Molecular Magnetism*, (Elsevier, Amsterdam, 1999).
[32] O. Waldmann and H. U. Güdel, Phys. Rev. B **72**, 094422 (2005).
[33] M. Tinkham, *Group Theory and Quantum Mechanics*, (McGraw-Hill, New York, 1964).
[34] R. A. Klemm and M. Ameduri, Phys. Rev. B **66**, 012403 (2002).
[35] D. M. Barnhart, D. L. Clark, J. C. Gordon, J. C. Huffman, J. G. Watkin, and B. D. Zwick, J. Am. Chem. Soc. **115**, 8461 (1993).
[36] R. A. Klemm and M. Luban, Phys. Rev. B **64**, 104424 (2001).
[37] A. Bencini and D. Gatteschi, *Electron Paramagnetic Resonanceof Exchange Coupled Systems*, (Springer, Berlin, 1990).
[38] T. Moriya, Phys. Rev. **120**, 91 (1960).
[39] I. Dzyaloshinskii, J. Phys. Chem. Solids **4**, 241 (1958).
[40] J. D. Jackson, *Classical Electrodynamics, 3rd Edition* (Wiley & Sons, Hoboken, NJ, 1999), p. 186.
[41] H. Goldstein, *Classical Mechanics*, (Addison-Wesley, Reading, MA, 1965), p. 109.
[42] M. Alcántara Ortigoza, R. A. Klemm, and T. S. Rahman, Phys. Rev. B **72**, 174416 (2005).
[43] R. Valenti, C. Gros, and W. Brenig, Phys. Rev. B **62**, 14164 (2000).
[44] H. Katsura, N. Nagaosa, and A. V. Balatsky, Phys. Rev. Lett. **95**, 057205 (2005).
[45] S.-W. Cheong and M. Mostovoy, Nature Materials **6**, 13 (2007).
[46] J. Schnack, M. Brüger, M. Luban, P. Kögerler, E. Morosan, R. Fuchs, R. Modler, H. Nojiri, R. C. Rai, J. Cao, J. L. Musfeldt, and X. Wei, Phys. Rev. B **73**, 094401 (2006).
[47] O. Waldmann, J. Hassmann, P. Müller, D. Volkmer, U. S. Schubert, and J.-M. Lehn, Phys. Rev. B **58**, 3277 (1998).
[48] O. Waldmann, Coord. Chem. Rev. **249**, 2550 (2005).
[49] R. A. Klemm, C. T. Rieck, and K. Scharnberg, Phys. Rev. B **61**, 5913 (2000).
[50] V. V. Kostyuchenko, Phys. Rev. B **76**, 21204 (2007).
[51] D. V. Efremov and R. A. Klemm, unpublished.
[52] S. Carretta, P. Santini, G. Amoretti, T. Guidi, R. Caci-

uffo, A. Candini, A. Cornia, D. Gatteschi, M. Plazanet, and J. A. Stride, Phys. Rev. B **70**, 214403 (2004).
[53] A. Cornia, A. C. Fabretti, P. Garrisi, C. Mortalò, D. Bonacchi, D. Gatteschi, R. Sessoli, L. Sorace, W. Wernsdorfer, and A.-L. Barra, Angew. Chem. Int. Ed. **43**, 1136 (2004).
[54] E. Rastelli and A. Tossi, Phys. Rev. B **75**, 13414 (2007).
[55] G. Amoretti, S. Carretta, R. Caciuffo, H. Casalta, A. Cornia, M. Affronte, and D. Gatteschi, Phys. Rev. B **64**, 104403 (2001).
[56] J. M. Clemente-Juan, H. Andres, J. J. Borrás-Almenar, E. Coronado, H. U. Güdel, M. Aebersold, G. Kearly, H. Büttner, and M. Zolliker, J. Am. Chem. Sic. **121**, 10021 (1999).
[57] L. Lecren, W. Wernsdorfer, Y.-G. Li, O. Roubeau, H. Miyasaka, and R. Clérac, J. Am. Chem. Soc. **127**, 11311 (2005).
[58] M. Koikawa, M. Ohba, and T. Tokii, Polyhedron **24**, 2257 (2005).
[59] J.-N. Rebilly, L. Catala, E. Rivière, R. Guillot, W. Wernsdorfer, and T. Mallah, Inorg. Chem. **44**, 8194 (2005).
[60] M. Ameduri and R. A. Klemm, J. Phys. A: Math. Gen. **37**, 1095 (2004).
[61] J. L. Musfeldt, private comuunication.